



US Army Corps
of Engineers
Waterways Experiment
Station

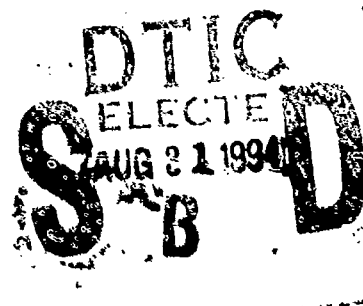
Technical Report SL-94-1
July 199

AD-A283 904



Development of a Large-Diameter Gas Gun for Studies of Gage Validation and Dynamic Material Properties

by Howard G. White



WES

Approved For Public Release; Distribution Is Unlimited

94-27987



DTIC QUALITY INSPECTED 8

The contents of this report are not to be used for advertising, publication, or promotional purposes. Citation of trade names does not constitute an official endorsement or approval of the use of such commercial products.



PRINTED ON RECYCLED PAPER

Development of a Large-Diameter Gas Gun for Studies of Gage Validation and Dynamic Material Properties

by Howard G. White

U.S. Army Corps of Engineers
Waterways Experiment Station
3909 Halls Ferry Road
Vicksburg, MS 39180-6199

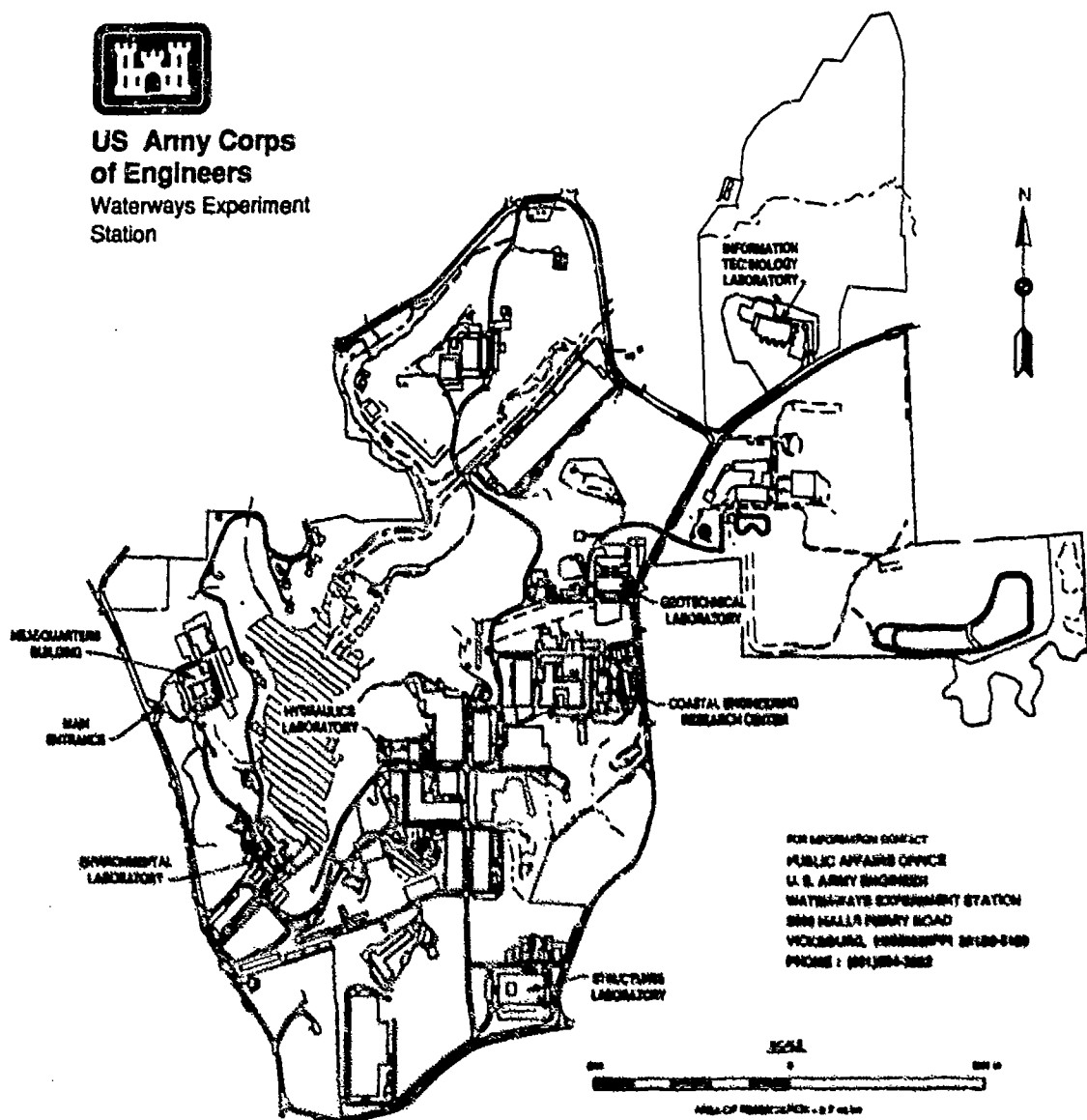
Final report .

Approved for public release; distribution is unlimited

Prepared for Defense Nuclear Agency
6801 Telegraph Road, Alexandria, VA 22310-3398



**US Army Corps
of Engineers**
Waterways Experiment
Station



Waterways Experiment Station Cataloging-in-Publication Data

White, Howard G.

Development of a large-diameter gas gun for studies of gage validation and dynamic material properties / by Howard G. White ; prepared for Defense Nuclear Agency.

170 p. : ill. ; 28 cm. -- (Technical report ; SL-94-16)

Includes bibliographic references.

1. Nuclear explosions -- Simulation methods -- Equipment and supplies. 2. Military geology -- Instruments -- Testing -- Equipment and supplies. 3. Blast effect -- Environmental aspects -- Simulation methods. 4. Projectiles -- Testing -- Equipment and supplies. I. United States. Army. Corps of Engineers. II. U.S. Army Engineer Waterways Experiment Station. III. United States. Defense Nuclear Agency. IV. Structures Laboratory (U.S.) V. Title. VI. Series: Technical report (U.S. Army Engineer Waterways Experiment Station) ; SL-94-16.

TA7 W34 no.SL-94-16

PREFACE

The work described in this report was sponsored by the Headquarters, Defense Nuclear Agency. Funding was provided under MIPR's 90-594, 91-571, 92-573, and 93-567, with Mr. Mark Flohr, DNA/TDTR, Project Manager.

This study was conducted by the Explosion Effects Division (EED), Structures Laboratory (SL), U.S. Army Engineer Waterways Experiment Station (WES), Vicksburg, MS.

This effort was performed under the overall direction of Mr. Howard G. White. Dr. Charles Welch and Mr. Alan Ohrt of the EED, WES, provided technical assistance. Numerous persons have assisted in various aspects of testing with the gun. These include Messrs. Rodney Walters and Cecil Dorrell of the EED, WES; Messrs. John Byrne, Jeff Hales, Fred Williams, and Graymond Jolly, contractors to the EED, WES; Messrs. Charles Thompson, Bruce Barker, Sonny Johnson, Jim Holder, and Bill Strahan of the Instrumentation Services Division, WES; Mr. Billy Neely of the Concrete Technology Division, WES; and Messrs. Gene Logan, Ron Wood, Mickey Blackmon, Bill Tennant, Paul Beatty, Buttons Crum, and numerous others of the Engineering and Construction Services Division, WES.

The author expresses his appreciation to his advisor, Prof. Robert Miller, and other members of the committee, Prof. James Phillips and Prof. Richard Weaver, Department of Theoretical and Applied Mechanics, University of Illinois at Urbana-Champaign, for their insight and suggestions in preparing this thesis.

During this investigation, Mr. Landon K. Davis was Chief, EED, and Mr. Bryant Mather was Director, SL.

At the time of publication of this report, Director of WES was Dr. Robert W. Whalin. Commander was COL Bruce K. Howard, EN.

The contents of this report are not to be used for advertising, publication, or promotional purposes. Citation of trade names does not constitute an official endorsement or approval for the use of such commercial products.

CONVERSION FACTORS, NON-SI TO SI
(METRIC) UNITS OF MEASUREMENT

Non-SI units of measurement used in this report can be converted to SI (metric) units as follows:

<u>Multiply</u>	<u>By</u>	<u>To Obtain</u>
atm	101352.93	Pascals
degrees (angle)	0.01745329	radians
feet	0.3048	meters
feet/sec	0.3048	meters/sec
g's (standard free-fall)	9.80665	meters/sec/sec
inches	25.4	millimeters
mil	0.0254	millimeters
pounds (force)	4.448	Newtons
pounds (force)/square inch	6.894757	kiloPascals
pounds (mass)	0.4535924	kilograms

Accession For	
NTIS GRA&I	<input checked="" type="checkbox"/>
DTIC TAB	<input type="checkbox"/>
Unannounced	<input type="checkbox"/>
Justification	
By	
Distribution/	
Availability Codes	
Dist	Avail and/or Special
A-1	

TABLE OF CONTENTS

CHAPTER

1	INTRODUCTION.....	1
1.1	Background/Requirement.....	1
1.2	Review of Existing Facilities/Techniques.....	4
1.3	Scope.....	7
2	DESCRIPTION OF WES 4-FT-DIAMETER VERTICAL GAS GUN.....	10
2.1	Gun Operation.....	10
2.2	Quick-Release Trigger Mechanism.....	13
2.3	Projectile Design.....	14
2.4	Projectile Velocity and Planarity Measurements...	19
3	MODELLING GUN PERFORMANCE.....	21
3.1	Mathematical Model.....	21
3.2	Comparison of Test Results with Mathematical Model.....	25
3.3	Planarity and Pressurization Data.....	29
4	DETERMINATION OF NUISANCE EFFECTS: PREDICTIONS AND MEASUREMENTS.....	31
4.1	Ground Motion.....	31
4.2	Airblast.....	35
5	TESTING WITH THE WES 4-FT-DIAMETER VERTICAL GAS GUN...	41
5.1	Testing Philosophy and Objectives.....	41
5.2	Safety Tests and Considerations.....	43
5.2.1	Hydrostatic Testing.....	43
5.2.2	Vacuum Testing.....	45
5.2.3	Safety Features and Safety Plan.....	49
5.3	Target Construction and Typical Instrumentation Layout.....	52
5.4	Testing Procedure.....	57
6	EXPERIMENT DATA AND ANALYSIS.....	61
6.1	Active Measurement Data.....	61
6.2	Projectile-Soil Interaction Model.....	63
6.2.1	Model Development.....	63
6.2.2	Comparison of Test Data with PSI Model.....	67
6.3	Time-of-Arrival Data and the Determination of Dynamic Material Properties.....	68
6.3.1	Propagation Velocity of Loading Wave.....	69
6.3.2	Propagation Velocity of Relief Wave.....	70

6.3.2.1	Graphical Method.....	71
6.3.2.2	Analytic Method.....	73
6.3.2.3	Determination of Relief Wave Velocity Using a Varying Loading Wave Velocity.....	75
6.4	Construction of a Material Model for Ottawa Sand.	78
7	SUMMARY AND CONCLUSIONS.....	79
7.1	Summary.....	79
7.2	Conclusions.....	80
	TABLES.....	81
	FIGURES.....	86
	REFERENCES.....	142
	APPENDIX A.....	148
	APPENDIX B.....	152
	APPENDIX C.....	154

LIST OF SYMBOLS

A	area of barrel
A_p	area of projectile
A_t	area of target
C	loading wave velocity
C_L	average loading wave velocity in a target
C_{L1}	loading wave velocity between the target surface and the lower instrumented depth in a target
C_{L2}	loading wave velocity between the lower instrumented depth and the bottom of a target
C_r	loading wave velocity
C_v	relief wave velocity
E	yield energy of TNT explosive
F	force on projectile and reaction mass
g_c	gravitational constant
H_p	thickness of projectile
H_t	thickness of target
H_1	upper instrumented depth in a target
$H_1(t_4)$	location of an instrument originally at the upper depth in a target, at TOA of the relief wave
H_2	lower instrumented depth in a target
$H_2(t_3)$	location of an instrument originally at the lower depth in a target, at TOA of the relief wave
KE	kinetic energy
L_p	distance traveled by projectile
L_r	distance traveled by reaction mass
M_p	mass of projectile
M_{p1}	mass of projectile before impact

M_{p2}	mass of projectile after impact
M_r	mass of reaction mass
M_{t1}	mass of target before impact
M_{t2}	mass of target after impact
P	peak pressure amplitude total pressure in system
P_e	effective pressure
P_{init}	initial pressure acting on projectile and reaction mass
P_{ref}	reference pressure
PSI	projectile-soil interaction (model)
R	range from source
SPL	sound pressure level
t	time
TOA	time of arrival (of shock wave)
t_1	initial TOA at a gage in the upper depth
t_2	initial TOA at a gage in the lower depth
t_3	TOA of the relief wave at a gage in the lower depth
t_4	TOA of the relief wave at a gage in the upper depth
U_t	particle velocity of soil in the target
V	total system volume
V_{cham}	volume of chamber between projectile and reaction mass
v_i	peak vertical particle velocity for impact
v_p	projectile velocity
V_{pv}	volume of pressure vessel
v_{p1}	projectile velocity at impact
v_{t1}	target velocity at impact

x	displacement of projectile
y	displacement of reaction mass
z	position of shock front in a target
z_g	depth of gage in a target
γ	ratio of specific heats for a gas
ρ	density of reaction mass
ρ_p	density of projectile
ρ_t	density of target
σ_t	stress in the target

CHAPTER 1

INTRODUCTION

1.1 Background/Requirement

The study of explosives and explosive phenomena is an inherent interest of the military. During recent years, particular attention has been focused on the survival (or destruction) of underground military targets. Because the Limited Test Ban Treaty of 1963 prohibited the detonation of nuclear devices in the atmosphere, high-explosive testing schemes have been developed to simulate the effects of nuclear detonation. Part of the mission of the Explosion Effects Division (EED), Structures Laboratory, Waterways Experiment Station (WES), is to develop transducers capable of surviving and measuring extreme-shock environments, such as those produced in the earth near a simulated nuclear explosion.

Ground motion (acceleration, velocity, and displacement) and stress are among the most important parameters measured during explosive tests. Particle velocities up to 300 ft/sec in acceleration fields exceeding 100,000 g, and stress fields up to 100,000 psi are not uncommon. The time regime of interest varies from microseconds to seconds. A variety of specialized instruments are used to monitor these parameters. Data measured on these tests are used to evaluate the accuracy of material models used in calculating the response of a medium to an explosive source.

An inherent problem in using these instruments is the validation of their operation in the manner of their intended use. That is, explosive tests are highly dynamic events, and transducers are typically calibrated statically. Also, typical calibration procedures do not include the geologic material in the calibration process. For example, the inclusion of a gage in a soil medium disrupts the stress field and potentially induces either stress concentrations or reliefs, depending on gage stiffness and geometry and the properties of the medium. For several types of particle-velocity measurement systems, an accelerometer is placed inside a protective canister. The effect of the rigid-body motion of the canister on the ability of the package to track the medium is critical to the fidelity of these measurements (Rickman and White, 1986; White, 1989a; and Welch, 1993)*. Other factors not included in the calibration process are placement procedures. For example, in some test geometries a borehole is drilled in the medium and an instrument is grouted in place. The gage measurements must be corrected for the difference between the material response of the medium and that of the grout in order to determine the values that would have been measured had the gages been embedded directly in the medium rather than grout (Welch, 1982; Germain, 1992; and King, 1992).

As mentioned above, data measured on various tests are used to evaluate the accuracy of material models. These models are

* References are listed alphabetically by author, beginning on page 142.

used to predict explosion-induced effects. A fallacy with the development of a model for a given geology is that the properties determined may be localized, i.e., the material is likely to have different properties over a very small range. For instance, in a jointed rock, the orientation and density of the joints, and the interface conditions between them could vary drastically within a range of just a few feet. A tool for isolating the effect of each of these parameters could aid in developing dynamic "macroscopic" material properties for the medium.

The U. S. Army Engineer Waterways Experiment Station has developed a 4-ft-diameter vertical gas gun, under funding from the Defense Nuclear Agency, to provide a mechanism for addressing the problems stated above. Gas guns are used to generate localized shock environments in materials, for shock physics studies, by high-velocity impacts of a projectile against samples of the materials under study. A gas gun's ability to produce controlled and repeatable shock inputs is an attractive alternative to high-explosive techniques, which are more commonly used to test the performance of ground shock transducers. Typically, gas guns accelerate projectiles which are small (6-in. diameter or less) and achieve high velocities. Small gun bores, however, limit the suitability of existing gas guns to test transducers in soils, since they cannot produce the large one-dimensional fields that are desirable for such tests. The purpose of the large-bore (4-ft) gun is to generate these large, one-dimensional stress and motion fields in various geologic

materials of interest. These fields can then be used for controlled tests of ground shock transducers, as well as for other shock physics studies.

Some of the desired attributes of the 4-ft diameter gun are that it:

- require no explosive;
- produce repeatable inputs;
- provide an efficient and cost-effective testing method;
- generate minimal noise levels (allowing use in relatively inhabited areas);
- have a vertical orientation (for easier testing).

1.2 Review of Existing Facilities/Techniques

Blast and shock simulators may be categorized as:

- large/small-scale high-explosive (HE) configurations;
- shock tubes;
- blast chambers;
- mechanical shock equipment.

Large/small-scale HE configurations produce a shock wave that propagates through the air, earth, or water, to impinge on a test object. These tests, typically conducted at established test ranges, provide a very realistic simulation of a nuclear device. However, large-scale tests are infrequent and costly and rarely afford instrumentation development studies. Small-scale HE field tests are sometimes used for instrumentation studies, though not necessarily for validation purposes. One method for

simulating HE airblast and airblast-induced ground motion is the High-Explosive Simulation Technique, or HEST. This simulator is constructed to suit specifications on a suitable site for one-time use. The test objects (gages, in our case) are installed in a target which is overlaid with an array of explosive strands placed in polystyrene foam forms and bermed over with earth. The explosive array is ignited at one end and the explosive strands produce a travelling airblast wave that simulates a high-level large-yield nuclear airblast wave. As explosive simulations go, this technique produces a particularly planar input to the target. The fundamental problem with any explosive-driver technique is the characterization and repeatability of the driver. Of course, there are also the safety problems of storing, handling, and detonating the explosives.

Another type of blast simulator, the shock tube, is basically a long horizontal tunnel with a compressed gas or explosive driver at one end that produces a shock wave which propagates down the tunnel to impact a test object contained in a test chamber. Some shock tubes include a soil bed for testing objects that are partially or completely below the ground surface. Some of the advantages of shock tubes over HE field tests are that the tests are easily scheduled, are repeatable, and are less costly. However, shock tubes are generally intended for conducting airblast and airblast instrumentation studies and are not suited for the instrumentation and/or material properties studies that were the impetus for the 4-ft-diameter gas gun.

Blast chambers are used to simulate only the overpressure portion of airblast. This pressure pulse may be used to simulate ground shock. A blast chamber is simply a strong container for simulating blast overpressure on a test object or the soil over a buried object. The pressures can be created by an explosive or a compressed gas and the release can be controlled to simulate the decay of a passing airblast wave. The size of available blast chambers could accommodate the geometry necessary for gage validation or material property studies. However, these devices have the same drawbacks as other simulation techniques mentioned in that they require explosives for generating the shock delivered to the target. Static instrumentation studies have been conducted using blast chambers (Ohrt, 1994). These tests used air pressure to load a water bag in contact with the target. These tests were successful in determining the static response of stress instruments in various types of soils.

Mechanical shock equipment imposes airblast or ground shock directly onto a test object through a number of methods. These include drop tests, mechanical shakers, static and dynamic loaders, gas guns, etc. The only method of mechanically shocking a material to conduct dynamic instrumentation or material properties studies that is similar in scale (or capability) to the 4-ft gas gun is known in the explosive effects community as the flyer-plate technique. The technique uses an explosively driven steel plate to impact a target. The plate is typically 4 or 8-ft in diameter and achieves an impact velocity on the order

of 1,500 ft/sec, producing stresses in a sand target of about 70,000 psi. Drawbacks to this technique are its expense and use of explosives.

More information on all the techniques discussed above are reported by Gould (1990). This comprehensive reference contains an extensive listing of facilities and techniques used for the simulation of nuclear weapons effects.

While there are several techniques to simulate nuclear weapons effects, most require explosives. There are numerous problems when testing with explosive, e.g., tests are inherently dangerous, special training is required for personnel handling the explosives, the tests must be performed in remote locations or at special test sites, the tests are usually expensive, the source input to a target is difficult to quantify, and it is difficult to produce a repeatable input to a target.

The 4-ft gas gun was developed to overcome these problems and to fill the need in the explosion effects community for a device that could become the standard for gage validation studies and provide a mechanism for conducting dynamic material properties studies.

1.3 Scope

The scope of the material presented here is somewhat limited compared with the total development effort, but this thesis is not intended to be an exhaustive review of every aspect of the project. Instead the focus is centered on the general aspects of

the development effort. It is the intent of the author to have the reader understand how the gun operates, how targets are constructed, how tests are conducted, and how the data is used.

To achieve these goals, the thesis is organized into seven chapters. A description of the gun and its method of operation is given in Chapter 2. A mathematical description of the operation of the gun is developed in Chapter 3 and compared with test results. Chapter 4 presents predictions and data on the nuisance effects (far-field ground motion and noise) associated with testing. The philosophy behind the initial tests with the gun is described in Chapter 5, along with discussion of safety considerations, results from safety tests, and procedures for target construction and firing the gun. Results from tests using sand targets and typical data analysis procedures are presented in Chapter 6. A summary of the development effort is presented in Chapter 7.

The development of the gas gun was a substantial research program, involving large amounts of funding spanning several years. For the sake of efficiency and cost-effectiveness, many individuals contributed to the work effort (as was mentioned in the Acknowledgments). So as to not mislead the reader, and assign credit properly, two particularly significant contributors are recognized again here. The barrel and pressure vessel of the gun were designed by Mr. Alan Ohrt, with follow-on design of the trigger mechanism, control systems, etc., performed by the author. Also, the original mathematical model of the gun was

developed by Dr. Charles Welch and Mr. Alan Ohrt. Several revisions and improvements to the mathematical model have been made by the author. Virtually all other development efforts described in this thesis are entirely, or primarily, the work of the author.

CHAPTER 2

DESCRIPTION OF WES 4-FT-DIAMETER VERTICAL GAS GUN

2.1 Gun Operation

A cut-away view of the 4-ft-diameter gas gun is given in Figure 2-1', and a schematic of the gun is shown in Figure 2-2. The gun is approximately 21 ft long, 8 ft in diameter (at its widest point), and weighs approximately 16 tons. It consists of a large annular pressure vessel surrounding a vertical barrel. A series of orifices is machined in a 28 in. long section of the barrel located about one-third of the barrel height below the top. The orifices allow the compressed air from the vessel to expand into the barrel. When the gun is in the cocked position, a one and one-half ton projectile containing o-ring seals at the top and bottom straddles the orifices, and prevents the compressed air from being released into the barrel. The projectile is held in place by a quick-release trigger mechanism. A water reaction mass fills the top portion of the barrel above the trigger mechanism. The bottom of the barrel may be sealed with a diaphragm to allow a partial vacuum to be created in the barrel section below the projectile.

To fire the gun, the projectile is first released by the trigger mechanism. The weight of the projectile causes it to move downward. As the top o-ring clears the orifices, the compressed air expands into the barrel. The incoming air

* Figures are collected at the end of the thesis, beginning on page 86.

simultaneously drives the projectile downward and the water reaction mass upward. Theoretically, the mass of the water can be adjusted so that the "bottom" of the water mass will exit the top of the barrel at the same time the projectile clears the bottom of the barrel. Water was chosen as the material for the reaction mass for convenience and to eliminate any hazards as the mass falls back to the earth after a test. The gun has a maximum operating range of 300 psi, which produces a projectile velocity of about 230 ft/sec.

Photographs of the gas gun at its permanent location at WES are presented in Figures 2-3 and 2-4. There are several interesting items of note in the photographs. For a sense of scale, notice the man at top of the gun in Figure 2-3. The gun is surrounded by an earthen berm, except for an access road (not visible in the photographs). Directly adjacent to the gun are three buildings. The cinder block building is used as a work room and storage room. The small portable building behind the cinder block building (seen in Figure 2-4) is used as a storage facility. The shed behind the gun in Figure 2-4 houses several components of the fill system used in operating the gun (see Section 5.2.3). Also seen in Figure 2-3 are instrument cables running along the tops of poles. These cables terminate in the Control Trailer, barely visible behind the trees in the top left corner of Figure 2-3. The Control Trailer is the control center for conducting a test. Instrument recorders and the control panel used for operating the fill system are located in the

trailer. The Control Trailer is also the closest range (175 ft) at which a test may be viewed by spectators. Various parts used in conducting a test are also seen in the two photographs, e.g., the three components of the projectile (carriage, energy-absorbing foam, and impact plate, described in Section 2.3), the tripod for loading the projectile into the gun, and the canvas covered frame used for moving the projectile and targets into the trench beneath the gun.

The use of the projectile as a plug for a series of orifices which allow venting of a high pressure gas is not unlike that described by Stewart and Tatu (1972). However, that is where the similarity between this gas gun and other guns end. There are many unique features of the 4-ft gas gun, including:

- the use of a water reaction mass to resist temporarily the 550,000 lb (maximum) jet force;
- incorporating replaceable barrel extensions and a replaceable barrel liner to minimize damage and repair costs to the gun should a mishap occur, such as the projectile lodging in the barrel during a test (Ohrt, 1988);
- the quick-release mechanism used to support and release the projectile;
- the multi-layered projectile used with the gun.

The latter two of these items as well as the procedure used for making projectile velocity and planarity measurements are discussed in the sections below.

2.2 Quick-Release Trigger Mechanism

The trigger mechanism for the gas gun must be capable of supporting both the weight of the projectile and the vacuum load applied to the bottom of the projectile. It must also provide a swift, smooth, central release of the projectile so as to not cause the projectile to get "caught" in the barrel. A schematic of the trigger is shown in Figure 2-5.

The trigger mechanism is supported within the barrel using two perpendicular crossmembers. Attached to the crossmembers is the housing piece for the three latches used in supporting the projectile. The weight of the projectile and the vacuum load tend to rotate the top of the latches away from the housing. This rotation is prevented by the retaining collar. The gas gun is fired by lifting the retaining collar (using four pneumatic cylinders), thus allowing the latches to rotate, and the projectile to move downward.

A safety feature incorporated into this design is a potential well at the top of the latches. Notice in Figure 2-5 that the mating surface of the latch and retaining collar is not simply vertical. This interface is designed such that when the retaining collar is lifted vertically, the latch must rotate into its housing. This rotation lifts the projectile slightly prior to firing. This lifting action requires a significant force in order to fire the gun, greatly reducing the chance of misfire. A photograph of the quick-release trigger mechanism is contained in Figure 2-6.

2.3 Projectile Design

The projectile is, of course, a critical element of the 4-ft-diameter gas gun. In addition to acting as the loading mechanism for a test specimen, it serves as the "plug" for the pressure vessel. When in its loaded position, o-rings at the top and bottom of the projectile seal the pressure vessel above and below the orifices in the permanent barrel section. After being released by the trigger mechanism, the projectile weight initiates the projectile's descent down the barrel. The top o-ring then clears the top row of orifices, allowing the pressurized air to expand into the barrel section.

The projectile design is shown schematically in Figure 2-7. A photograph of the projectile is contained in Figure 2-8. The projectile consists of a 34-in. long by 4-ft diameter carriage. Suspended beneath the carriage is a 47-in. diameter impact plate, which is typically made of steel or concrete, and is 2 to 12 inches thick. Rigid polyurethane foam is sandwiched between the impact plate and the carriage to reduce the impact-induced loads on the carriage and prevent damage.

The carriage section is comprised of two concentric right circular cylinders attached to a 3/4-in. thick bottom plate. The total height of the carriage is 34 inches. Eight equispaced gussets are used as stiffeners for the outer cylinder. The projectile is supported by the trigger mechanism using a flange bolted to the top of the inner cylinder (see Figure 2-9). O-rings located at the top and bottom of the carriage seal the

pressure vessel. As the projectile travels in the barrel, it "rides" on the o-rings. Guides along the outer surface of the projectile aid in centering the projectile in the barrel when being loaded. The weight of the carriage is approximately 2,100 lb.

A disposable pressure plate may be attached to the top of the carriage. The use of a pressure plate, suggested by Miller (1990), increases the projectile velocity for a given vessel pressure. The pressure plate acts as a lid over the carriage, providing a bearing surface for the driving pressure. This pressure will be greater as a result of reducing the initial volume in the barrel into which the gas must expand prior to acting on the projectile. The greater driving pressure will produce a higher projectile velocity. A photograph of the projectile after a 23 psi test is presented in Figure 2-10. Notice the deformation of the 3/16-in. thick aluminum pressure plate. The wavy pattern resulted from support provided by the gussets inside the carriage. For tests with a vessel pressure above 75 psi, the plate sheared around the gussets. Thus, a much thicker plate and/or a steel plate would be required to support the driving pressure effectively. However, the advantage gained by using the plate is diminished by the additional weight it adds to the total weight of the projectile.

Several issues were considered in the design of the projectile. They include:

a. Compression of the o-rings. Two primary factors were considered in the design/selection of the o-rings. The first is that the o-ring must be compressed sufficiently to provide adequate sealing for the pressure vessel. Secondly, the friction developed as the projectile travels down the barrel is a function of the compression of the o-ring and the choice of o-ring material. The sealing ability of the o-ring is influenced by the stretching of the o-ring around the projectile, and the interference fit between the o-ring and the barrel. Three diameter o-rings were investigated: 3/4-in., 11/16-in., and 5/8-in. The two smaller sizes provided adequate sealing (between 4 and 19 percent compression) during hydrostatic testing. A nitrile compound with a Type A durometer hardness of 70 was selected for the o-ring material. Nitrile compounds are good for general purpose sealing and are resistant to attack from oils and fluids. The 70-durometer material is a suitable compromise for the hardness level. It is soft enough to seal properly the pressure vessel while being hard enough to minimize friction as the projectile travels in the barrel. The Parker O-Ring Handbook (1990), used in the design of the carriage o-rings, is an excellent reference for o-ring design and material selection.

b. Tolerance between the carriage and the barrel liner. The radial clearance between the carriage and the barrel wall is 0.075 in. The maximum rotation of the carriage (about its central axis) as it travels in the barrel is 0.25 degrees. That is, one side of the impact plate could be as much as 0.212 in.

higher than the opposite side at the time of impact, assuming the impact plate is parallel to the bottom of the carriage.

c. Deflection of the sidewalls of the carriage. The pressure acting through the orifices on the sidewalls of the carriage (while in the ready-to-fire position) works against the sealing action of the o-rings. Excessive deflections could cause a leak to develop. The carriage design minimizes these deflections through the use of eight stiffening gussets between the inner and outer cylinders.

d. Deflection of the bottom plate of the carriage. There are two sources which could cause the bottom plate of the carriage to deform. The less significant source is the driving pressure acting on the back side of the plate (inside the carriage) which propels the projectile down the barrel. The maximum pressure at which the gun may be fired is 300 psi, but the only resistance to this force is the friction between the o-rings and the wall of the barrel. Therefore, the contribution of the driving pressure to the deformation of the bottom plate of the carriage is considered to be relatively small. The greatest possibility for damage to the carriage is from impact-induced stresses. These stresses could be several thousand psi and last several milliseconds.

The gussets positioned between the inner and outer cylinders are welded to the back side of the bottom plate of the carriage along their lower edge. This configuration provides significant support for the bottom plate to resist deformation. However, it

is not sufficient to prevent damage without making the bottom plate extremely thick, and hence massive.

The projectile configuration shown in Figure 2-7 was chosen for several reasons. The energy-absorbing foam allows for a lighter carriage, which in turn allows for higher projectile velocities. The foam may be altered to change the pulse shape delivered to the target. Also, a variety of impact plates may be used with the carriage to change the pulse shape.

A rigid closed-cell polyurethane foam was selected as the energy-absorbing material for use with the projectile. As the projectile velocity increases, for increased testing levels, the kinetic energy of the carriage to be absorbed by the foam increases. One of the material properties of the foam is the impact energy density, i.e., the kinetic energy per unit volume absorbed by the foam. This parameter is a function of the foam density. Typically foam weighing 15 or 20 lb/ft³ is used in the projectile. Since the diameter of the foam used in the projectile is fixed at 47 in., the thickness of the foam layer is increased, as required, to limit the stress applied to the bottom plate. More information on the material properties of the foam used with the projectile is given by Henry (1991). More information on the use of foams in energy-absorbing applications is contained in Henry, (1991); Gibson and Ashby, (1988); and White, (1989b).

2.4 Projectile Velocity and Planarity Measurements

Six piezoelectric pins, located at the base of the barrel of the gun, were used to monitor the velocity and planarity of the projectile as it exited the barrel. Shown in Figure 2-11 are a plan view and a section view of the location of the 6 pins. Pins T-1A and T-3A are located 1 in. above the plane containing the 4 pins designated T-1B, T-2, T-3B, and T-4. A schematic showing the orientation of the piezoelectric pin within its bushing, and the projectile within the barrel of the gun, is shown in Figure 2-12. A Time of Arrival Data System (TOADS) box (Schneider, 1989), running at a clock speed of 1 MHz, was used to record the time-of-arrival (TOA) of the projectile at each pin location. The projectile velocity was evaluated by measuring the TOA of the projectile at the locations T-1A/T-1B and T-3A/T-3B. The planarity at which the projectile exited the barrel was computed by comparing the measurements at pin locations T-1B, T-2, T-3B, and T-4. The redundant pin was included to evaluate the consistency of the TOA data.

Several factors determine the accuracy of the velocity/planarity measurements. These include the accuracy of machining the holes in the barrel and the holes in the pin bushing, the flatness of the impact plate, the assembly of the projectile, and the positioning of the pins within the bushing. The accuracy of the location of each pin was determined to be ± 0.023 in. Therefore, the actual distance between two pins used to measure the projectile velocity could be as much as 1.046 in. or as

little as 0.954 in. Hence, the accuracy of the velocity measurement is ± 4.6 percent. Likewise, pins assumed to be located in a common horizontal plane could have a relative difference in their vertical position of 0.046 in. The tolerance on the planarity measurement depends on the location of the two pins exhibiting the greatest disparity in TOA. For pins located 90° apart the tolerance is ± 1.44 milliradians and for pins located 180° apart the tolerance is ± 1.02 milliradians. The frequency response of the piezoelectric pin and the recording system is high enough to eliminate any significant contribution to the error of these measurements.

The impact velocity at which the projectile strikes a target placed beneath the gun will not change significantly from the value at which it exited the barrel. However, the planarity with which the projectile strikes the target could change drastically, depending on the levelness of the top of the target and whether or not the target surface is parallel to the impact plate surface. Beginning with Test 23, piezoelectric pins were placed in jigs at the surface of the target to quantify the impact velocity and planarity. Results on the velocity and planarity of travel of the projectile are presented in Sections 3.2 and 3.3.

CHAPTER 3

MODELLING GUN PERFORMANCE

3.1 Mathematical Model

A mathematical model of the gas gun operation was formulated in order to calculate projectile velocity as a function of initial vessel pressure.

Consider the simplified view of the gas gun shown in Figure 3-1. The view on the left shows the initial positions of the projectile and reaction mass, M_p and M_r , respectively. The chamber between the two masses, V_{cham} , is that portion of the barrel containing the trigger mechanism and its supporting members. The volume of the annular pressure vessel is denoted V_{pv} . The area of the barrel is given by A . The view on the right in Figure 3-1 shows the positions of the projectile and reaction mass at some time, t , after firing the gun. The displacement of the projectile is given by the variable x and that of the reaction mass is given by the variable y . Hence, the total volume at any time is

$$V = V_{pv} + V_{\text{cham}} + A(x+y) \quad (3.1)$$

Let the pressure at any time after firing be P . Since the area of the projectile and reaction mass are the same, the gas exerts an equal force, $F = PA$, on each. Frictional forces between the barrel walls and the projectile and reaction masses are ignored; hence, Newton's second law produces

$$F = M_p \ddot{x} = M_r \ddot{y}$$

Rearranging and integrating twice yields

$$y = \frac{M_p}{M_r} x \quad (3.2)$$

Substituting Equation (3.2) into Equation (3.1) yields

$$V = V_{pv} + V_{cham} + Ax \left(1 + \frac{M_p}{M_r} \right) \quad (3.3)$$

For a given projectile displacement, x , Equation (3.3) provides the volume of gas, V , of the system. Adiabatic expansion of the gas is assumed; hence, the pressure, P , of that volume has the relation

$$PV^\gamma = \text{constant}$$

where γ is the ratio of specific heats for the gas (about 1.4 for air). If the pressure and volume are known at any time, say P_1 and V_1 , then the pressure and volume as a function of time are given by

$$P(t) = \frac{P_1 V_1^\gamma}{(V(t))^\gamma} \quad (3.4)$$

Before the projectile and reaction masses are driven by the gas, the gas must first expand into the chamber between the two masses. The pressure (P_{pv}) and volume (V_{pv}) of the pressure

vessel, and the chamber volume (V_{chan}) are known. The initial pressure acting on the masses can be calculated using Equation (3.4):

$$P_{\text{init}} = \frac{P_{pv} V_{pv}^{\gamma}}{(V_{pv} + V_{\text{chan}})^{\gamma}} \quad (3.5)$$

The pressure acting on the projectile that produces a given projectile displacement, x , may be found by substituting Equations (3.3) and (3.5) into Equation (3.4):

$$P = P_{\text{init}} \left[\frac{V_{pv} + V_{\text{chan}}}{V_{pv} + V_{\text{chan}} + Ax \left(1 + \frac{M_p}{M_r} \right)} \right]^{\gamma} \quad (3.6)$$

The work done on the projectile by this pressure is given by

$$W = \int dW = \int PdV = \int_0^{L_p} PAdx$$

where L_p is the distance traveled by the projectile.

Substituting Equation (3.6) in the last of these expressions yields

$$W = \int_0^{L_p} P_{\text{init}} \left[\frac{V_{pv} + V_{\text{chan}}}{V_{pv} + V_{\text{chan}} + Ax \left(1 + \frac{M_p}{M_r} \right)} \right]^{\gamma} Adx \quad (3.7)$$

After integration, this expression becomes

$$W = \frac{P_{init}(V_{pv} + V_{chan})}{(\gamma-1)\left(1 + \frac{M_p}{M_r}\right)} \left[1 - \left(\frac{V_{pv} + V_{chan}}{V_{pv} + V_{chan} + AL_p\left(1 + \frac{M_p}{M_r}\right)} \right)^{(\gamma-1)} \right] \quad (3.8)$$

The velocity of the projectile, v_p , may be found by equating the work done on the projectile to the kinetic energy of the projectile. This assumption ignores the kinetic energy of the compressed air moving behind the projectile and is an upper-bound calculation of the projectile's velocity. Thus

$$KE = \frac{1}{2}M_p v_p^2 = W$$

Substituting Equation (3.8) and solving for v_p yields

$$v_p = \sqrt{\frac{2P_{init}(V_{pv} + V_{chan})}{M_p(\gamma-1)\left(1 + \frac{M_p}{M_r}\right)} \left[1 - \left(\frac{V_{pv} + V_{chan}}{V_{pv} + V_{chan} + AL_p\left(1 + \frac{M_p}{M_r}\right)} \right)^{(\gamma-1)} \right]} \quad (3.9)$$

Equation (3.9) gives the velocity of the projectile, for a given vessel pressure, after it has travelled a distance L_p .

The reaction mass, M_r , is (theoretically) selected such that the pressure simultaneously vents out of both ends of the barrel. The height of the reaction mass is made equal to the distance it must travel, L_r , before the bottom exits the barrel. The distance the projectile travels before leaving the barrel is L_p ; therefore, the travel distance of the reaction mass, L_r , is given by

$$L_r = \frac{M_p}{M_r} L_p \quad (3.10)$$

But $M_r = AL_r\rho$, where ρ is the density of the reaction mass.

Substituting Equation (3.10) and rearranging, we have

$$M_r = \sqrt{M_p L_p A \rho} \quad (3.11)$$

The projectile velocity, v_p , as a function of vessel pressure, P_{pv} , is predicted using Equations (3.5) and (3.11) in Equation (3.9). The computer code GG4PV, listed in Appendix A, was written to automate the calculation.

3.2 Comparison of Test Results with Mathematical Model

The terms in the three Equations (3.5), (3.11), and (3.9) are easily defined. The area of the barrel, A , is 12.57 ft², and the volume of the pressure vessel, V_{pv} , is 355 ft³. These are determined from the actual physical dimensions of the gun. The density of the water reaction-mass, ρ , is 1.939 slugs/ft³.

The remaining terms, other than the vessel pressure, P_{pv} , are determined by the projectile configuration. As discussed in Section 2.3, the projectile is comprised of three parts: the carriage, the layer of energy-absorbing foam, and an impact plate. The carriage is a hollow right-circular cylinder with a bottom, like a cup. When the trigger mechanism releases the projectile and the gas is released from the vessel into the barrel, it expands in the volume V_{cham} . If a "lid", called a

pressure plate, is placed over the top of the carriage, V_{cham} is decreased, thus increasing P_{init} (see Equation (3.5)). The use of a pressure plate results in a more efficient action of the gun, i.e., a higher projectile velocity for a given vessel pressure. However, at higher vessel pressures (75 psi and above) the thickness of the plate required to support the pressure adds substantially to the mass of the projectile, thereby eliminating its effectiveness. When a pressure plate is used on the projectile, V_{cham} is 33 ft³; otherwise V_{cham} is 63.7 ft³.

The mass of the projectile, M_p , is obtained by adding the weights of the various components. The measured weight of the carriage is 2,125 lb. The weight of the energy-absorbing foam and impact plate are calculated for each test. The total projectile weight depends on the amount and type of foam and the particular impact plate used for a test. The weight of the projectile has varied from 2,125 lb to 3,950 lb.

The length over which the projectile travels, L_p , depends on when the velocity measurement is required. The velocity may be predicted after the leading edge of the projectile has travelled a length that corresponds to the location of time-of-arrival pins located at the bottom of the barrel. These pins are used to measure the projectile velocity and planarity (see Section 2.4). In this case L_p is 128-3/8 in. minus the thickness of the layer of foam and the thickness of the impact plate. The predicted velocity at this location would be a close estimate of the actual impact velocity onto a target, were a target placed near the end

of the barrel. The thickness of the foam has varied between 4 and 12 in. The impact plates have typically been 2-in. thick steel or 6- or 12-in. thick concrete.

Most tests with the gas gun had the target placed at the base of the trench beneath the gun. For this type of placement, impact occurs just after the entire projectile exits the barrel. The velocity may be predicted as the back of the projectile exits the barrel within the GG4PV code. This prediction is used to approximate the impact velocity in these cases by setting L_p to 166 in., the distance the projectile travels before gas is vented at the bottom of the barrel.

Listed in Table 3-1* are the test conditions for all tests with the gas gun that used the 2,125 lb carriage. The first four tests with the gun were preliminary tests, and have been omitted from the table. The vessel pressure in these tests varied from 0 to 300 psi and the projectile velocities varied from 18 to 230 ft/sec. Multiple tests were conducted at several vessel pressure levels to investigate the repeatability of the gun's performance with regard to nuisance factors (ground vibration and noise) associated with testing, projectile velocity, and induced ground shock in a target.

The measured projectile velocities for tests with the current gas gun projectile are shown in Figure 3-2. The circles in this figure represent the predicted velocity for a given

* Tables are collected at the end of the thesis, beginning on page 81.

vessel pressure and projectile configuration. The projectile velocity data from Table 3-1 is indicated by the small squares in the figure. In each case the velocity listed in Table 3-1 and plotted in Figure 3-2 is the velocity measured/predicted as the leading edge of the projectile passes the location of the TOA pins at the end of the barrel. The accuracy of the velocity measurement is ± 4.6 percent (discussed in Section 2.4). The use of carefully placed piezoelectric pins proved to be a reliable method of measuring the projectile velocity, with the exception of a few tests where the recording equipment was faulty or operator error precluded proper recording of the data.

The measured projectile velocity was, on the average, about 94 percent of the predicted value (see Table 3-1). The discrepancy between the predicted and measured values may perhaps be attributed to the friction between the projectile o-rings and the barrel (not accounted for in the mathematical model), and the weight of the water reaction mass at the top of the barrel. Between tests 4 and 5 the projectile was redesigned. The new three-part design (discussed above and in Section 2.3), that includes the carriage, energy-absorbing foam, and impact plate, resulted in an increase in weight from 1,675 lb to approximately 3,120 lb. To obtain the theoretical maximum projectile velocity, a further increase of 1,800 lb in the reaction mass is required. The mass of the water has not been increased since the redesign of the projectile, since that would require increasing the height of the upper barrel section that contains the water by

approximately 28 in. It would be prohibitively expensive to modify the gun for a relatively small gain in projectile velocity.

3.3 Planarity and Pressurization Data

The planarity of the projectile was measured near the end of the barrel using piezoelectric pins (see Section 2.4). The rotation of the projectile was typically between 2 and 5 milliradians. When targets were placed near the end of the barrel, the surfaces of the impact plate and target were mated to effect a more normal impact. Since impact occurs while the carriage of the projectile is still in the barrel, it is expected that the values for planarity measured at the end of the barrel would be similar to values measured at the impact surface. Tests 23-28 included planarity measurements at the impact surface. Of these experiments, the targets for tests 26-28 were located near the end of the barrel. Note in Table 3-1 the similarity of the measured data between tests 26-28 and tests 5-22.

For targets placed at the bottom of the trench beneath the gun, as was the case for most tests, the entire projectile exits the barrel prior to impact. For this testing configuration the impacting surfaces were not mated and the normality of impact degraded. Targets for tests 23-25 were located at the bottom of the trench and included planarity measurements at the impact surface. Note in Table 3-1 the larger angle of impact measured at the impact surface for these tests.

Also listed in Table 3-1 (and presented in Figure 3-3) is the time required for the air compressor to pressurize the gas gun to a given level. The air compressor currently in use can be run only intermittently at pressures greater than 200 psi, to prevent overheating of the compressor. The delay to allow the compressor to cool causes a slight increase in the amount of time required to pressurize the 4-ft gun reservoir to the higher operating pressures.

CHAPTER 4

DETERMINATION OF NUISANCE EFFECTS: PREDICTIONS AND MEASUREMENTS

There was no experience base available for estimating the probable range of nuisance effects associated with the operation of a gas gun as large as the 4-ft-diameter gun. Accordingly, an assessment had to be made of the potential nuisance-level noise and far-field ground motions that would be generated by the operation of the gun. This assessment included the development of upper bound predictive equations for the induced far-field ground motion, and careful monitoring of the induced noise and far-field ground motions during the tests, to insure that these quantities were within acceptable limits. Predictive equations and far-field data gathered during the tests are presented in the following sections.

4.1 Ground Motion

In order to evaluate potential hazards to buildings in the vicinity of the 4-ft gas gun, calculations of far-field ground motions were performed for various projectile impact velocities.

Wallace and Fowler (1973) developed a relationship for peak vertical particle velocity as a function of range from the impacts of spheres dropped onto soil surfaces from a given height. The equations convert the kinetic energy of the sphere's impact into an equivalent-explosion energy yield for TNT explosives. This relationship is

$$v_i = 600 \left(\frac{E}{R^3} \right)^{1/2} \quad (4.1)$$

where

v_i = peak vertical particle velocity for impacts (in./sec)

E = yield energy (lbs of TNT)

R = range from the impact or explosion point (ft)

By determining the explosion energy yield, in pounds of TNT, equivalent to the kinetic energy of the 4-ft gas gun projectile at the time of impact, the far-field motions can be predicted.

Figure 4-1 shows the predicted upper bound impact velocity (as a function of vessel pressure) for a 3,260 lb projectile. In this calculation, adiabatic expansion of the air is assumed, and the friction between the projectile and the barrel walls is ignored. A detailed development of the mathematical model used to predict projectile impact velocity is presented in Section 3.1.

The kinetic energy, KE (lb_f-ft), of the projectile at the time of impact is given by

$$KE = \frac{M_p v_p^2}{2 g_c} \quad (4.2)$$

where

M_p = projectile mass (lb_m)

g_c = gravitational constant (32.174 lb_m-ft/lb_f-sec²)

v_p = projectile impact velocity (ft/sec)

Substituting Equation (4.2) into Equation (4.1), and using a TNT equivalence of 1.41×10^6 lb_f-ft/lb-TNT yields

$$v_i = 600 \sqrt{\frac{M_p v_p^2}{2R^3 g_c (1.41 \times 10^6)}} \quad (4.3)$$

where

v_i = peak vertical particle velocity (in./sec)

R = range from the impact (ft)

The computer code PARTVEL (listed in Appendix B) was written using Equation (4.3) to calculate the peak vertical particle velocity for projectile velocities between 0 and 295 ft/sec for various ranges of interest. The ranges of interest are listed in Table 4-1.

The threshold of human perception of ground vibration is significantly lower than the levels associated with the onset of structural damage. Subjective human response to vibratory ground motion, based on earthquake studies, has shown that motions of 0.004 in./sec amplitude are the absolute lower limit of human perception, and amplitudes of less than 0.04 in./sec are rarely perceived for short-period, explosion-produced motions (Ristvet, 1987). Ristvet lists a level of 0.8 in./sec as "unpleasant," and Siskind et al. (1990) gives 0.7 in./sec as the level of "discomfort," or producing a "startle" effect. Siskind also lists thresholds of 2.2 in./sec and 4.4 in./sec for an onset of interference with activity or proficiency, and a health limit, respectively.

Peak particle velocity is usually taken as the significant parameter in the development of damage criteria for structures. Listed in Table 4-2 is a summary of damage thresholds for residential structures, taken from several references. In general, these criteria state that no structural damage should occur below a peak particle velocity of 2 in./sec.

The results of PARTVEL calculations for the 30-ft range are shown in Figure 4-2. Though this prediction indicates that a building at this range could incur structural damage when testing with projectile velocities greater than 90 ft/sec, no damage to the storage building, located at the 30-ft range, was noticed after testing at even the highest projectile velocities.

Shown in Figure 4-3 are the predicted peak vertical particle velocities as a function of projectile velocity for the remaining ranges of interest. Triaxial motion measurements (vertical, radial and tangential) were made at three far-field ranges on several tests with the gas gun. These ranges were 175 ft, 255 ft, and 765 ft. The peak value of the three measurements, at a given range, for a single gas gun test is shown in Figure 4-3. These data are tabulated in Table 4-3. Note that, at the nearest residential building outside the WES boundary (765 ft), the measured values of ground motion are two orders of magnitude less than that level typically regarded as a hazard to residential structures. At the location of the nearest personnel (the control trailer at 175 ft, as stipulated in the testing safety plan, White (1991a)), the levels are a factor of five lower than

the allowable threshold (2 in./sec). Personnel located at the 175-, 255-, and 325-ft ranges could feel the impact for most projectile velocities.

The calculations presented in Figures 4-2 and 4-3 do not consider the topography of the area, which perhaps accounts for the discrepancy between predicted and measured values. The elevation of the gun is 165.1 ft. An embankment adjacent to the gun rises to an elevation of 180 ft before dropping to 136.6 ft at a nearby creek, some 470 ft away. The elevation rises to 189.2 ft at the nearest residential structure located outside of the WES boundary. These severe changes in grade that exist between the gun and locations of interest apparently aided in attenuating the ground shock.

4.2 Airblast

During a gas gun test, the pressurized air driving the projectile and reaction mass will vent at both the top and bottom of the barrel. This pressure release into the atmosphere will cause an airblast wave in the vicinity of the gas gun. Personnel in the area will sense the airblast wave by hearing it, and if close enough, by feeling it. In order to evaluate potential hazards to personnel (hearing damage) and buildings (window breakage), calculations were performed to predict the airblast/nuisance levels from testing with the gun. Sound pressure level measurements were made during several tests at all five ranges of interest (see Table 4-1). In addition,

measurements of airblast were made at three far-field ranges (175, 255, and 765 ft) on several tests.

Sound pressure level data gathered during tests with the WES 12-in. diameter vertical gas gun were used to predict the airblast level, for the ranges of interest, when testing with the 4-ft gun. The noise level associated with the airblast at these ranges was then determined.

During the performance evaluation tests of the 12-in. gun, sound pressure level measurements were made at the 30- and 110-ft ranges for several different vessel pressures. These data are presented in Figure 4-4. Note from this figure that, with the exception of the two measurements made at the 110-ft range for a vessel pressure of 50 psi, the data are relatively constant for a given range. Therefore, an average value of the sound pressure level (using all data points) was determined for each range. The peak airblast pressure amplitude associated with a given sound pressure level measurement may be determined from the relations (Kinsler et al., 1982)

$$P = \sqrt{2} P_e \quad (4.4)$$

and

$$SPL = 20 \log \left(\frac{P_e}{P_{ref}} \right) \quad (4.5)$$

where

P = peak pressure amplitude

P_e = effective pressure

P_{ref} = reference pressure (20 μ Pa)

SPL = sound pressure level (dB)

Solving for P_e in Equation (4.5), substituting into Equation (4.4), and including a units conversion factor yields the peak pressure amplitude, P (in psi):

$$P = \frac{\sqrt{2} P_{ref} 10^{\left(\frac{SPL}{20}\right)}}{6895} \quad (4.6)$$

Substituting the average value of the SPL data for the 12-in gun into Equation (4.6) yields the peak pressure amplitude at the two ranges.

In order to use the 12-in. gun data for predicting the peak pressure amplitude at various ranges of interest for the 4-ft gun, each range was normalized by dividing by the gun diameter (11.5 in.). The results of Equation (4.6) for the 12-in. gun data are tabulated as a function of the normalized range in Table 4-4 and presented graphically in Figure 4-5. Listed in Table 4-5 are the peak pressure amplitude and SPL predictions (scaled from the linear fit to the 12-in. gun data presented in Figure 4-5) at the ranges of interest for the 4-ft gun. The ranges are also expressed in normalized values (range/gun diameter (4 ft)).

The sound pressure level corresponding to the scaled values of pressure for the 4-ft gun may be determined by solving for P_e in Equation (4.4) and substituting into Equation (4.5):

$$SPL = 20 \log \left(\frac{P(6905)}{\sqrt{2} P_{ref}} \right) \quad (4.7)$$

where a units conversion factor has been included and P has units of psi and SPL has units of dB. By substituting the scaled peak pressure amplitudes for the 4-ft gun into Equation (4.7), the predicted SPL's can be tabulated (Table 4-5) and presented graphically (Figure 4-6). Also included in Figure 4-6 are the sound pressure level data, for the various ranges of interest, as a function of normalized range.

OSHA regulations (Federal Register, May 29, 1971) state that exposure to impulsive or impact noise should not exceed 140 dB peak sound pressure level. This threshold is included in Figure 4-6 for comparison to predicted and measured noise levels at the various ranges of interest for testing with the 4-ft gun. For the 4-ft gun, the 30-ft range is the only one of concern that lies above the 140 dB limit. As mentioned previously, the closest range at which personnel were located during testing was 175 ft. As with the ground shock calculations, this analysis does not take into account the natural terrain (hills and trees) effects that will tend to mitigate the airblast wave and thus reduce noise levels.

Presented in Figure 4-7 are the sound pressure level data, for the various ranges of interest, as a function of vessel pressure. Note from this figure and Figure 4-6 that, although the measured levels are relatively high, they are well below

limits requiring safety precautions (i.e., ear protection).

Personnel located approximately 2 miles from the gun, aware that a test was imminent, heard the gun during tests at the very highest levels, i.e., 250 psi and greater.

The most likely component of an ordinary structure to sustain damage from a blast wave is a window. Therefore most damage criteria are based on window pane breakage. Not all window panes will break at the same blast pressure level, so the study of this phenomenon is statistically based. Some large plate glass windows may break at a pressure level of 0.03 psi. At 0.1 psi some windows break and at 1.0 psi most windows break. At a pressure level of 3.0 psi conventional structures are severely damaged (Blaster's Handbook, 1980). The 0.03 psi threshold for window pane damage is included in Figure 4-5. From this figure, or from Table 4-5, it was determined that windows in buildings located at the 30-, 175-, and 255-ft ranges might sustain damage. The probability of window damage cannot be determined from this analysis. However, it is interesting to note that the close-in data point for the 12-in. gun is located above the 0.03 psi threshold and windows at that range were not damaged during performance testing with the 12-in. gun.

The windows of the building at the 30-ft range were covered with a sheet of plywood to prevent possible breakage during a test with the 4-ft gun. No windows were damaged, at any location, during any test with the 4-ft gas gun.

Additional analyses to predict the airblast/nuisance levels associated with testing with the 4-ft gas gun are reported in White (1991d). An equivalent spherical TNT charge was determined that would produce the pressure level measured at a given range for the 12-in. gun. The peak pressure was then determined, for the "equivalent" charge weight, at ranges of interest for the 4-ft gas gun using an empirically based formula. The results of this analysis confirmed the prediction presented above, namely that damage was possible at only the 30-ft range.

CHAPTER 5

TESTING WITH THE WES 4-FT-DIAMETER VERTICAL GAS GUN

5.1 Testing Philosophy and Objectives

A safety-oriented and conservative approach was taken throughout the entire development effort with the gun. Initial hydrostatic and vacuum tests (described below) were conducted to investigate the structural integrity of the gun prior to placing it in service. A Safety Plan was developed (White 1991a) to provide a systematic method of conducting tests in a safe manner. A peer-review panel was briefed on the operating principle of the gun, the safety plan, and the test plan for the gun prior to pressurized testing. The panel provided useful suggestions that were incorporated into the development effort, including the safety calculations to predict the potential for damage to buildings and the nuisance effects (see Chapter 4).

Early in the testing phase of the gun's development, it was realized that each test presented an opportunity to meet additional objectives (White, 1991b; 1992; and "Test Plan for Tests 1-28 ...", 1991-1993). These objectives evolved naturally from determining the performance characteristics of the gun to analyzing the ground shock generated in a target, or in other words, from tests "on" the gun to tests "with" the gun. The primary objectives for initial tests with the gun were to determine:

- the performance of various gun components (barrel, projectile, trigger mechanism, instrumentation, etc.) and their interaction with one another;

- the projectile velocity as a function of vessel pressure;
- the nuisance effects associated with testing.

As more tests were conducted and these objectives were being met, the primary objectives were changed to focus on the results obtained from instrumented targets placed beneath the gun. These objectives included:

- determination of the stress and motion fields within a dry sand target;

- comparison of data from various types of stress instruments;

- comparison of data from various types of ground-motion instruments;

- testing new stress and ground-motion instruments;

- determination of dynamic material properties for a dry sand target.

The results from the initial tests on targets identified deficiencies in the construction techniques for sand targets. Objectives were then expanded to include developing target construction and testing techniques such that identical tests could be conducted with the gun, i.e., identical stress and ground-motion fields generated in successive tests. This is one of the fundamental objectives for the gun's intended use: to

provide a standard for the dynamic calibration/validation of weapon's effects instrumentation.

Twenty-eight tests have been conducted with the 4-ft-diameter gas gun in addition to hydrostatic and vacuum tests. Over 630 diagnostic channels and 170 target channels have been recorded on the tests. Various aspects of testing with the 4-ft gun are described in the sections below. The topics include:

- safety tests and considerations;
- construction techniques for preparing sand targets;
- typical target and diagnostic instrumentation;
- testing procedures.

5.2 Safety Tests and Considerations

5.2.1 Hydrostatic Testing

Hydrostatic testing was performed to ensure the structural integrity of the pressure vessel and the projectile o-ring seals before placing the 4-ft gas gun in service. The initial phase of hydrostatic testing was conducted immediately following the construction of the projectile carriage. The second phase was conducted to increase the operating level to the maximum design level of 300 psi.

Figure 5-1 illustrates the test set-up for both the initial hydrostatic tests and vacuum tests. The gun was oriented horizontally for the initial tests. The carriage was first loaded into the barrel. The o-ring material used for sealing around the carriage for the first hydrostatic test was a 70-

durometer nitrile compound with a 3/4-in. material diameter. For the hydrostatic tests, the vessel was filled with water. Compressed air was then applied to the water-filled tank. The only air in the system was that in the hose connecting the compressor to the gun. Testing revealed that the 3/4-in. diameter o-ring was inadequate for sealing around the carriage. The failure was a result of several lacerations in the o-ring, created while loading the carriage. As the o-ring moved along the orifices in the barrel, it extruded into the orifices, and was nicked when it passed beyond the top of the orifices.

The second hydrostatic test in the initial series used 5/8-in. diameter, 70-durometer nitrile o-rings in place of the 3/4-in. o-rings. The smaller thickness o-ring extruded less into the orifices, and prevented damage to the o-ring. The vessel was then pressurized to 330 psi. The 5/8-in. o-ring adequately sealed around the carriage. In addition, the welds of the pressure vessel were determined to be sound, verifying the structural integrity of the vessel for conducting tests using pressurized air up to 220 psi. A third hydrostatic test, identical to the second test, verified these results.

A second series of hydrostatic tests was performed to increase the operating level of the gun up to its maximum design limit of 300 psi. These tests were conducted after the gun had been placed in use and tested with air up to a pressure of 200 psi. The set-up for the second series of hydrostatic tests is shown in Figure 5-2. The gun was in its normal testing

orientation (vertical) for these tests. As with the previous successful hydrostatic tests, 5/8-in. o-rings were used to seal around the carriage.

After filling the vessel with water, nitrogen was used to increase pressure within the vessel. The pressure was raised to 450 psi using a pressure regulator to control the flow of nitrogen. A minimal loss of pressure within the vessel was noted after several minutes at the 450 psi level. The test was repeated to verify the results.

Under existing Army Corps of Engineers safety regulations (EM 385-1-1, 1987), tests can be conducted with the gas gun using pressurized air at the maximum design limit (300 psi) of the gun, i.e., two-thirds of the hydrostatic test pressure.

5.2.2 Vacuum Testing

Testing with smaller bore gas guns typically involves evacuating the air from the portion of the barrel between the projectile and the target. This is done for several reasons: (a) to initiate movement of the projectile, (b) to minimize or eliminate the air precursor in front of the projectile, and (c) to increase the projectile velocity by increasing the pressure differential on either side of the projectile. When conceptualizing the large diameter gas gun, it was envisioned that these three uses for a vacuum would be required. Both the 12-in. and 4-ft diameter guns were designed with this in mind; for example, much care was taken to seal along various sections

of the gun barrel, and systems were developed to evacuate the barrel.

Tests with the 12-in. gun used a 30-lb aluminum projectile. For this gun, a vacuum force was required to overcome the friction between the projectile o-rings and the barrel. Once the projectile was released by the trigger mechanism, the vacuum and gravitational forces initiated downward motion of the projectile, allowing the pressurized gas to flow into the barrel behind the projectile.

Immediately following the initial hydrostatic tests on the 4-ft gun, vacuum testing was performed by evacuating the barrel of the gas gun beneath the carriage. A schematic of the test set-up is shown in Figure 5-1. The purpose of these tests was to evaluate:

- the practicality of pulling a vacuum in the lower portion of the barrel;
- the performance of the o-ring seals on the barrel and around the projectile carriage;
- the suitability of candidate diaphragm materials used for sealing the end of the barrel;
- the ability of the trigger mechanism to support the vacuum load on the projectile.

The first vacuum test used 3/4-in. diameter o-rings, made from 70-durometer nitrile material, for sealing around the projectile. A diaphragm of 0.040-in.-thick fiberglass reinforced polyester sealed the bottom end of the barrel. After running the

vacuum pump approximately 135 seconds, the diaphragm failed at a vacuum level of roughly 460 mm of mercury (Hg), or 40 percent vacuum.

As of result of the failure of the fiberglass reinforced polyester, a second test was conducted using a 1/2-in. aluminum plate over the end of the barrel. This test used projectile o-rings made from 5/8-in. diameter, 70-durometer nitrile material. During this test, the vacuum pump was run intermittently while observing both the vacuum gage and the deflection of the aluminum plate. The effectiveness of the various seals was assessed by observing the loss of vacuum while the pump was off. Approximately 25 mm Hg (3 percent vacuum) was lost during a two-minute span. The rate of loss was fairly constant over the entire range of vacuum. The maximum deflection at the center of the aluminum plate was measured as 1/2 in.

In order to determine the time required to pull a "full" vacuum, a third test was conducted during which the pump ran continuously, except for brief stops for taking vacuum level readings. The maximum attainable vacuum was approximately 740 mm Hg, which was achieved in 15 minutes. After running the pump for 40 minutes, no change in the vacuum level was evident. The pump is capable of pulling down to a vacuum pressure of 10 microns, but there are sufficient leaks in the system that prohibit pulling a vacuum greater than approximately 740 mm Hg.

Also observed on the vacuum test was movement of the carriage. The manner in which the quick-release trigger

mechanism is constructed (Figure 2-5) allows for a slight backward rocking motion of the three supporting latches when they are in the cocked position and not carrying a load. The pretest placement of the carriage was such that the latches of the trigger mechanism were not loaded. After the test, the latches were tight against the retaining collar and could not be rocked backward, indicating that the trigger mechanism was indeed loaded by the vacuum.

The vacuum tests described above were conducted again after the gun was relocated to the testing site. The second series of tests confirmed the results of the initial vacuum tests. For these tests, the trigger mechanism was subjected not only to loading from the vacuum force (26,000 lb), but also the gravitational force on the carriage (2,125 lb).

It is not clear that testing with a vacuum is feasible with the 4-ft gas gun. A vacuum is not required to fire the gun, i.e., the projectile will begin moving within the barrel under its own weight, once released by the trigger mechanism. To remove more than 40 percent of the air from the barrel requires a thick (1/2 in. or greater) diaphragm at the base of the barrel. This plate could affect the planarity of impact due to its presence or its deflection under the vacuum loading. Also, another gas such as helium, which has a lower density and higher sonic velocity than air, could be flooded into the barrel to displace the air and perhaps minimize any precursor effect.

Should a vacuum be required on a test with the gun, the rate of loss of vacuum (12.5 mm Hg/min) was determined to be acceptable. It is not a requirement to hold a vacuum for an extended period of time. Because of the displacement capability of the vacuum pump, it is possible to simply cycle the pump on and off just prior to firing the gun to obtain the desired vacuum level.

The vacuum tests were considered successful. The critical components of the trigger mechanism were tested and found to perform satisfactorily. In addition, the sealing capability of the o-rings within the gun was found to be adequate. For detailed results of the initial hydrostatic and vacuum tests results see White, (1990); or White et al., (1991). For more information on tests with the 12-in.-diameter gas gun see Joachim, (1985); Ohrt and Welch, (1989); and White et al., (1991).

5.2.3 Safety Features and Safety Plan

Safety issues have received the highest priority in the development of the 4-ft-diameter gas gun. Some of the safety features included in the design and siting of the gas gun are:

- a. Pressure Vessel. The pressure vessel is designed for a maximum working pressure of 300 psi. This design includes a minimum factor of safety of four in all components (Ohrt, 1988). A manway is incorporated to provide entry to the vessel for

periodic inspection. A relief valve is attached to the vessel to prevent overpressurizing.

b. Trigger Mechanism. A "potential energy" well has been incorporated into the design of the trigger mechanism (Figure 2-5) used to fire the gas gun. The mating surface of the latch and the retaining collar of the trigger mechanism is designed such that, when the retaining collar is lifted vertically, the latch must rotate into its housing. This rotation slightly lifts the projectile prior to firing. Requiring the application of a significant force in this manner in order to fire the gun greatly reduces the chance of a misfire.

c. Operation Controls. The controls for operation of the gas gun (Figure 5-3) are located away from the immediate vicinity of the gun. These controls operate the "fill" system used in conducting a gas gun test. The fill system, illustrated schematically in Figure 5-4, is comprised of three components: the pressure system, the vacuum system, and the firing system. The pressure and vacuum systems incorporate valves to bleed off the pressure in the vessel and the vacuum in the barrel, should a test be aborted. Figure 5-5 is a photograph showing most of the components of the pressure and vacuum systems, which are located in the shed adjacent to the gun (seen in Figure 2-4). Also included in the control panel is a master switch that prevents firing the gun until all fill system components are in their proper state, in which all valves are closed and the air compressor and vacuum pump are shut off. The Standard Operating

Procedure (White, 1991c) for conducting a test is posted on the control panel in plain view of the operator.

d. Location of Gas Gun. The gas gun is situated over a trench 7 ft deep and 28 ft long. Steps located at one end of the trench and a ladder at the other provide access into and out of the trench. The Engineering and Construction Services Division at WES was consulted to ensure that the shoring in the trench, handrails along the steps, and railing along the side of the trench comply with the US Army Corps of Engineers Safety and Health Requirements Manual, EM 385-1-1.

e. Test Plan. A cautious and conservatively safe plan was followed for testing of the gun. The plan called for initial testing with atmospheric vessel pressure, followed by tests with gradual increases in vessel pressure. The performance of various gun components (barrel, projectile, instrumentation, etc.) were carefully evaluated after each test.

A Safety Plan was developed for the 4-ft-diameter gas gun (White, 1991a). The plan prescribes the safety policies and procedures for testing with the gas gun and applies to all personnel participating on a test. The requirements listed below were mandatory for all gas gun tests:

- The Standard Operating Procedure was followed when conducting a test.

- All components of the gun were inspected on a regular basis.

- When the projectile was in the loaded position between tests, the battery power to the four-way directional valve (used for firing the gun) was disconnected. Two safety chains were used to secure the projectile's position within the barrel between tests.

- No personnel were allowed in close proximity (175 ft) to the gun once pressurization of the vessel began.

- A manned road block was placed at the entrance of the service road to the test site prior to pressurizing the vessel.

- The WES Public Affairs Office and Security Office were notified that a test was imminent.

- A warning horn was sounded just prior to firing the gun.

- A standard procedure for reentering the test site was followed. As a minimum, this procedure included a visual inspection of the concrete pads, the platform supporting the gun, and the trench shoring.

- A pump was maintained on-site to remove any water in the trench.

5.3 Target Construction and Typical Instrumentation Layout

Twenty-six pressurized tests have been conducted with the 4-ft gas gun. Fifteen of these tests included a sand testbed as the target. These tests occurred during the period April 1991 through August 1993. Nine of the tests used a brown masonry sand, three tests used Socorro Plaster sand, and three tests used a fine Ottawa sand as the target material. To use the gas gun to

perform validation experiments for developmental instrumentation, it is necessary to produce known and repeatable stress and motion fields in the target. The predictability and repeatability with which the gas gun can deliver the projectile to a target is evident in Figure 3-2. However, to produce the same shock field in successive tests also requires the target to be identical from test to test. The target material parameters used to determine the "quality" of the target are the density and moisture content. If the material is packed at its maximum density it is less likely to change density as other layers (or lifts) in the target are prepared or when the target is moved from the preparation area to its final location beneath the gun. It was found that the best method for obtaining the maximum density was to use a poorly-graded sand for the target material. This type sand, with a majority of the grains identical in size, produces less variations in the density because there are fewer smaller grains that may be packed between larger grains. The maximum density at which the material can be placed also depends on the moisture content. It was found that the sand could be placed with a more uniform density if it was virtually dry, i.e., the moisture content was below 1 percent.

The disposable target container was a 54-in. diameter by 30-in. high corrugated 12-gauge steel pipe with a welded 12-gauge steel bottom. The target for each test was constructed by placing four lifts (typically 6-8 in.) of sand in the steel container. After a lift of sand was placed into the container

(see Figure 5-6), it was smoothed by hand to obtain a generally level surface. A thin aluminum plate was placed over the layer of sand and a vibratory compactor was used to pack the sand to a maximum density. A photograph of personnel operating the compactor is shown in Figure 5-7. The wet density and moisture content were measured at two locations in each lift of a target using a nuclear densitometer (see Figure 5-8). The accuracy of the nuclear densitometer for measuring moisture content is questionable, however, because the source and receiver are both in the base of the gage, and experience has shown that the moisture content is measured only to a depth of approximately 2 in. (Phillips, 1991). For that reason, the moisture content was also measured for several tests by weighing samples of the sand before and after drying in a microwave oven, pictured in Figure 5-9. The references by Gilbert (1988, 1990) contain more information on the use of a microwave oven for determining the moisture content of soils. Density and moisture content profiles through the depth of the target for several tests are presented by White and Byrne (1994). A representative profile is presented in Figure 5-10. The values presented in the figure represent the average of two measurements at each depth. For all the targets tested with the gun, the values for the average density of the entire target were between 100 and 112 lb/ft³, and values for moisture contents were between 0.1 and 5 percent. A target was considered to have a uniform density if the measured values were within 1 lb/ft³ of the average value of the entire target. A

target was considered to have a uniform moisture content if the measured values were within 0.5 percent of the average value of the target.

The total depth of each target was 24 in. Two depths in a target were instrumented on each test. These two depths (6 in. and 12 in.) typically included a variety of stress and velocity instruments. The stress gages included the WES-designed Column-Based Stress (CBS) Gage (Joachim and Welch, 1985; and Rocco et al., 1994), a modified version of the CBS gage, called the New CBS (NCBS) Gage (Welch, White, and King, 1992; and Rocco et al., 1994), and the Kulite Corporation High-Range SE (HRSE) Gage. The HRSE gage is a high-range version of the SE soil stress gage described in Ingram (1968).

The ground-motion gages placed in the targets included the WES Log and Wedge Canisters (Welch, 1986), the WES Micro-Accelerometer Canister (Peekna, 1972), and the WES High-Fidelity Particle Velocity (HiFi) Gage (Welch et al., 1994). The Log and Wedge Canisters contained Endevco Corporation accelerometers mounted on miniature shock-isolated systems described in Welch and White (1987), and White (1989a). Ground-motion sensors included on the tests by other organizations included the Electromagnetic Velocity Gage from Sunburst Recovery, Inc. (Young et al., 1992), and the Fiber Optic Accelerometer from Geo-Centers, Inc. (Landry, 1994).

A schematic of a typical gage layout is presented in Figure 5-11. Gages were placed in the correct lift as the target

was being built (see Figure 5-12). The instruments located at the 12-in. depth were typically placed at a radius of 6 in. from the vertical centerline of the target specimen, and the instruments at the 6-in. depth were placed at a radius of 12 in. For some tests a gage was placed in the center of the target at one of the two levels. Several tests also included piezoelectric crystals, spaced every 3 in. through the depth of the target, to mark the time-of-arrival (TOA) of the loading wave as it propagated through the target. Shown in the photograph of Figure 5-13 are instruments located at the 12-in. depth in a target. The large instrument in the center is a single canister that contains both the NCBS and HiFi gages. Spaced at a 6-in. radius from the central gage is a HiFi gage, a TOA crystal, and a HRSE gage (starting from the left and looking clockwise). A short length of cable was routed from each gage, through the target, and terminated just outside of the target container. The instrument cables can be seen in the photograph of a completed target, shown in Figure 5-14.

The time required to build a target, once all materials were on hand (gages, sand, vibrator, microwave oven, tools, etc.), was approximately one and one-half days per test. An efficient method for testing with the gun was to prepare several targets at a time, since most objectives for subsequent tests were not contingent on results from previous tests. Typically, two or three targets were prepared (in a sheltered area) on successive

days. The targets were moved to the facility, as required for testing, using a fork lift.

In addition to the target instrumentation, several types of diagnostic measurements were included on each test. Two pressure gages were located in the reservoir of the gas gun. One served as a direct readout gage used to monitor system pressure, prior to firing, at the control panel for the gun. The second gage was used to monitor the pressure drop in the vessel during a test. An accelerometer was mounted on the base of the gun to monitor acceleration levels in the vertical direction on several tests. Six piezoelectric pins at the bottom of the barrel of the gun were used to measure the projectile velocity and planarity as the forward face exited the barrel. Several tests also included piezoelectric pins and copper foil switches at the surface of the target to monitor projectile impact velocity and planarity (described in Sections 2.4 and 3.3). Triaxial seismic stations and microbarograph gages were fielded at three different ranges on several tests to monitor far-field ground motions and airblast. Sound pressure level measurements were also made at several ranges on many tests (described in Chapter 4 and White, 1993). A video camera was used to photograph each test.

5.4 Testing Procedure

The projectile for each test was assembled prior to loading it into the barrel of the gas gun. The configuration of the projectile varied depending on the vessel pressure planned for

the test. As test levels increased (higher vessel pressures and projectile velocities), thicker pieces of foam were required at the base of the projectile to absorb the impact energy, and thus protect the carriage from damage (see Section 2.3). The mass of the projectile varied slightly as a result of changing the foam thickness. A 2-in. thick steel impact plate was used for each test with a sand target. The mass of the projectile for most of these tests was 3,260 lb. The vessel pressure for the tests varied from 50 to 200 psi and the projectile velocity (as the leading edge exited the barrel) varied from 92 to 193 ft/sec. The test level, projectile configuration, and projectile velocity for each test are listed in Table 3-1. The projectile was raised into its cocked position via a chain hoist attached to a tripod at the top of the barrel. Two chains were used to lift the projectile, and two were used as safety chains during the loading process. The two safety chains remained in place after the projectile was locked into position with the quick-release trigger mechanism.

After the projectile was loaded into the gun and secured with safety chains, sand was placed over the earthen portion of the trench bottom located directly beneath the barrel of the gun. Several (4-in. by 6-in.) timbers were placed in the sand base to support the target. The target was moved into position beneath the barrel of the gun via a trolley that ran along channels cast into the concrete walls on either side of the trench. The target was centered beneath the gun using a plumb bob suspended from

temporary crosshairs at the bottom of the barrel. Final leveling of the target was achieved using a carpenter level to guide placement of shims between the steel bottom of the target and the timbers. The surface of the target was typically located about 48 in. below the end of the barrel, allowing the entire projectile to exit the barrel prior to impact. An advantage of supporting the target with timbers is that it essentially provided a "free" surface at its base (see Figure 5-15). The shock wave reflecting off this free surface is identifiable in the stress waveforms, and thus may be used to investigate the relief wave speed of the target material (see Section 6.3.2).

After the target was positioned beneath the gun, instrument cables were spliced to cables running to the Control Trailer. After all electrical checkouts were completed, the safety chains on the projectile were removed. A 0.040-in.-thick fiberglass diaphragm and plastic liner, used for containing the water reaction mass, were placed above the quick-release trigger mechanism in the upper portion of the barrel. The depth of the water reaction mass for all tests was about 53 in., which corresponds to a mass of 3,460 lb. After placing the reaction mass, the firing system for the trigger mechanism was enabled by supplying pressurized gas to the system and by connecting battery power to a solenoid valve used to control the flow of gas. Prior to clearing the test site, water was supplied to the in-line aftercooler in the pressure system and the video camera(s) were started.

Instrument recording and remote operation of the gun were performed at the Control Trailer, located approximately 175 ft from the gun. The trailer can be seen in the background of Figure 2-3. A photograph of the recording equipment is shown in Figure 5-16. The control panel used for operating the pressure system, the vacuum system, and the firing system for the gun is shown in Figure 5-3. None of the tests reported here used a vacuum in the lower section of the barrel. The pressure vessel was filled by a high-pressure, high-volume air compressor. After the desired testing level was reached, the air compressor was stopped. The time required to pressurize the gun for these tests varied between 13 and 54 minutes. A master switch was then used to ensure all components of the pressure system were in their proper state, i.e., all valves closed and the air compressor shut off. The master switch also provided power to the firing system. After sounding a warning siren and a final check with instrumentation personnel, the gun was fired by energizing the 4-way solenoid valve in the firing system. The action of the valve allowed gas pressure to activate the quick-release trigger mechanism, which released the projectile. On average, about 450 msec were required for the trigger mechanism to release the projectile. The additional time required for the projectile to travel the length of the barrel was between 100 and 400 msec, depending on the test level and length of the projectile.

Approximately two to three days were required for conducting a single test.

CHAPTER 6

EXPERIMENT DATA AND ANALYSIS

6.1 Active Measurement Data

As mentioned in Chapter 5, over 170 target channels have been included on tests with the 4-ft gas gun. The inclusion of each waveform here is beyond the scope of the thesis; however, the reader may refer to White and Byrne (1994) for a complete set of the data waveforms (stress, integrated impulse, acceleration, integrated velocity, and doubly-integrated displacement) for Test 6 through Test 22. Results from the tests were very good, with waveforms containing identifiable features of the test geometry, e.g., a relief wave reflected from the free surface at the base of the target. Peak stresses varied from 1,000 to over 15,000 psi in the different tests in sand, depending on the impact velocity and target material. The average particle velocity varied from 60 to 110 ft/sec.

Data presented here are limited to a series of three identical tests (Tests 23, 24, and 25). The primary objective of these tests was to determine to what degree the stress and velocity fields could be reproduced, in a granular material (Ottawa sand), using the 4-ft gas gun.

Presented in Figure 6-1 are stress waveforms from a single test containing various types of stress transducers. These instruments were positioned at two depths in the target similar to the gage layout presented in Figure 5-11. Some of the apparent disagreement seen in the figure is due to the inertial

response of a gage. A gage in the sand target has an inertial resistance to acceleration, which causes the stagnation of sand against the gage face. Until the gage achieves equilibrium with the free-field velocity, the gage is exposed to an inertial (or stagnation) stress significantly higher than the free-field stress. Also, the impedance mismatch between the gage and the surrounding media tends to cause the gage to over-register the free-field stress. Considering these factors when comparing the output of the different gage types, the data of Figure 6-1 are considered quite good. More information on the response of the type of stress gages used in these experiments may be found in Rocco et al., (1994); Veyera and Rinehart, (1986); and Rinehart, (1993).

Presented in Figure 6-2 are velocity wave forms from a single test. Noted in the figure is the response of an internal shock mount used in one of the accelerometer canisters. This low frequency ringing is typical for this type mount. The response of the other three accelerometers are considered good.

Presented in Figure 6-3 are stress measurements from the three identical tests (i.e., similar impact velocity and target material) as monitored by a single type of stress gage. The repeatability of the environment from test to test may be seen more readily by comparing a single type of gage, because the inertial and impedance mismatch effects would be identical for each test. The consistency of the data in the figure is very good. Figure 6-4 contains velocity waveforms from two identical

tests with the gun; Test 25 was omitted because of gage failures. The consistency of the measured data from these tests shows the repeatability of the ground shock generated by the gun from test to test.

6.2 Projectile-Soil Interaction Model

While the data from Tests 23, 24, and 25 indicate that the same stress and velocity environments can be reproduced well using the 4-ft gas gun, they do not quantify the stress and velocity levels in the target. A combination of computational and experimental efforts is required to develop the standardized target desired for gage validation. As a first step in calculating the stress and motion fields in a target tested with the gun, a projectile-soil interaction (PSI) model was utilized. This model is similar to that reported by Anderson et al., (1987); Renick et al., (1987); and Rinehart, (1987). The development of the model and comparisons with test data follow in the sections below.

6.2.1 Model Development

The following assumptions/conditions are made in the development of the PSI model:

- planar one-dimensional flow in the target; relief waves from the edges of the target are ignored and only uniaxial strain is considered. In an experiment this assumption requires the placement of gages away from the edges of the target.

- known boundary conditions; the momentum of the projectile (i.e., mass and velocity) as it impacts the target is required.

- constant loading wave velocity in the target material; the velocity at which the shock wave travels through the target is constant, regardless of the stress level at a particular depth.

- zero strain recovery in the target material; this is commonly referred to as a "locking" or "snowplow" soil model, and it implies that the material is compressed to its maximum strain state by the shock wave with insignificant strain recovery upon unloading. This assumption may also be thought of as the material having an infinite relief wave velocity; hence, all particles behind the shock front, and the projectile, are moving with the same velocity.

The impact of the projectile onto a target, shown schematically in Figure 5-15, is represented in a more generic fashion in Figure 6-5, both before and after impact. The projectile is modeled as a plate with thickness H_p , density ρ_p , area A_p , and impact velocity v_{p1} . The target has density ρ_t , area A_t , loading wave velocity C_t , and thickness H_t . The position of a gage in the target relative to the impact surface is denoted z_0 , and the position of the shock wave relative to surface is z . The particle velocity of the soil behind the shock front is U_t .

Conservation of momentum for an inelastic collision may be expressed as

$$M_{p1}v_{p1} + M_{t1}v_{t1} = (M_{p2} + M_{t2})U_t$$

where

M_{p1} = projectile mass before impact

v_{p1} = projectile velocity at impact

M_{t1} = entire target mass before impact

v_{t1} = target velocity at impact

M_{p2} = projectile mass after impact

M_{t2} = mass of target, i.e., that portion of the target through which the loading wave has traversed

U_t = velocity of the soil (and projectile) behind the shock front.

This equation may be rearranged to solve for the particle velocity of the soil:

$$U_t = \frac{M_{p1}v_{p1} + M_{t1}v_{t1}}{M_{p2} + M_{t2}} \quad (6.1)$$

The mass of the projectile before (and after) impact may be rewritten as $M_{p1} = M_{p2} = \rho_p A_p H_p$ using the terms defined in Figure 6-5. The mass of the target prior to impact is $M_{t1} = \rho_t A_t H_t$. The mass of the target after impact is $M_{t2} = \rho_t A_t z$. However, $z = C_t t$, where t is time; therefore, $M_{t2} = \rho_t A_t C_t t$. The projectile impact velocity, v_{p1} , is known for a given test and the initial target velocity, v_{t1} , is zero since the target is at rest prior to impact. Substituting these expressions into Equation 6.1 yields

$$U_t = \frac{(\rho_p A_p H_p) (v_{p1}) + (\rho_t A_t H_t) (0)}{\rho_p A_p H_p + \rho_t A_t C_t t}$$

This expression may be simplified since $A_p = A_t$; hence, the particle velocity of the soil as a function of time (or depth since $z = C_t t$) in the target is

$$U_t = \frac{\rho_p H_p v_{p1}}{\rho_p H_p + \rho_t C_t t} \quad (6.2)$$

Because uniaxial strain conditions have been assumed, the stress in the target, σ_t , may be determined from the familiar expression

$$\sigma_t = \rho_t C_t U_t$$

Substituting Equation (6.2) into this expression gives

$$\sigma_t = \rho_t C_t \left(\frac{\rho_p H_p v_{p1}}{\rho_p H_p + \rho_t C_t t} \right) \quad (6.3)$$

An interesting feature of this model is the state of stress behind the shock front. Recall that the locking soil model requires that all of the particles behind the shock front move at the same velocity, U_t . Therefore the projectile and the material through which the shock wave has traversed are moving together as a rigid body. Because the soil is acting as a rigid body, the stress through the depth of the "body" is constant. As time passes and the shock wave traverses deeper into the target, the

mass of the "body" increases and its velocity decreases, thus decreasing the stress.

The computer code 1DWAVE, listed in Appendix C, was written to automate calculations using Equations (6.2) and (6.3). Parameters input to the code are the density (ρ_p), thickness (H_p), and impact velocity (v_{pi}) of the projectile, and the density (ρ_t) and loading wave velocity (C_t) of the target. The location of a gage (z_g) in the target and the duration of the calculation are also input to the code. Program 1DWAVE treats the target as semi-infinite, i.e., there is no provision to account for the relief wave reflecting off the free surface at the bottom of the target container. This phenomenon is discussed in more detail in Section 6.3.2 below.

6.2.2 Comparison of Test Data with PSI Model

Representative data from Tests 23 through 25 (presented in Figures 6-3 and 6-4) are used for comparison with the PSI model. Recall that the projectile used with the 4-ft gas gun is composed of three parts: the carriage, energy absorbing foam, and impact plate. Illustrated in Figure 6-6 are two methods used to model the projectile in PSI model calculations. The first case, and lower bound, was to consider the impact plate only. For Tests 23 through 25 the impact plate was a 2-in. thick steel plate. An upper bound case conserved the total mass of the projectile. This was done by determining the thickness (6.28 in.) of a steel plate weighing 3,265 lb. Parameters for input to 1DWAVE were:

$$\rho_p = 496 \text{ lb}_m/\text{ft}^3 \text{ (steel)}$$

$$H_p = 2 \text{ in. (lower bound), } 6.28 \text{ in. (upper bound)}$$

$$v_{p1} = 155 \text{ ft/sec}$$

$$\rho_t = 110 \text{ lb}_m/\text{ft}^3$$

$$C_t = 2,670 \text{ ft/sec}$$

$$z_g = 6 \text{ in. (for stress comparison), } 12 \text{ in. (for velocity comparison)}$$

The lower and upper bound cases for the stress and velocity calculated using 1DWAVE are compared with test data in Figures 6-7 and 6-8. It is interesting to note that the measured stress seems to follow closely the upper bound calculation and the measured velocity seems more like the lower bound calculation. The reason for this discrepancy is not clear. Reasons for the difference in the measured and calculated peak stress (seen in Figure 6-7) are discussed briefly in Section 6.1 above. The PSI model provides bounds that may be used to predict the expected stress and velocity on a test with the gas gun.

6.3 Time-of-Arrival Data and the Determination of Dynamic Material Properties

Some very fundamental properties of a material may be determined from time-of-arrival (TOA) measurements made in a target tested with the 4-ft gas gun. By knowing the location of instruments in a target before and during the test, the propagation velocity of a loading wave and a relief wave traveling through the material may be derived. The sections

below describe how the TOA data and gage records are used to determine these material properties. Data presented here are limited to a series of identical tests in Ottawa sand (Tests 23, 24, and 25).

6.3.1 Propagation Velocity of Loading Wave

As each target was constructed, instruments were carefully located such that their positions with respect to the impact surface and each other were known. The TOA of the shock wave at each depth was determined from the data waveform at that location. In addition to stress and velocity instruments in the target, several tests also included piezoelectric crystals at various depths in the target for the purpose of marking the TOA of the loading shock wave. The TOA at each instrument location was plotted versus its depth in the target. The inverse slope of the best linear fit through the data represents the propagation velocity of the loading wave. In this analysis perfectly normal impact is assumed; i.e., the depth to the gage is a straight line down from the target surface. Also, by considering the entire target, a single value is determined for the propagation velocity, when in fact the propagation velocity will vary at different stress levels.

Presented in Figures 6-9 through 6-11 are TOA vs. depth plots for Tests 23, 24, and 25, respectively. Time-of-arrival measurements at the surface of the target were successful only on Test 24, and are included with the data presented in Figure 6-10.

The derived propagation velocities from the data of these tests were 2,990, 2,670, and 2,660 ft/sec, respectively. While the velocity from the first test is about 12 percent higher than that of the latter two tests, the repeatability is considered very good. It is also interesting to note that these values are more than two times higher than typical values for granular soils, increasing the range of stress that may be achieved in a target. The consistency of the derived propagation velocity demonstrates the potential use of the gas gun for gage validation studies, by providing a repeatable environment in which to test instruments.

6.3.2 Propagation Velocity of Relief Wave

A relief wave (or unloading wave) was generated in each target by the interaction of the shock wave with the free surface at the bottom of the container (and the sides as well). The initial compressive wave traveling through the target is reflected from the free surface as a tensile, or relief wave. The superposition of the tensile reflection and the still-impinging compressive wave will result in a decrease in stress and an increase in particle velocity at a gage location.

Two methods were used to determine the propagation velocity of the relief wave for several tests in sand. The two similar methods hinged on witnessing the TOA of the relief wave on individual gage records. The following assumptions were made in these analyses:

- the displacements of a stress gage and an accelerometer canister at the same depth are identical;
- the propagation velocity of the loading wave is constant;
- the propagation velocity of the relief wave is constant;
- there is perfectly normal impact onto the target.

6.3.2.1 Graphical Method

A schematic of the location of stress and velocity gages fielded in a target in their original position and at a later time is presented in Figure 6-12. Representative stress and velocity records from the 6-in. and 12-in. depths are shown in Figure 6-13. The TOA of the loading wave and relief wave at each gage location is noted in the figure. The amount an accelerometer canister displaces between the initial TOA and the TOA of the relief wave is measured from the double-integrated acceleration record. This displacement is added to the original gage position to determine the location of the gage at the TOA of the relief wave. This procedure is done for instruments at each depth in the target. As mentioned previously, TOA crystals were located at several depths in the target to monitor the TOA of the loading shock wave. One such measurement is made at the bottom of the target container, where the loading wave becomes a relief wave, thus providing an additional data point for consideration in determining the relief wave velocity.

Figure 6-9 (Test 23) is repeated in Figure 6-14, with additional data representing the location of various gages at the

TOA of the relief wave. The two data clusters represent gages at the two instrumented depths, 6 in. and 12 in. As was done when determining the propagation velocity of the loading wave, the inverse slope of the linear fit through the data represents the velocity of the relief wave. For Test 23 a value of 4,320 ft/sec was determined. Presented in Figure 6-15 is a similar plot for Test 24. Only the TOA measurement at the bottom of the target and the gages at the 12-in. depth were used to determine the relief wave speed. Only these gages were used in the analysis due to the failure of the acceleration measurements at the 6-in. depth prior to TOA of the relief wave, thus prohibiting a measure of the displacement of instruments at that depth. The linear fit through the data indicates a relief wave velocity of 4,280 ft/sec, which is very similar to that determined for Test 23. Test 25 was not analyzed because of failures or discrepancies in the acceleration measurements at both the 6-in. and 12-in. depths.

Theoretically, the two lines representing the best fit through the loading TOA and relief TOA should meet at the bottom of the target, i.e., at the 24-in. depth, represented by the dashed line in Figure 6-14 and 6-15. An error in any one of the assumptions or errors in placing the gages in the target could result in the discrepancy seen in the figures.

6.3.2.2 Analytic Method

The second method used to determine the propagation velocity of the relief wave in the soil is based on the geometry of the target and the determined loading wave velocity. After the shock wave impacted a stress gage, it continued until it impacted the free surface at the bottom of the target. The distance over which the shock wave traveled at the loading wave speed is known. The reflected tensile wave then traveled back through the target at the relief wave speed. The displacement of a gage during the time until the relief wave reached the gage was determined from a double-integrated acceleration record at the same depth. Hence, the position of the gage at the TOA of the relief wave is known. As before, the velocity of the loading and relief waves was assumed to be constant over the distance traveled.

In Figure 6-12 the original positions of gages at the upper and lower depths are denoted by H_1 and H_2 , respectively. The displaced positions at TOA of the relief wave are denoted by $H_1(t_4)$ and $H_2(t_3)$, respectively. The location of the bottom of the target is denoted by H_3 . In Figure 6-13 the initial TOA of the shock wave at each gage is labeled t_1 and t_2 . The TOA of the relief wave at the lower and upper depths is labeled t_3 and t_4 , respectively. The time for a shock wave to travel these two known distances and the propagation velocity over one of those distances is known; hence, the velocity over the second distance may be determined. At the upper depth and lower depth (respec-

tively), the difference in time between loading and relief wave arrival is given by:

$$(t_4 - t_1) = \frac{H_3 - H_1}{C_L} + \frac{H_3 - H_1(t_4)}{C_U}$$

$$(t_3 - t_2) = \frac{H_3 - H_2}{C_L} + \frac{H_3 - H_2(t_3)}{C_U}$$

where

C_L = the loading wave velocity

C_U = the relief wave velocity

These equations may be rearranged to solve for the relief wave velocity. For gages located at the upper depth,

$$C_U = \frac{H_3 - H_1(t_4)}{(t_4 - t_1) - \left(\frac{H_3 - H_1}{C_L} \right)} \quad (6.4)$$

For gages located at the lower depth, the relief wave velocity may be determined from

$$C_U = \frac{H_3 - H_2(t_3)}{(t_3 - t_2) - \left(\frac{H_3 - H_2}{C_L} \right)} \quad (6.5)$$

Equation (6.4) was applied to the gage records at the upper depth and Equation (6.5) was applied to the gage records at the lower depth for Test 23. The loading wave speed, C_L , used in

these calculations was that determined by the linear fit to the TOA data, i.e., 2,990 ft/sec (see Figure 6-9). The results are presented in Table 6-1. While all the determined values for C_v are similar, there appears to be a systematic difference in the values determined at each depth. The average values for C_v at the upper and lower depths are 4,260 and 3,880 ft/sec, respectively.

The variation in the determined relief wave speed at the two depths may be due to experimental error in placing gages in the target, or to the assumption that the displacement of the stress gage is identical to that of an adjacent accelerometer canister. Another explanation is perhaps the error in assuming that the loading wave travels at constant velocity through the depth of the target. This discrepancy may be seen in the values of C_v determined from the stress gage records at the lower depth. If a slower loading wave velocity is chosen for the depths where stresses are lower, the determined relief wave speed will be greater, perhaps bringing the values determined at the lower depth more in line with those determined at the upper depth.

6.3.2.3 Determination of Relief Wave Velocity Using a Varying Loading Wave Velocity

The premise described above was investigated for the data of Test 23. A loading wave speed, C_{L1} , was determined for that portion of the target between the surface and the lower instrumented depth from the inverse slope of the linear fit

through the TOA data in that region. A different loading wave speed, C_{L2} , was determined similarly from the TOA data at, and below, the lower instrumented depth. For gages at the upper depth, the mathematical description of the time required for the shock wave to make the round trip is

$$(t_4 - t_1) = \frac{H_2 - H_1}{C_{L1}} + \frac{H_3 - H_2}{C_{L2}} + \frac{H_3 - H_1(t_4)}{C_U}$$

where

C_{L1} = the loading wave speed between the target surface and lower instrumented depth

C_{L2} = the loading wave speed between the lower instrumented depth and the bottom of the target.

This relationship may be rearranged to solve for C_U :

$$C_U = \frac{H_3 - H_1(t_4)}{(t_4 - t_1) - \left(\frac{H_2 - H_1}{C_{L1}} + \frac{H_3 - H_2}{C_{L2}} \right)} \quad (6.6)$$

Equation (6.6) is used to determine C_U from the gage records at the upper depth. Equation (6.5) is still applicable for the gages at the lower depth by substituting C_{L2} for C_L .

The dashed line presented in Figure 6-16 is the linear fit through the TOA data of instruments between the target surface and the lower instrumented depth. The loading wave speed determined by the inverse slope of this line (3,240 ft/sec) is the value for C_{L1} over the distance from H_1 to H_2 within the

target. The solid line in Figure 6-16 is a linear fit through instrument TOA data at and below the lower depth. The wave speed determined from this data is 2,760 ft/sec. This value is substituted as C_{L2} in Equation (6.6) and as C_L in Equation (6.5) to determine the relief wave speed.

The results of this analysis are presented in Table 6-2. The average value of the determined relief wave speed using the instruments at the upper depth is 4,460 ft/sec. The average using instruments at the lower depth is 4,370 ft/sec. These two values are very similar, indicating that for some materials where the stress gradient is large through the target, the assumption of a constant loading wave speed may not be appropriate.

It is not clear, however, that the assumption of a constant loading wave speed for the Ottawa sand is invalid for this stress regime (15,000 psi). To evaluate further the consistency of the targets for Tests 23 through 25, C_{L1} and C_{L2} were determined, as described above, for Tests 24 and 25. The values determined for C_{L1} for the three tests were 3,240, 2,750, and 2,750 ft/sec, respectively. The values for C_{L2} were 2,760, 2,570, and 2,570 ft/sec. The similarity of the values of the latter two tests, both from test to test and between the different levels in a given test, indicate that perhaps the TOA data between the target surface and the lower instrumented depth in Test 23 is anomalous. However, the procedure by which the loading wave velocity may be determined, at various stress levels, has been demonstrated.

6.4 Construction of a Material Model for Ottawa Sand

If there is sufficient data from a test that supports the determination of a varying loading wave speed, a more complex (but still relatively simple) material model may be constructed. A constant loading wave speed and infinite relief wave speed were assumed when developing the projectile-soil interaction model. Using Test 23 as an example, the values of C_{L1} , C_{L2} , and C_U , may be used to determine the modulus of the soil over the various stress regimes. Shown in Figure 6-17 are the two loading wave velocities, as determined in Section 6.3.2.3, and the relief wave velocity, as determined in Section 6.3.2.1. The relationship $E=C^2\rho$ may be used to determine the modulus of the material. The result of this calculation for each value of C is shown in Figure 6-18. The "break" in the model at the 5,000 psi level reflects the nominal stress level at the 12-in. depth. This model for the sand could be used in more complex finite element or finite difference codes for predicting the stress in the target.

CHAPTER 7

SUMMARY AND CONCLUSIONS

7.1 Summary

The 4-ft gas gun is unique in its design and operating principle. It incorporates several novel features, including:

- a rearwardly exiting water reaction mass to resist jetting forces;
- a specially designed quick-release trigger mechanism;
- a multiple-layered projectile that uses energy-absorbing foam to protect a permanent carriage section;
- replaceable barrel liner and barrel extensions.

Twenty-eight tests have been conducted with the 4-ft gas gun to date. These tests were conducted over the entire range of operation of the gun (0 to 300 psi). The projectile velocity on these tests varied from 18 to 230 ft/sec. The projectile velocities were, on the average, about 94 percent of the values predicted by the mathematical model of the gun, and were consistent and predictable.

Tests on long-range effects indicate there is no potential for damage to buildings in the area from either ground shock or airblast. The noise generated from firing the gun, while relatively loud, has caused little disturbance in the surrounding area.

The gas gun overcomes the limitations of other dynamic testing techniques for gage validation by providing predictable

and repeatable stress and ground motion fields in a dry sand target.

7.2 Conclusions

The 4-ft gas gun provides a mechanism to conduct many interesting types of test. These include tests on new (and existing) instrumentation that evaluate gage response in a particular geologic material. The only target material discussed here was dry sand, but there are a myriad of materials of interest, e.g., saturated soils, clay, limestone, granite, marble, and various mixes of concrete.

The 4-ft gas gun also provides a means for obtaining ground motion data for ground shock transmission in jointed material under tightly controlled conditions. Tests could be conducted to investigate the relative effect of variations in joint properties (roughness, saturation, continuity, and orientation) on ground shock transmission, as well as the material's constitutive behavior. The data would provide a database for material modelers to develop "smeared" (or macroscopic) material models for a discontinuous material. These material models could be used as input to discrete element codes to predict ground shock and to determine the suitability or capability of continuum codes to predict the response of a jointed material.

TABLES

Table 3-1. Projectile configuration data, predicted and measured projectile velocity, planarity, and pressurization time from tests with the 4-ft gas gun.

Test No.	Proj. Mass lb.	Foam/Impact Plate Length in.	Pres. Plate Yes/No	Vessel Pres. psi	Predicted Projectile Velocity ft/sec	Measured Projectile Velocity ft/sec	Measured as Percent of Prediction ¹ percent	Projectile Planarity milliradians	Time to Pressurize min
5	2125	0/0	Yes	0	26.2 ²	17.6	67.2	2.5	0
6	3700	4/2	Yes	50	102	91.6	89.8	1.7	13.25
7	3260	7/2	Yes	75	132	121.7	92.2	2.6	18.25
8	3260	7/2	No	75	126	116.3	92.3	2.0	18.5
9	3260	7/2	No	100	146	ND	-	ND	25.75
10	3275	8/2	No	125	162	154.2	95.2	1.2	33.5
11	3245	7/2	No	147	177	165.1	93.3	0.6	38.25
12	3260	7/2	No	96	143	137.1	95.9	0.4	25.25
13	3260	7/2	No	149	178	173.2	97.3	5.2	40.25
14	3260	8/2	No	175	192	182.8	95.2	3.6	46.25
15	3260	8/2	No	200	205	193.4	94.3	3.2	54
16	3260	7/2	No	122	161	ND	-	ND	32.25
17	3260	7/2	No	169	189	ND	-	ND	47.45
18	3335	11/2	No	250	224	210.0	93.8	3.5	77.75
19	3335	11/2	No	249	224	206.8	92.3	5.2	ND
20	3335	11/2	No	300	246	ND	-	ND	94
21	3365	12/2	No	300	244	232.8	95.4	5.1	96
22	3245	6/2	No	125	164	153.5	93.6	2.5	32.75
23	3265	7/2	No	126	163	153.5	94.2	19.3 ³	34.5
24	3265	7/2	No	126	163	155.0	95.1	7.1 ³	33.25
25	3265	7/2	No	127	164	157.8	96.2	12.0 ³	33.5
26	3120	6/6	No	0	25 ²	20.7	82.8	1.3 ³	0
27	3120	6/6	No	44	98	90.6	92.4	3.6 ³	11
28	3950	4/12	No	55	95	87.3	91.9	2.4 ³	13.5

¹ (Meas. Vel.)/(Pred. Vel.) * 100

² Velocity calculated as $(2 \cdot g \cdot h)^{1/2}$

³ Impact planarity onto the target

ND = No Data

Table 4-1. Ranges of interest for testing with the 4-ft gun.	
Location	Range, ft
Nearest (uninhabited) bldg	30
Control Trailer, location of nearest personnel	175
Nearest inhabited WES bldg, not associated with testing	255
Guard at entrance road to site	325
Nearest residential bldg (outside station boundary)	765

Table 4-2. Structural damage thresholds from references.			
Damage Type	Particle Velocity Damage Threshold		
	Langefors et al. (1958)	Nicholls et al. (1971)	McPherson (1989)
None	< 2.8 in./sec	< 2.0 in./sec	< 2.0 in./sec
Fine plaster cracks	4.3 in./sec	2-4 in./sec	-
Plaster and masonry wall cracking/minor structure	6.3 in./sec	4-7 in./sec	5.4 in./sec
Major structural damage/serious cracking	9.1 in./sec	> 7 in./sec	7.6 in./sec

Table 4-3. Sound pressure level, far-field velocity, and airblast data from tests with the 4-ft gas gun.

Test No	Vessel Pres. psi	Projectile Velocity ft/sec	Sound Pressure Level dB					Far Field Data					
								Max Velocity ¹ , in./sec, Max Pressure, psi					
			30 ft Range	175 ft Range	255 ft Range	325 ft Range	765 ft Range	175 ft Range		255 ft Range		765 ft Range	
								Vel	Pres	Vel	Pres	Vel	Pres
3	23	105	135.0	114.5	101.5	112.5	105.5	0.106R	0.003	NF	NF	ND	ND
4	50	ND	137.0	116.0	110.0	102.5	105.5	0.148R	0.029	NF	NF	ND	ND
5	0	17.6	NF	NF	NF	NF	NF	NF	NF	NF	NF	NF	NF
6	50	91.6	126.5	107.5	106.5	116.0	108.0	0.111R	0.001	NF	NF	NF	NF
7	75	121.7	151.0	113.5	106.5	103.0	111.5	0.142R	NF	NF	NF	NF	NF
8	75	116.3	ND	113.5	111.0	103.0	ND	0.116R	NF	NF	NF	NF	NF
9	100	ND (146 ²)	134.0	ND	ND	106.0	100.5	0.168R	NF	NF	NF	0.022R	ND
10	125	154.2	ND	121.0	ND	111.0	109.0	ND	ND	NF	NF	0.018T	0.0024
11	147	165.1	ND	118.0	ND	ND	106.0	0.152R	ND	NF	NF	ND	ND
12	96	137.1	132.0	114.0	104.5	111.0	104.5	0.159R	NF	NF	NF	NF	NF
13	149	173.2	143.5	129.0	128.5	NF	112.0	0.158V	0.036	0.113V	0.012	0.0235R	0.0037
14	175	182.8	ND	126.5	NF	ND	ND	0.147V	0.033	0.113V	0.011	0.02R	0.0035
15	200	193.4	NF	NF	NF	118.5	112.5	0.198R	0.04	0.115V	0.0091	0.0188R	0.0046
16	122	ND (152 ³)	NF	NF	NF	NF	110.0	0.145V	0.02	0.117V	0.0104	0.0172R	0.0037
17	169	ND (180 ³)	NF	123.0	NF	NF	109.5	0.17V	0.0327	0.115V	0.0086	0.0282R	0.004
18	250	210.0	NF	127.0	126.0	NF	113.5	0.285R	0.0927	0.125V	ND	0.029V	0.0165
19	249	206.8	NF	125.5	126.5	NF	116.5	0.289R	0.049	0.126V	0.223	0.022V	0.0047
20	300	ND (236 ³)	NF	127.5	129.5	NF	117.0	0.344R	0.031	ND	0.166	0.023R	0.0047
21	300	232.8	NF	127.5	127.5	NF	116.0	0.347R	0.031	0.132V	0.131	0.022V	0.0038

¹ Max velocity from vertical (v), radial (R), or tangential (T) component

² Predicted value from GG4PV, used to plot results

ND = No Data

NF = Not Fielded

Table 4-4. Airblast/nuisance data for the 12-in gun.			
Range ft	Normalized Range	Peak Pressure psi	Avg. SPL dB
30	31	0.05	141.8
110	115	0.02	133.7

Table 4-5. Predicted airblast/nuisance data for the 4-ft gun.			
Range ft	Normalized Range	Peak Pressure psi	SPL dB
30	7.5	0.135	150.3
175	43.75	0.039	139.6
255	63.75	0.030	137.3
325	81.25	0.0255	135.9
765	171.25	0.0152	131.4

Table 6-1. Relief wave speed, C_v , as determined by the analytic method for Test 23, assuming a constant loading wave speed.

Gage Name/Type	Depth in.	C_v ft/sec
S&VA-1 (Accel)	6	4160
S&VS-1 (Accel)	6	4300
HRSE-1A (Stress)	6	4380
HRSE-1B (Stress)	6	4210
Average value at 6 in. depth = 4260 ft/sec		
S&VA-2 (Accel)	12	3720
HiFi-2 (Accel)	12	3840
HRSE-2 (Stress)	12	4070
Average value at 12 in. depth = 3880 ft/sec		

Table 6-2. Relief wave speed, C_v , as determined by the analytic method for Test 23, assuming a varying loading wave speed.

Gage Name/Type	Depth in.	C_v ft/sec
S&VA-1 (Accel)	6	4350
S&VS-1 (Accel)	6	4500
HRSE-1A (Stress)	6	4590
HRSE-1B (Stress)	6	4410
Average value at 6 in. depth = 4460 ft/sec		
S&VA-2 (Accel)	12	4170
HiFi-2 (Accel)	12	4320
HRSE-2 (Stress)	12	4610
Average value at 12 in. depth = 4370 ft/sec		

FIGURES

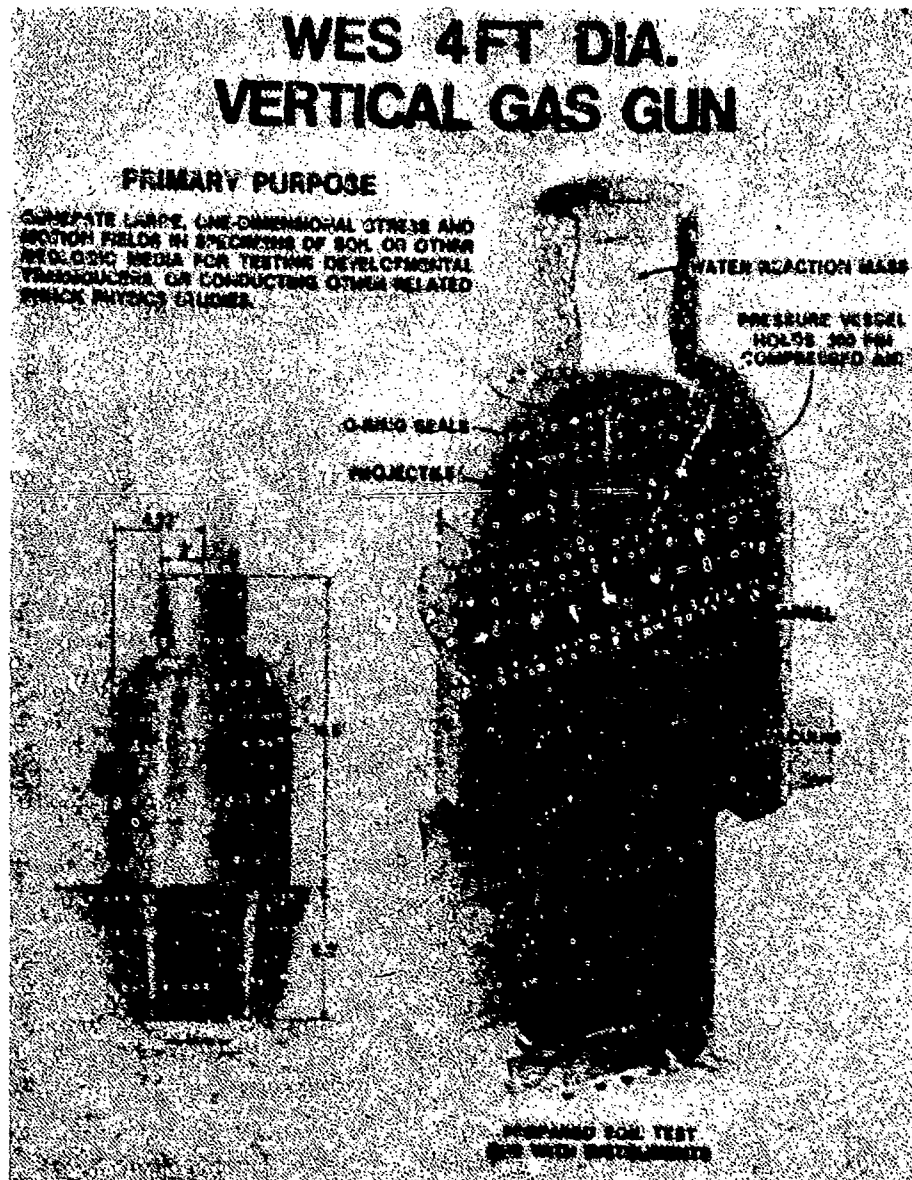


Figure 2-1. Cut-away view of the 4-ft-diameter vertical gas gun.

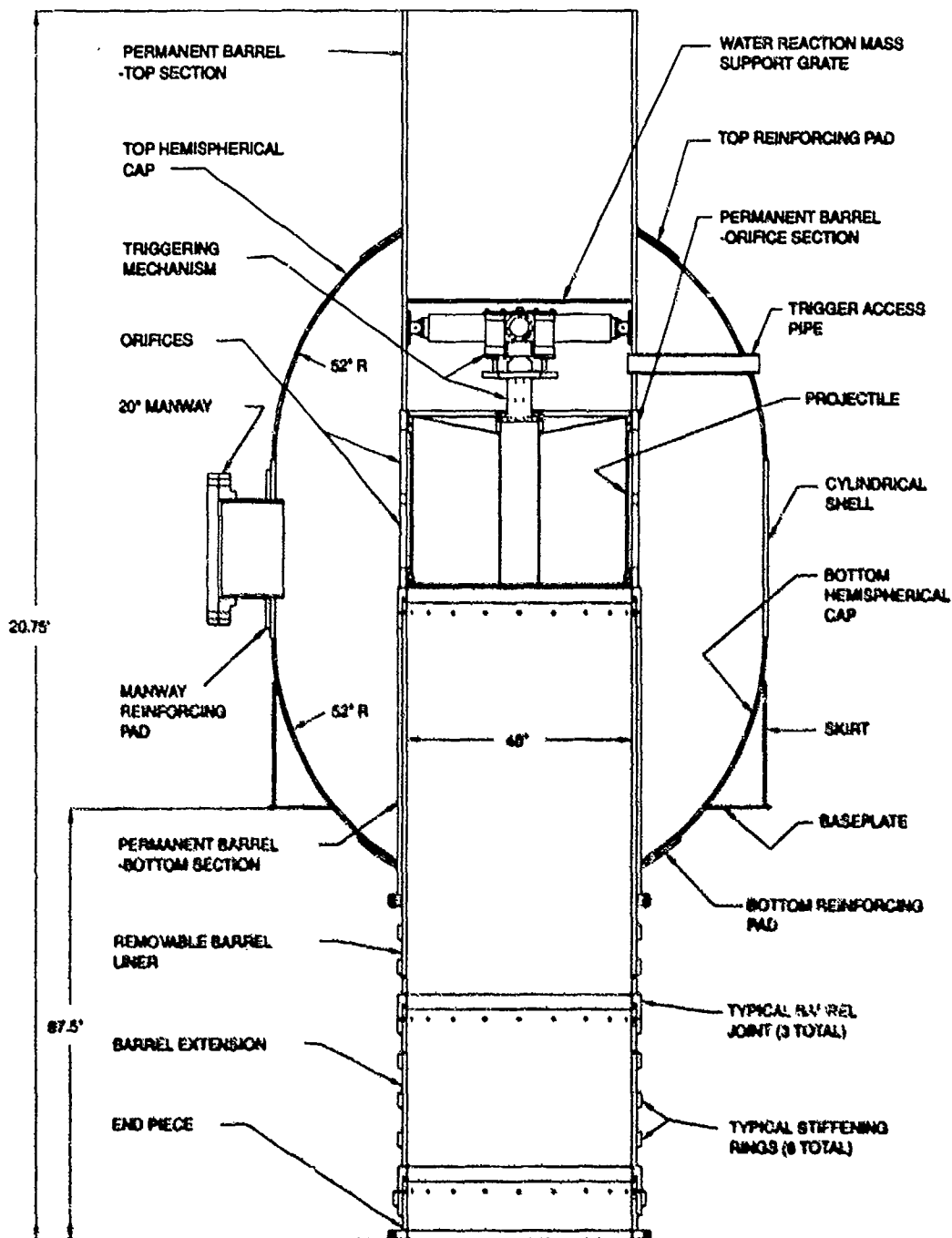


Figure 2-2. Schematic of the 4-ft-diameter vertical gas gun.

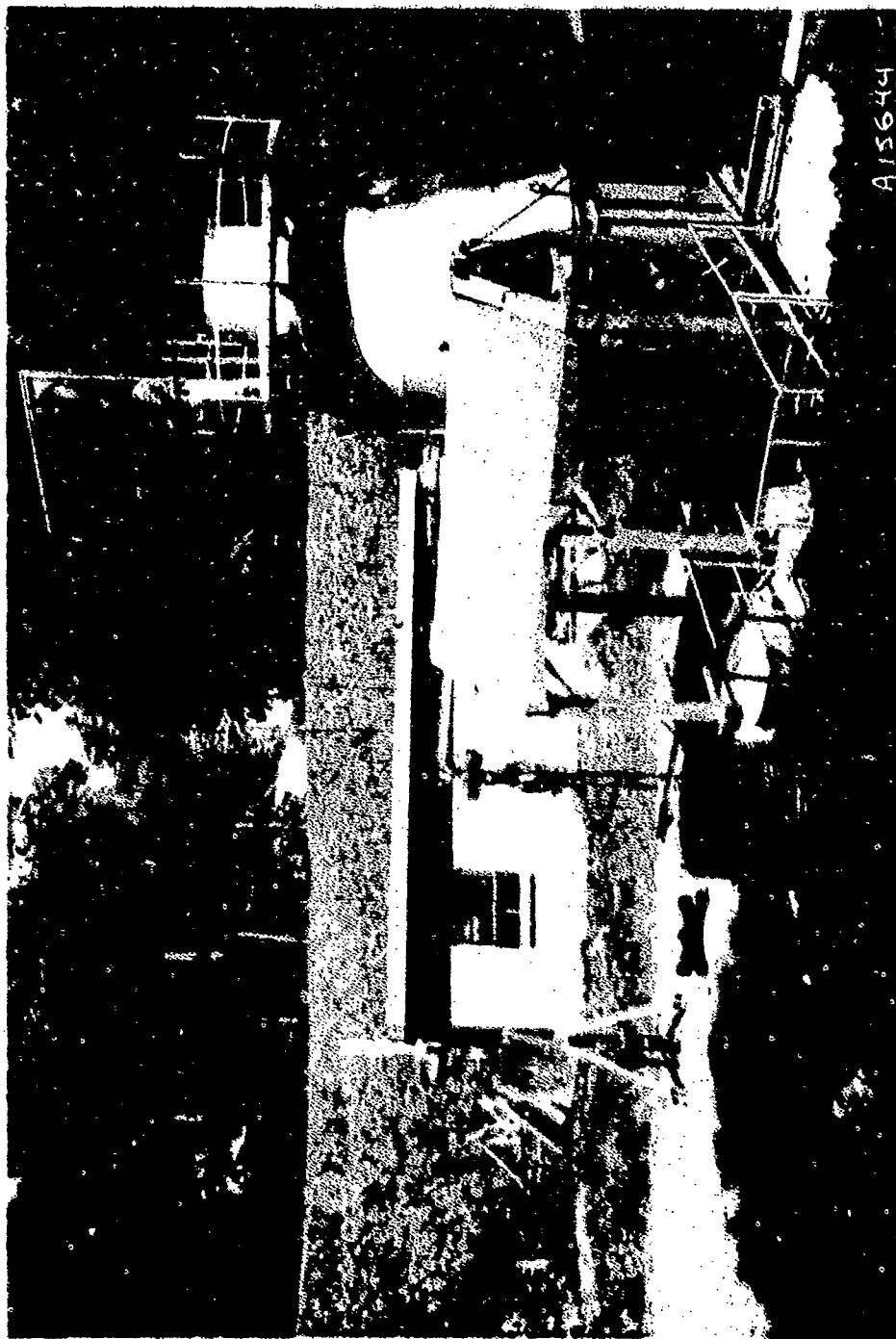


Figure 2-3. Photograph of the 4-ft gas gun and test site. Note the man at the top of the gun for scale.



Figure 2-4. Photograph of the 4-ft gas gun. The cinder block building is a work room, the portable building is a storage room, and the shed contains components of the fill system.

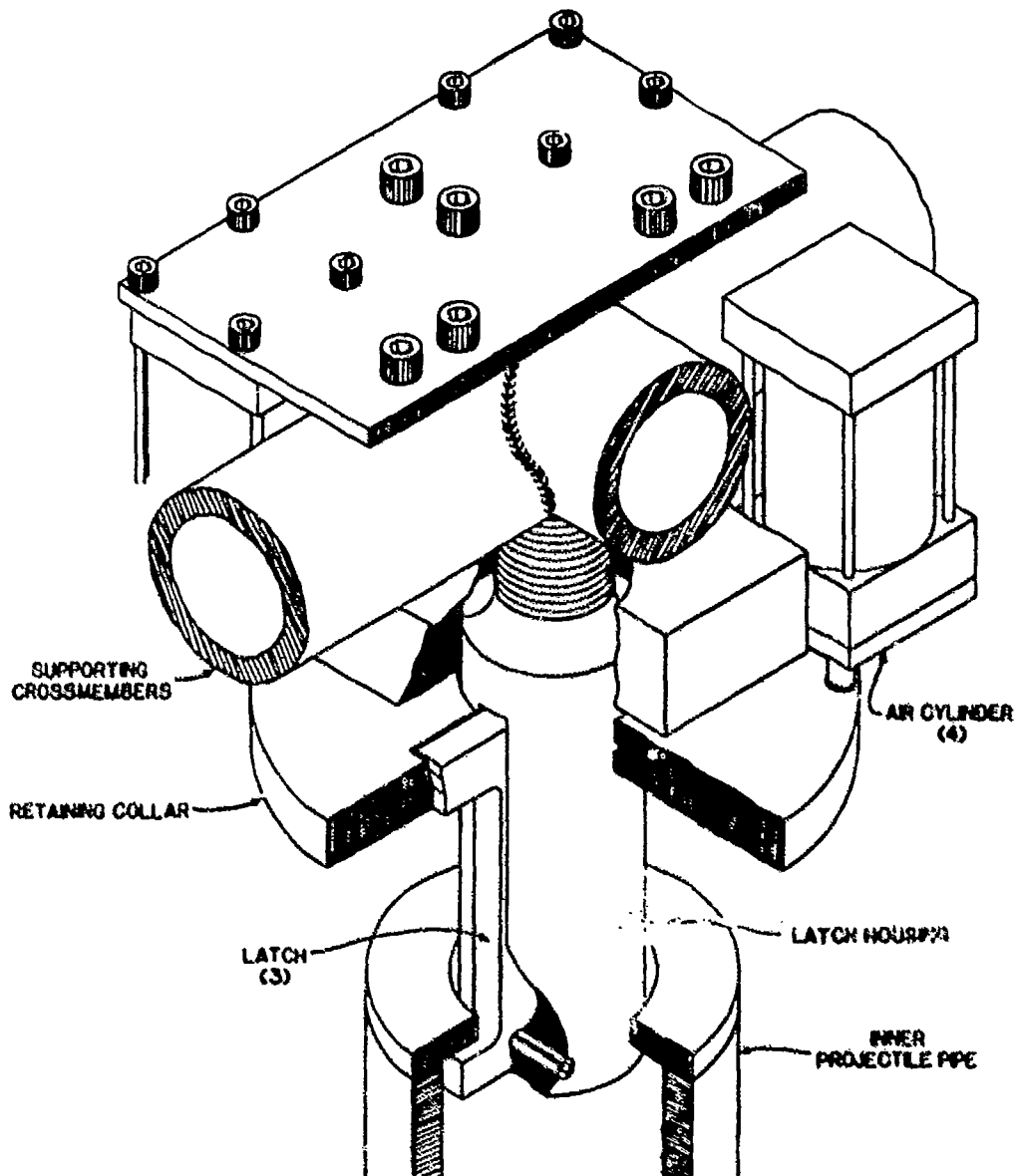


Figure 2-5. Cut-away view of the quick-release mechanism used with the 4-ft gas gun.

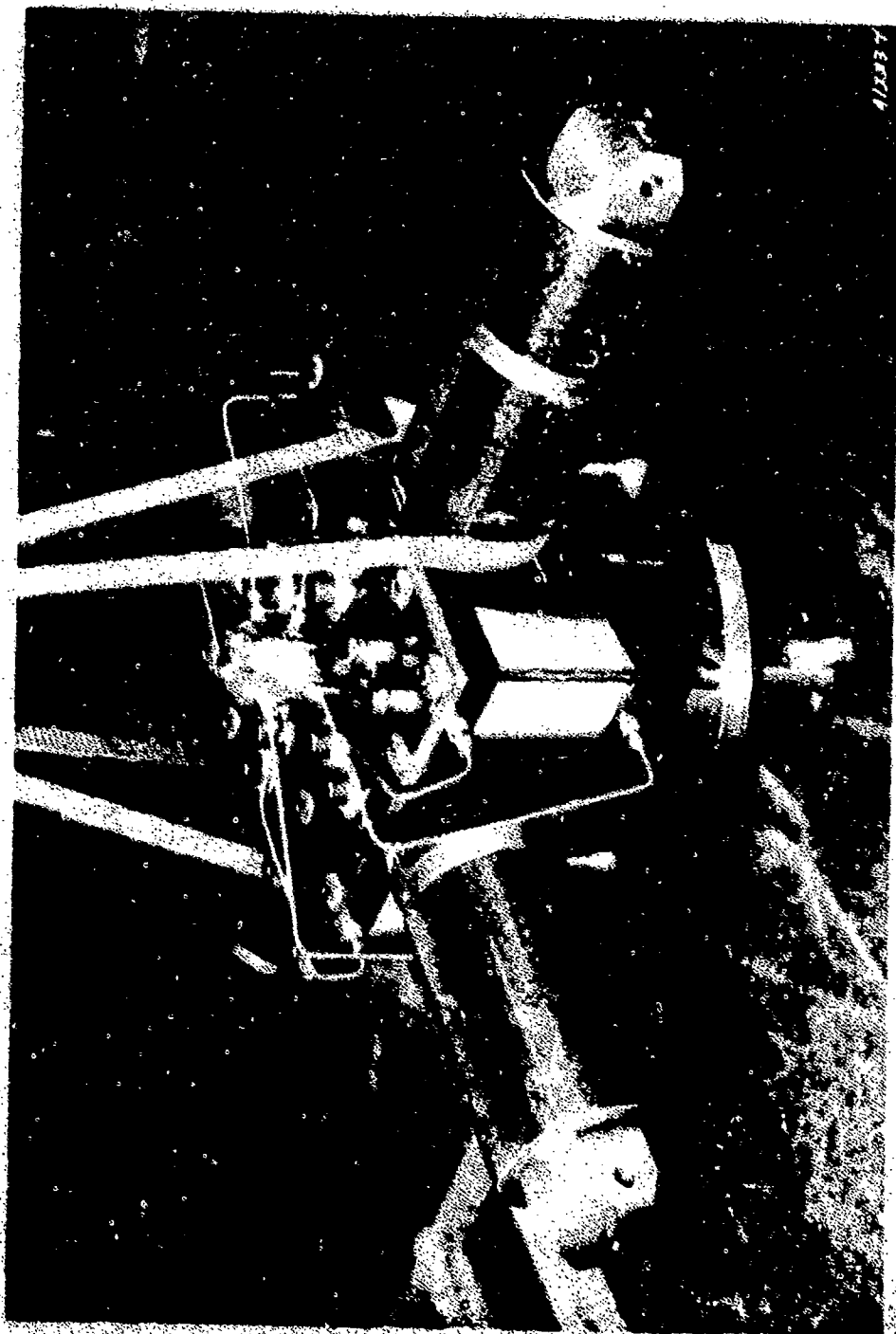


Figure 2-6. Photograph of the quick-release trigger mechanism used for supporting and releasing the projectile.

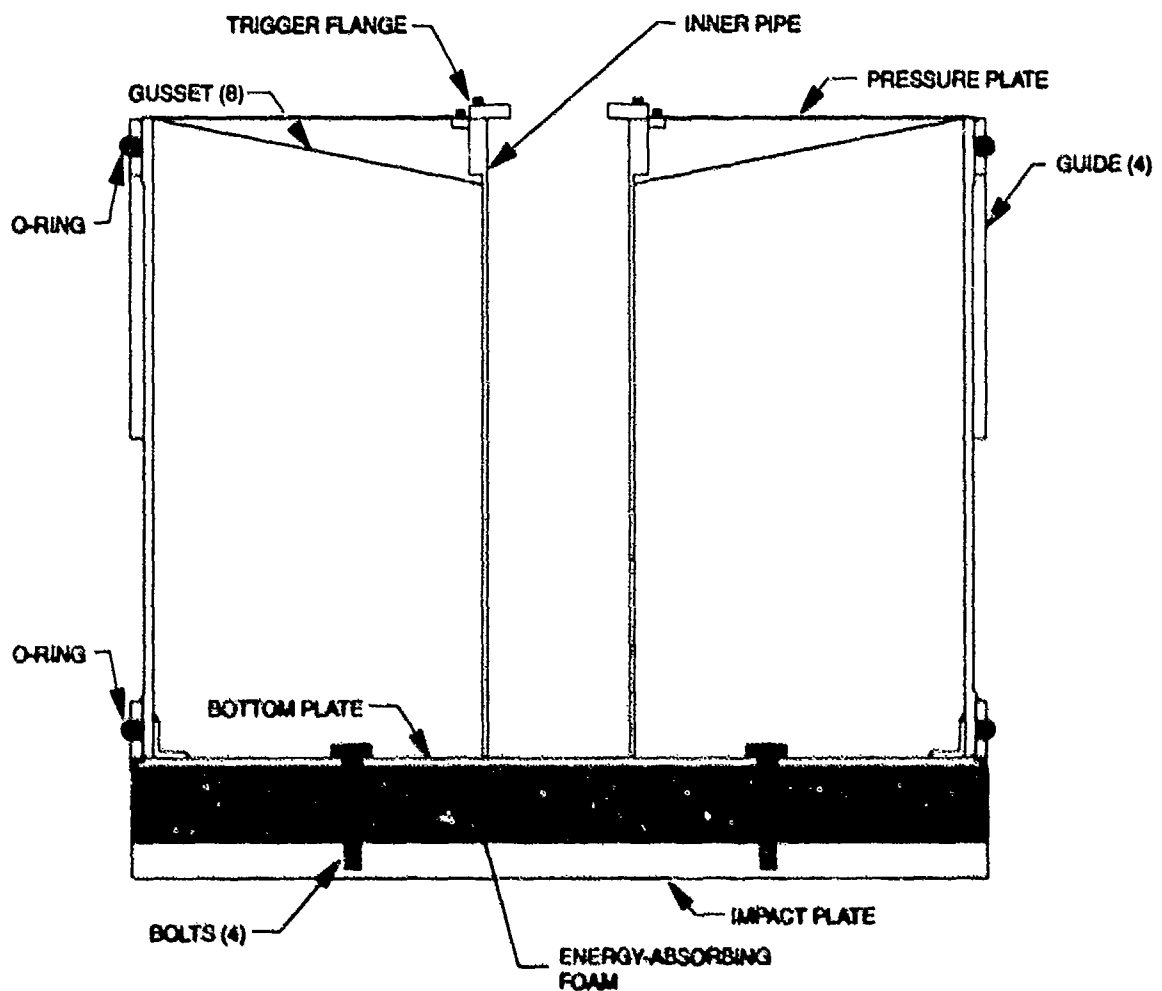


Figure 2-7. Schematic of the projectile used with the 4-ft-diameter gas gun.

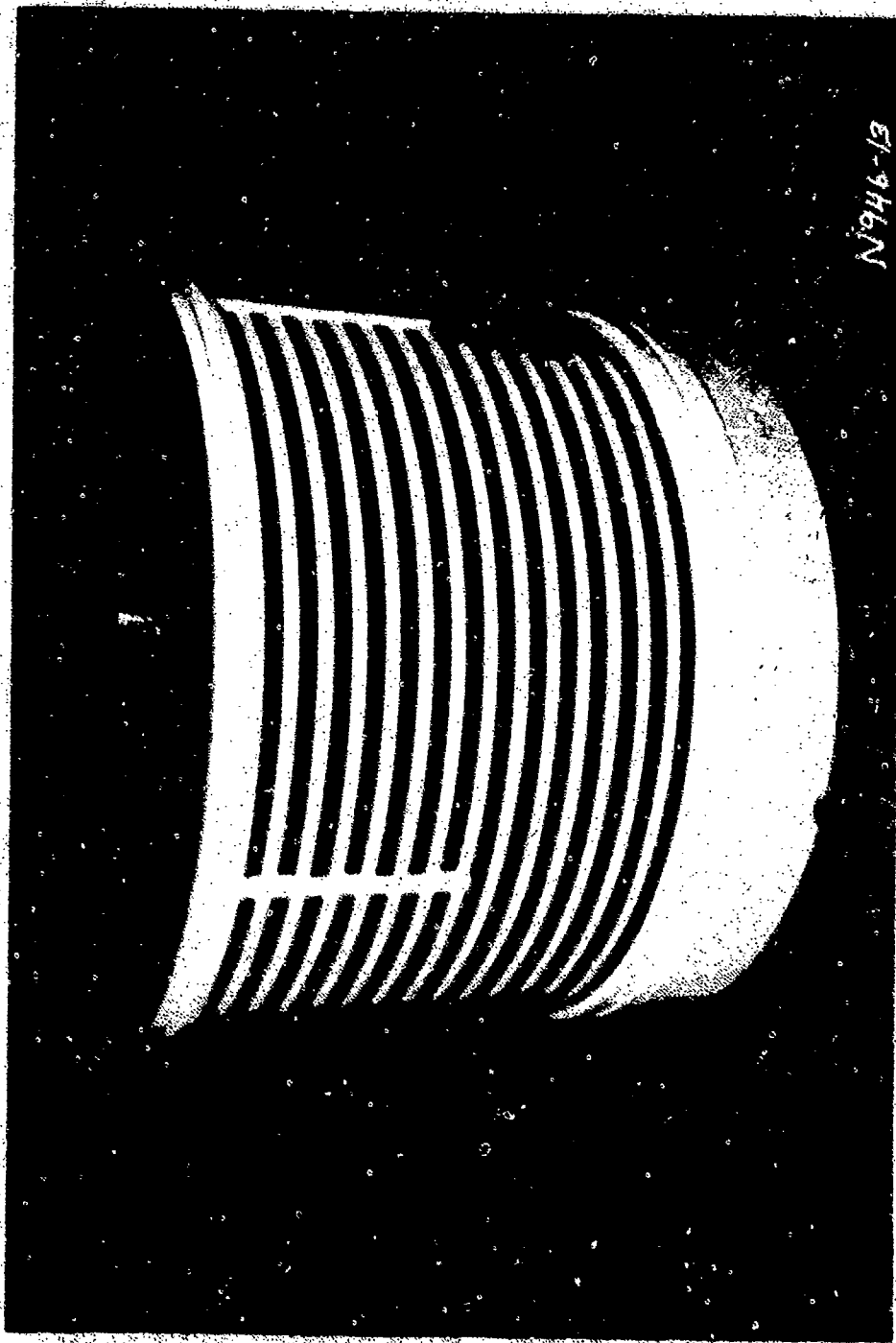


Figure 2-8. Photograph of the projectile used with the 4-ft gas gun. The three components of the projectile are the carriage (stripped in this photograph), energy-absorbing foam, and the impact plate.

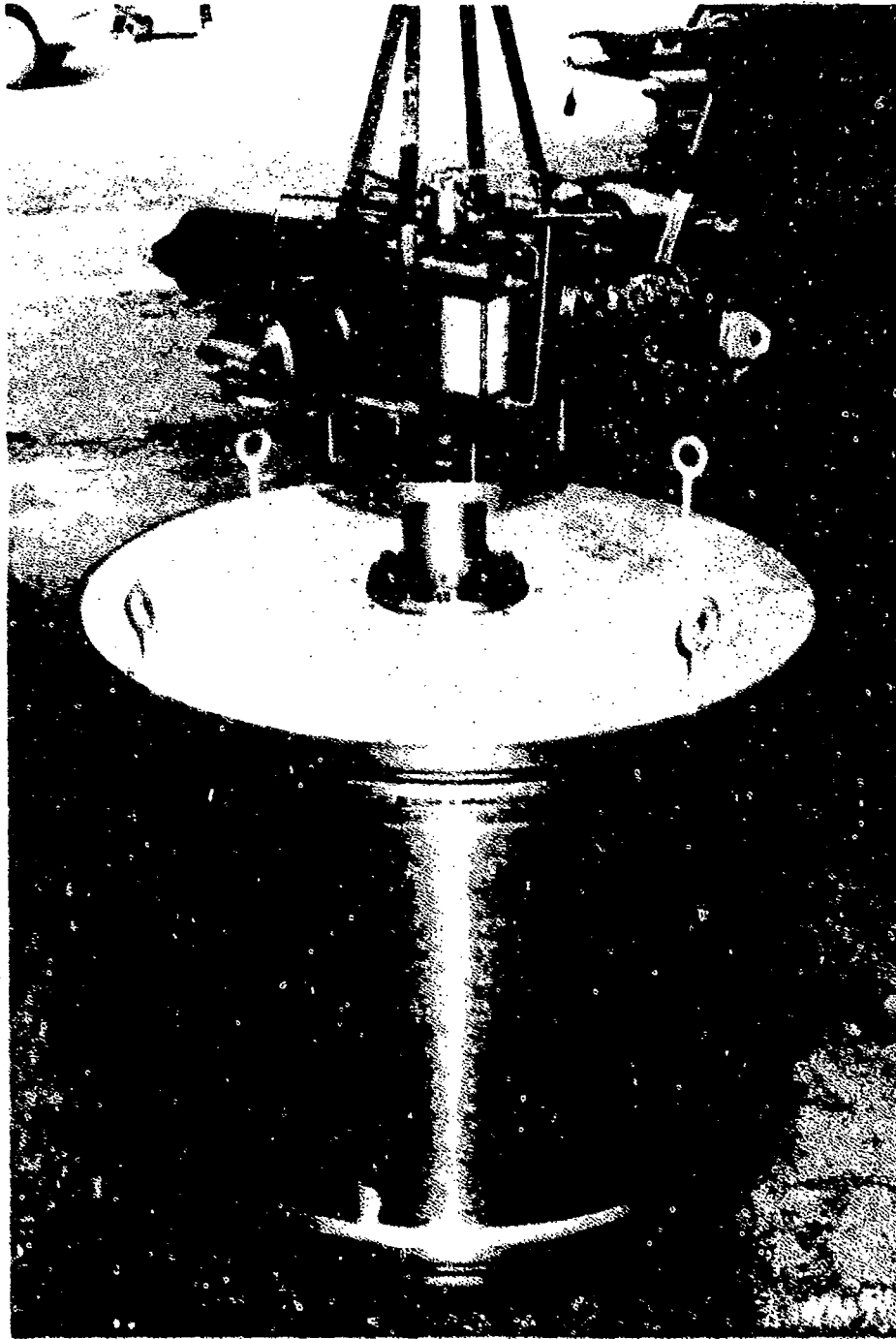


Figure 2-9. Photograph of the trigger mechanism supporting the carriage section of the projectile.



Figure 2-10. Photograph of the projectile after a test. Note the deformation of the pressure plate.

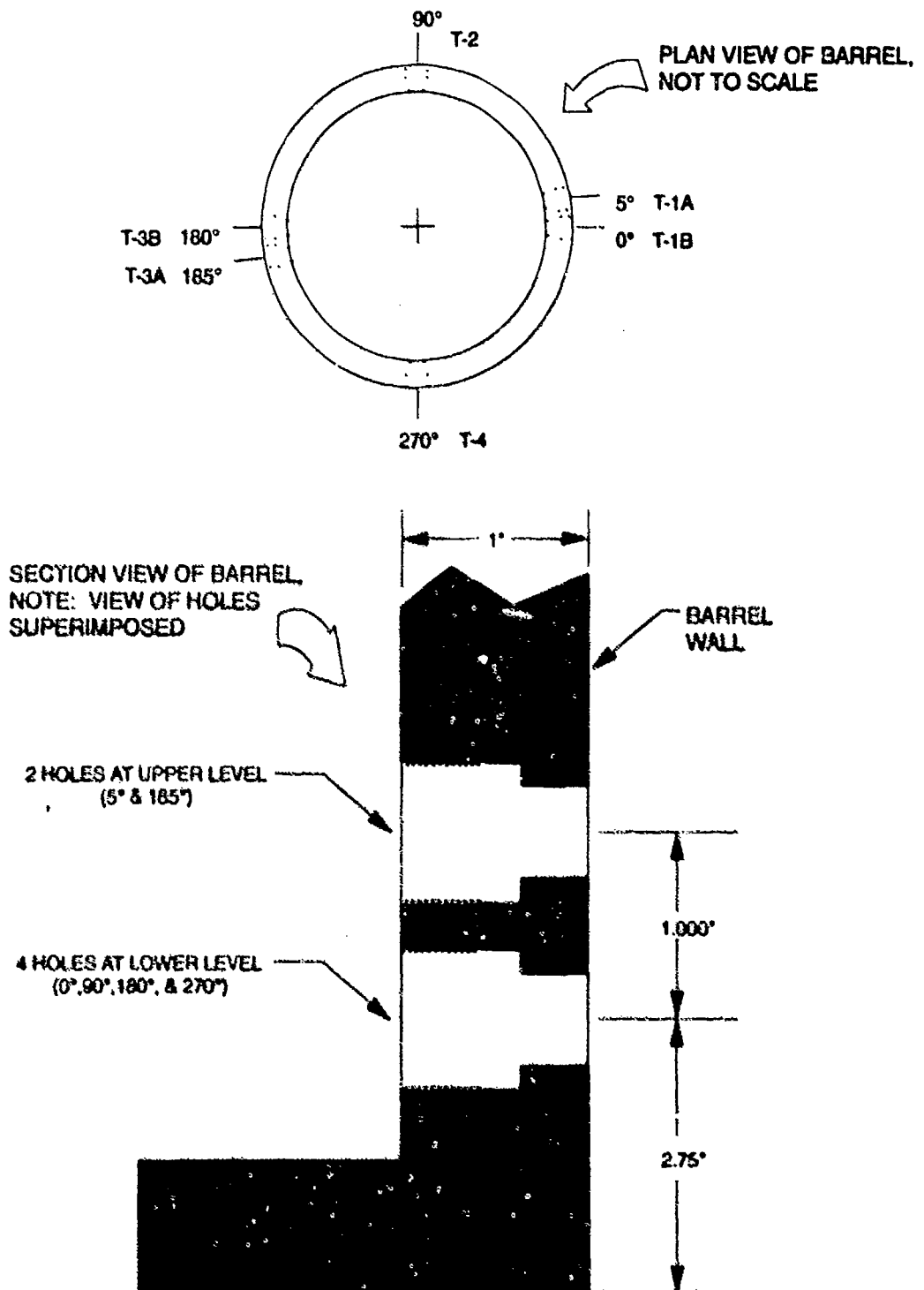


Figure 2-11. Piezoelectric pin locations, in the barrel of the gun, for velocity and planarity measurements.

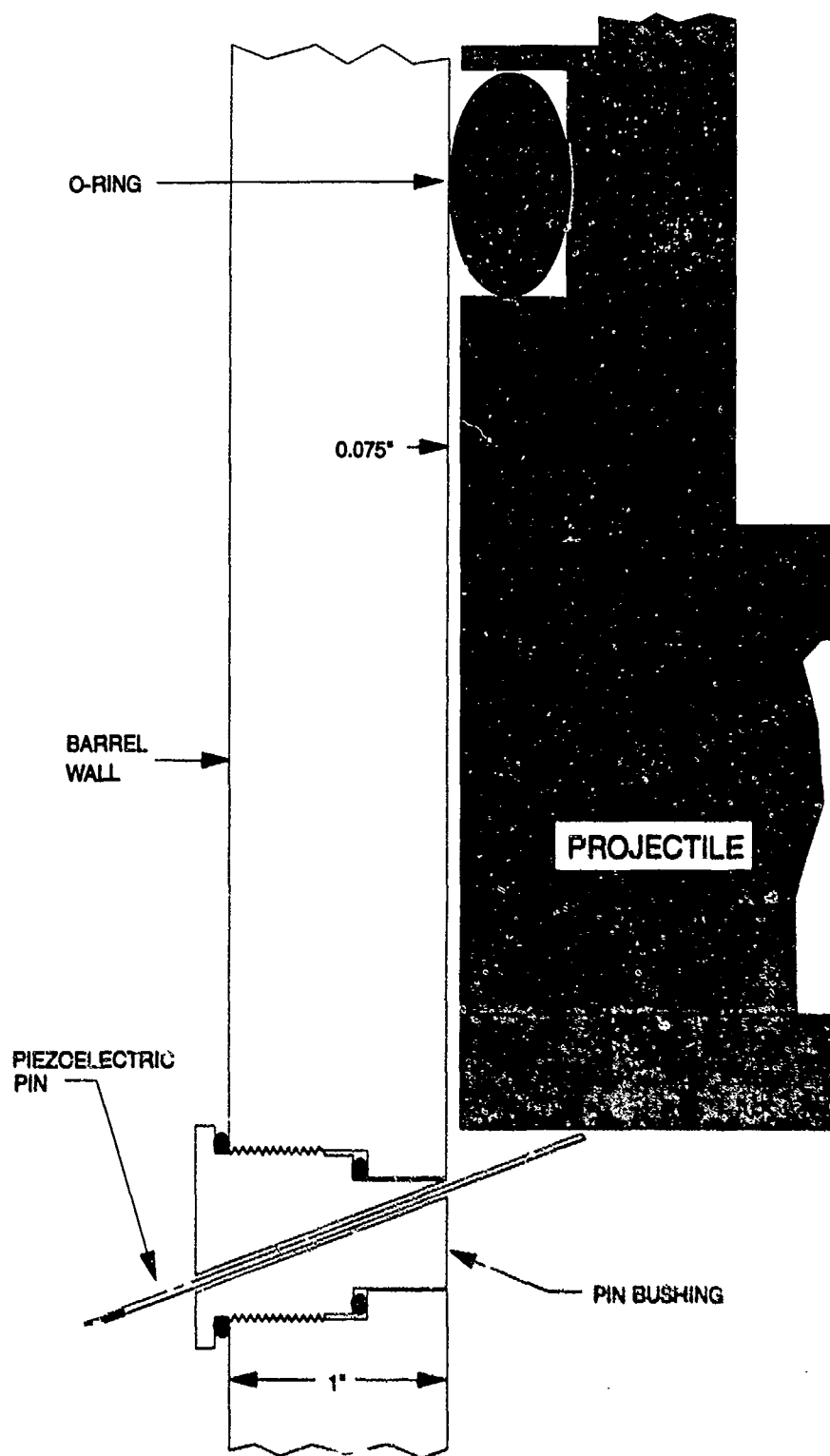


Figure 2-12. Schematic of orientation of piezoelectric pin used in measuring projectile velocity and planarity.

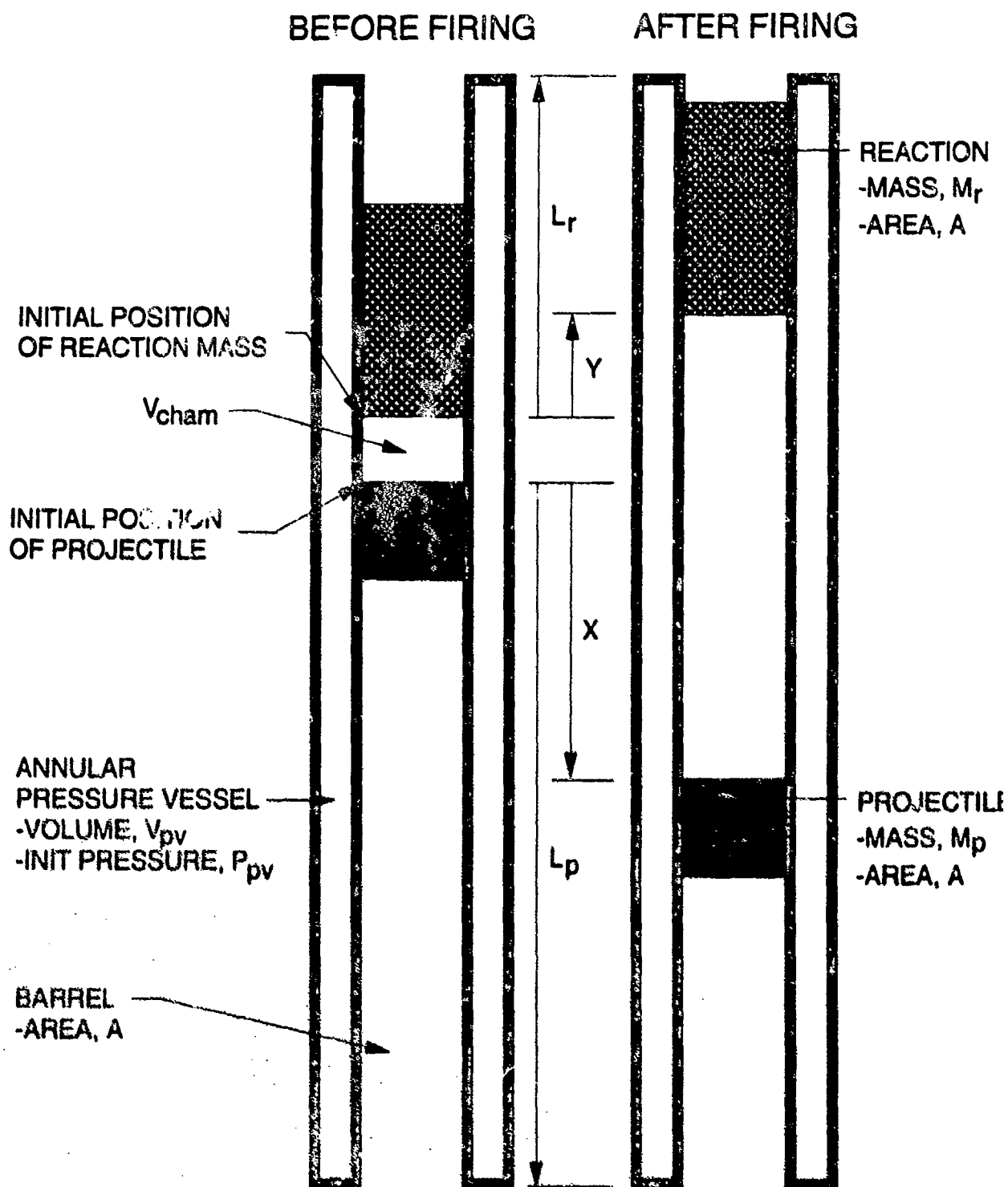


Figure 3-1. Parameters used in developing the mathematical model.

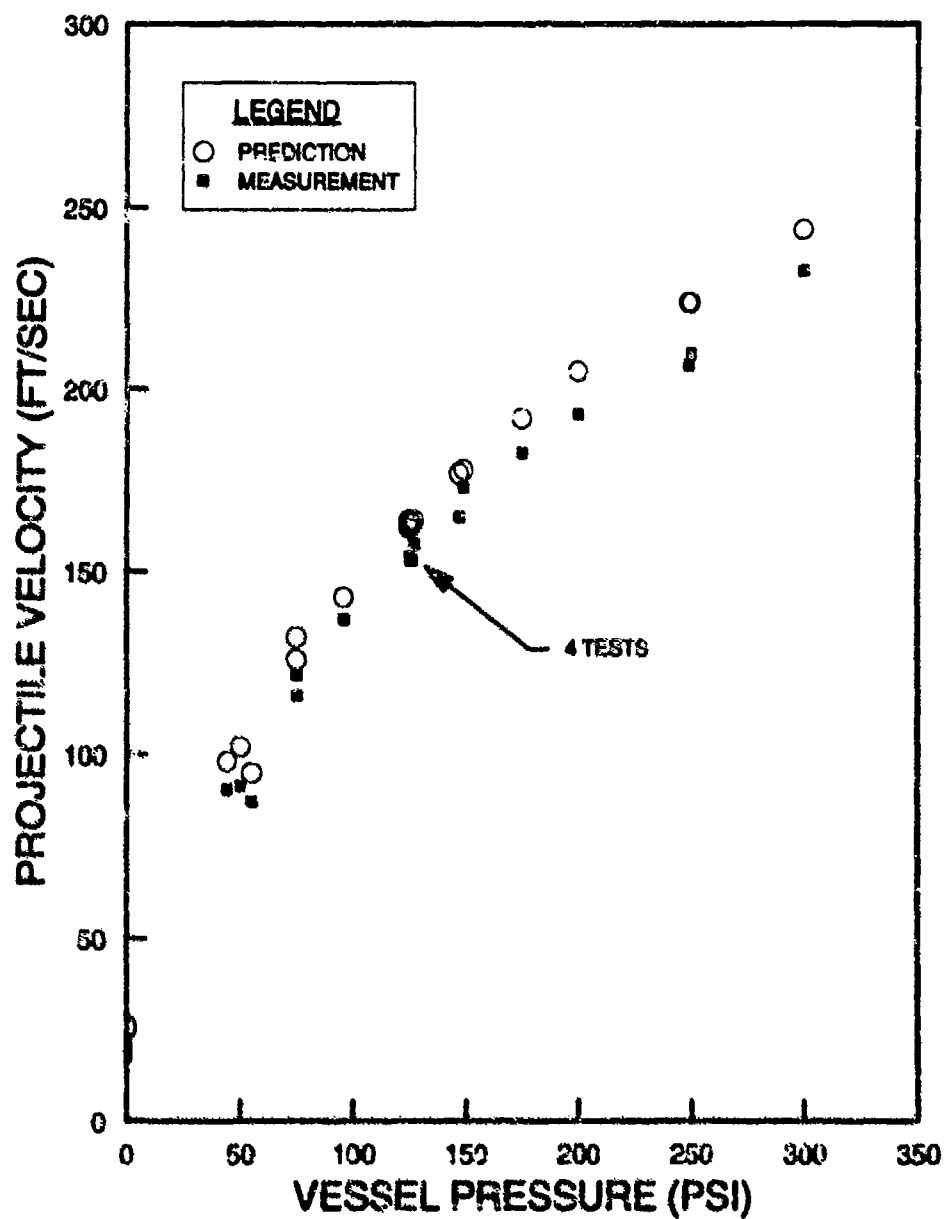


Figure 3-2. Predicted and measured projectile velocities for the 4-ft-diameter gas gun.

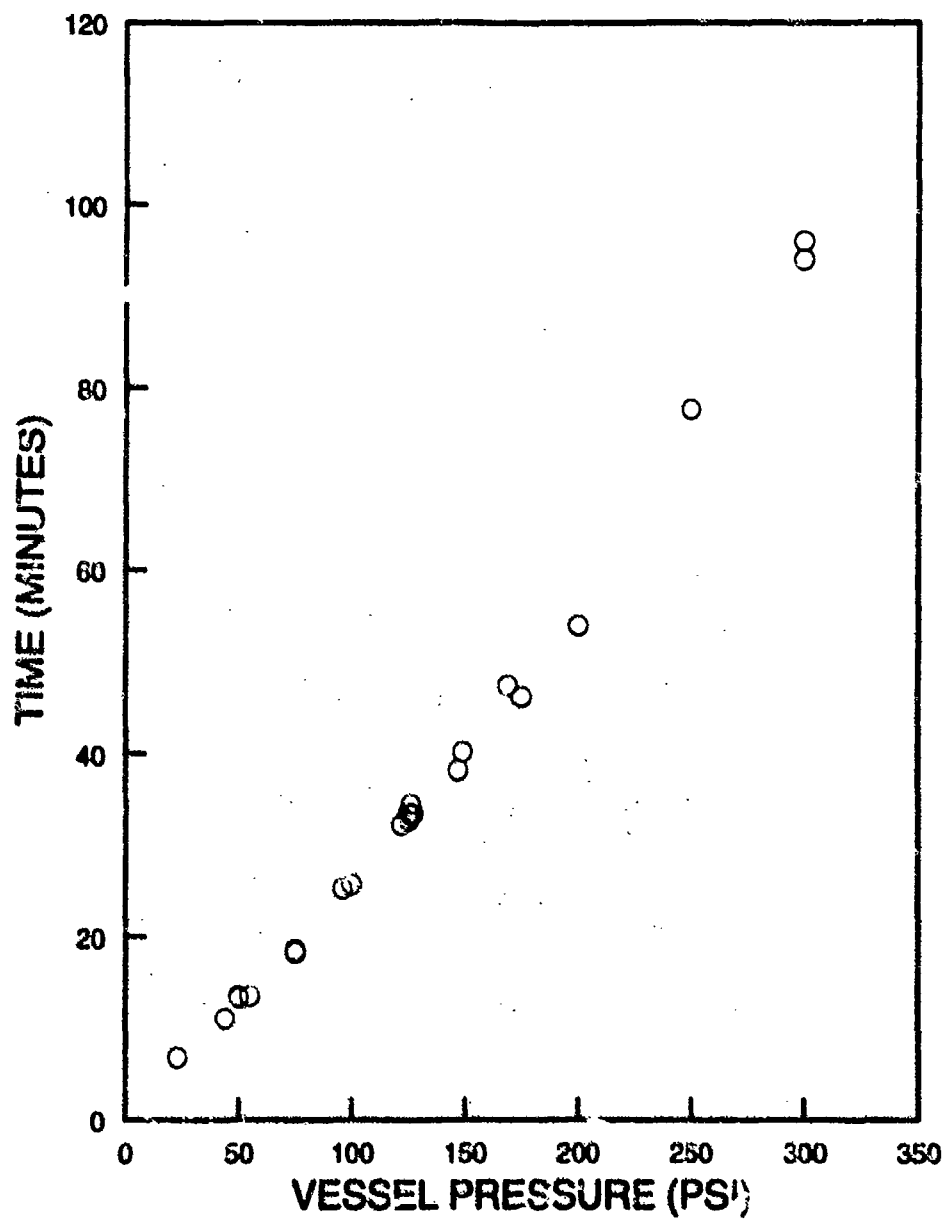


Figure 3-3. Time required to pressurize the gas gun.

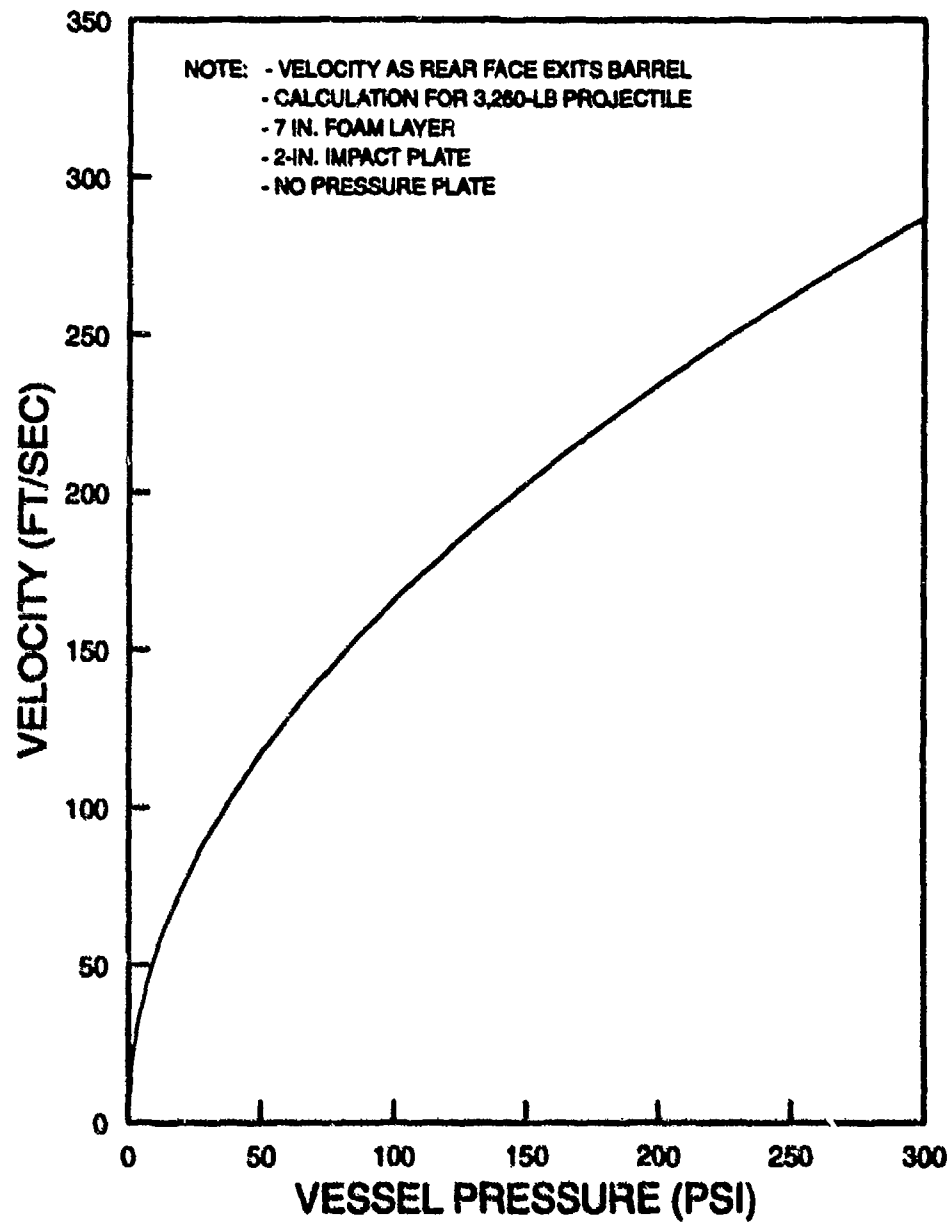


Figure 4-1. Predicted velocity for a 3,260-lb projectile.

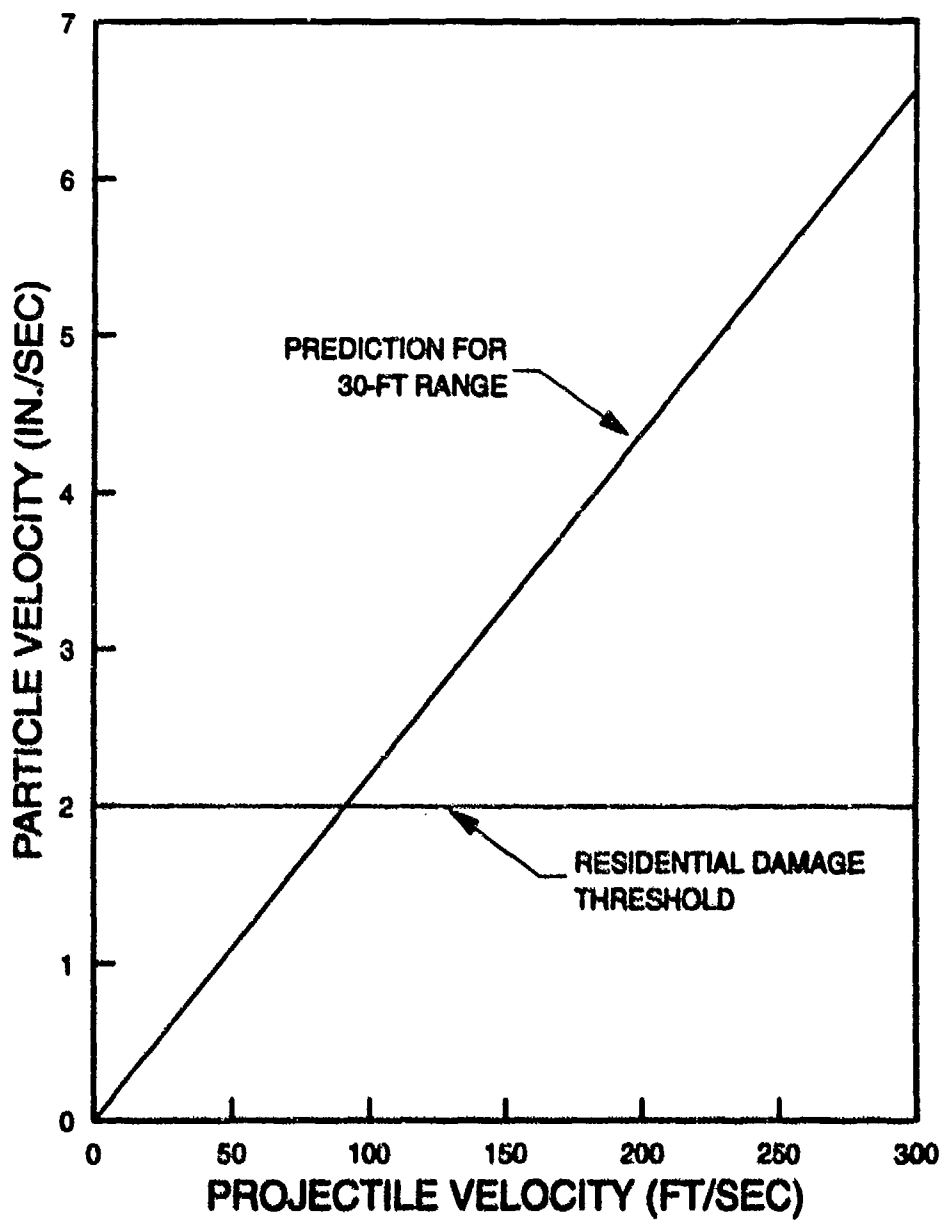


Figure 4-2. Predicted peak particle velocity as a function of projectile velocity for the 30-ft range.

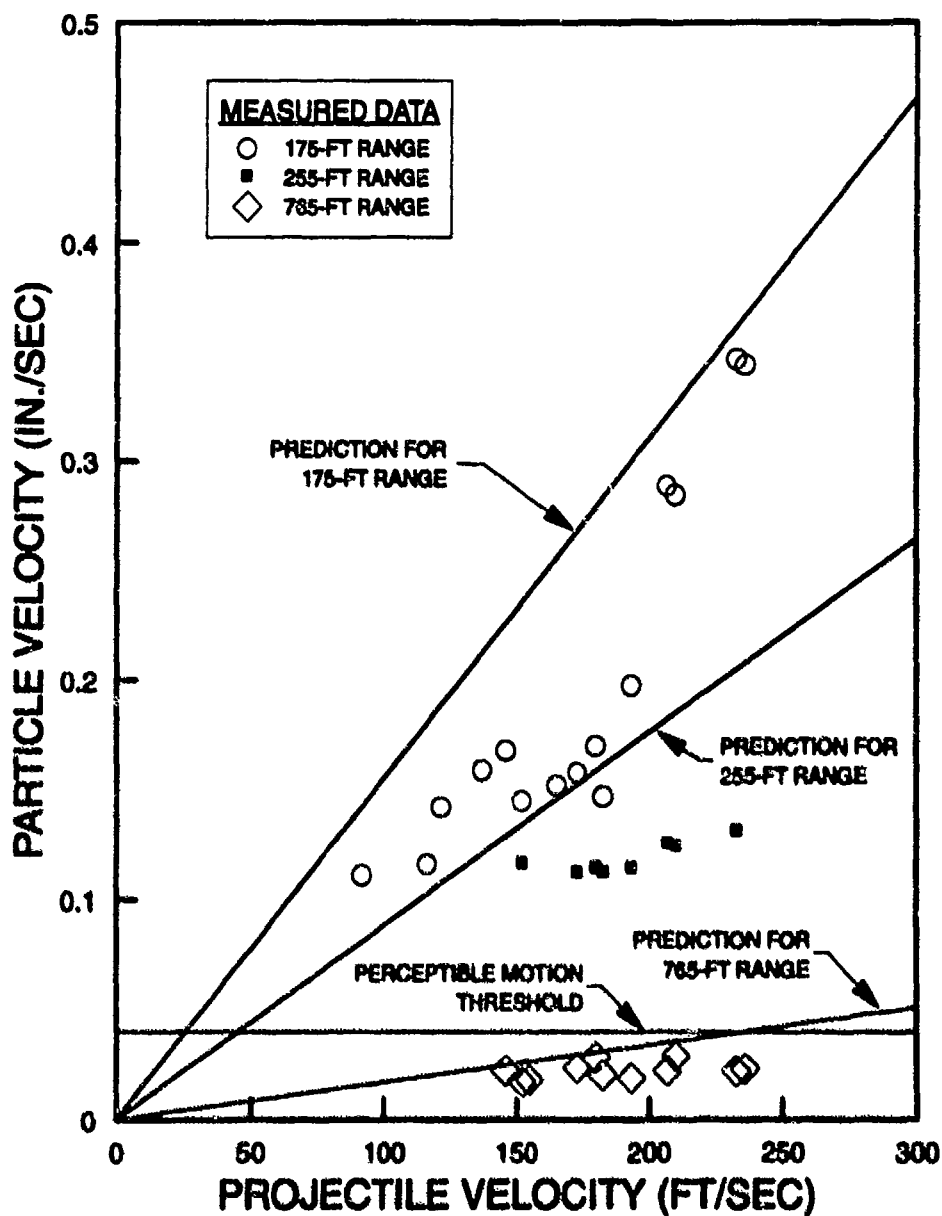


Figure 4-3. Predicted peak particle velocity as a function of projectile velocity for various far-field ranges.

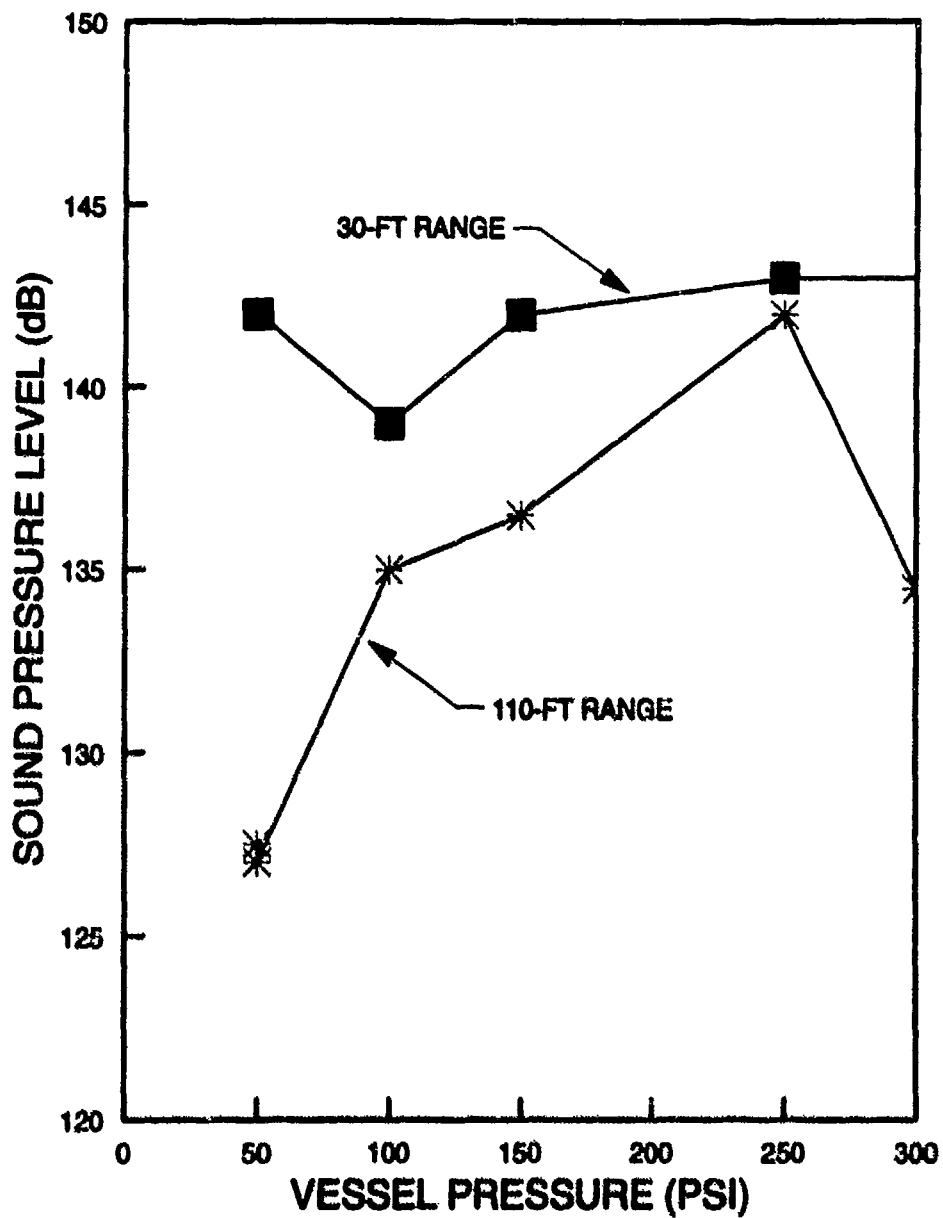


Figure 4-4. Sound pressure level measurements made when testing with the 12-in.-diameter gas gun.

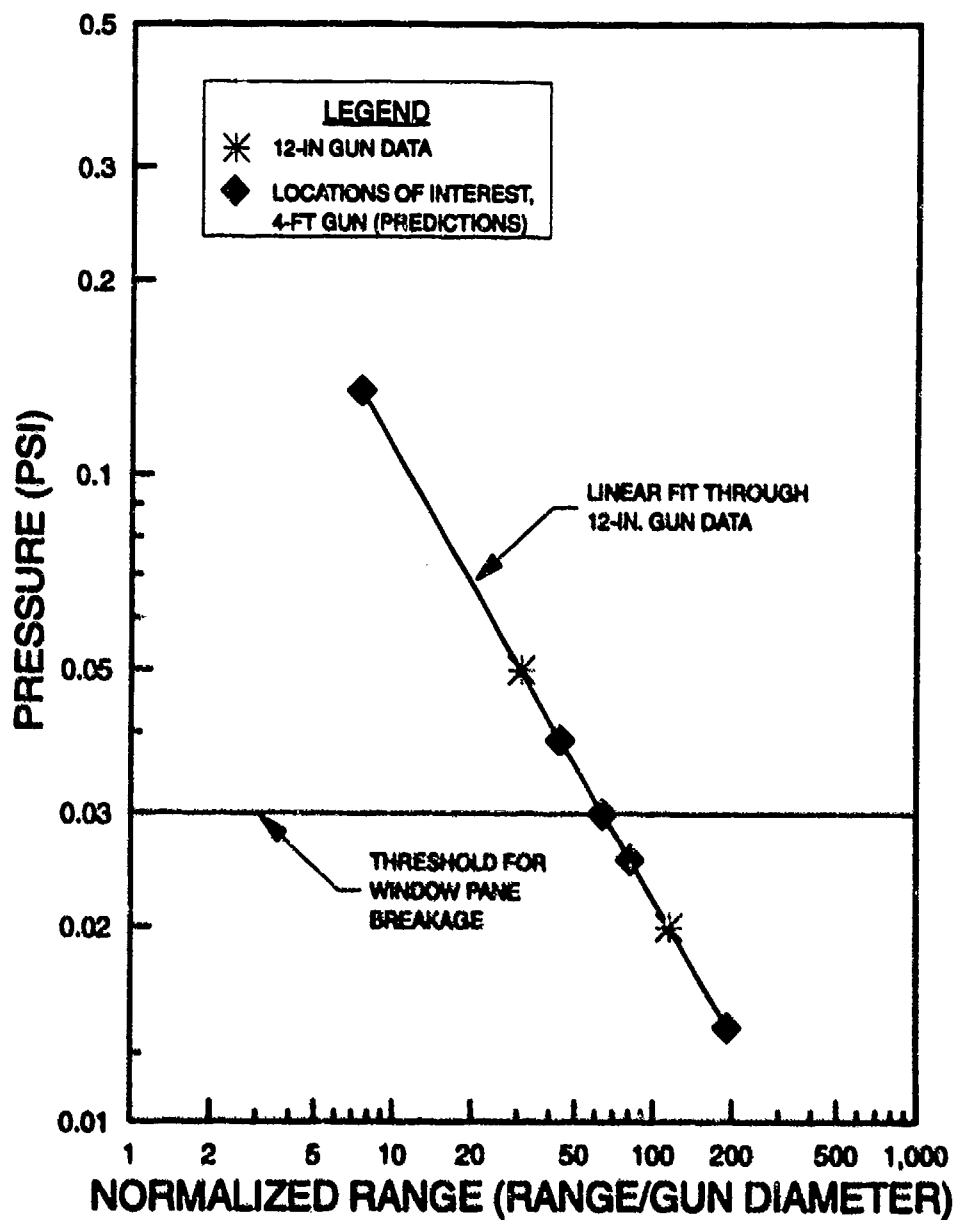


Figure 4-5. Airblast pressure measurements and predictions as a function of normalized range for gas gun testing.

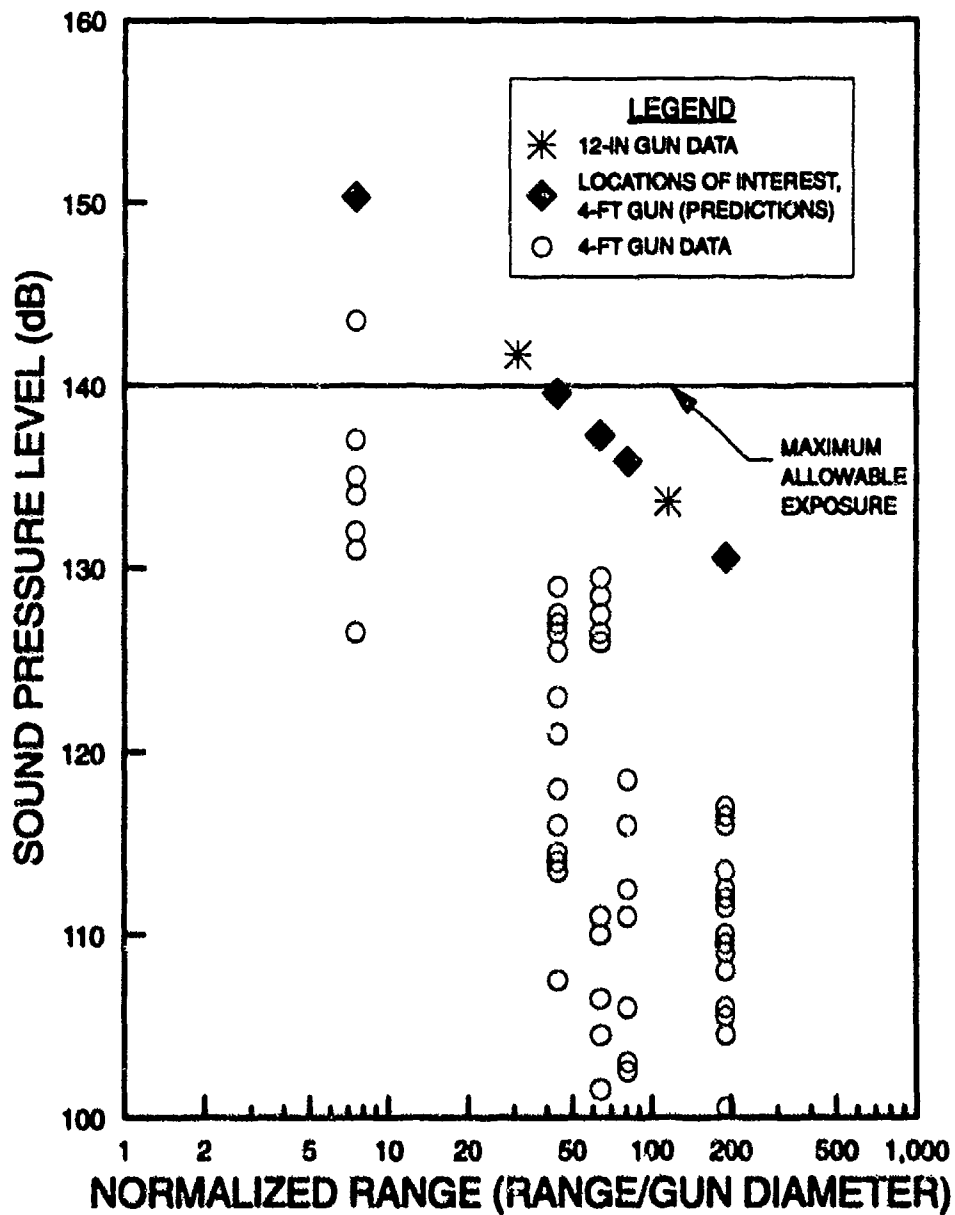


Figure 4-6. Measured and predicted sound pressure levels as a function of normalized range for the 4-ft gas gun tests.

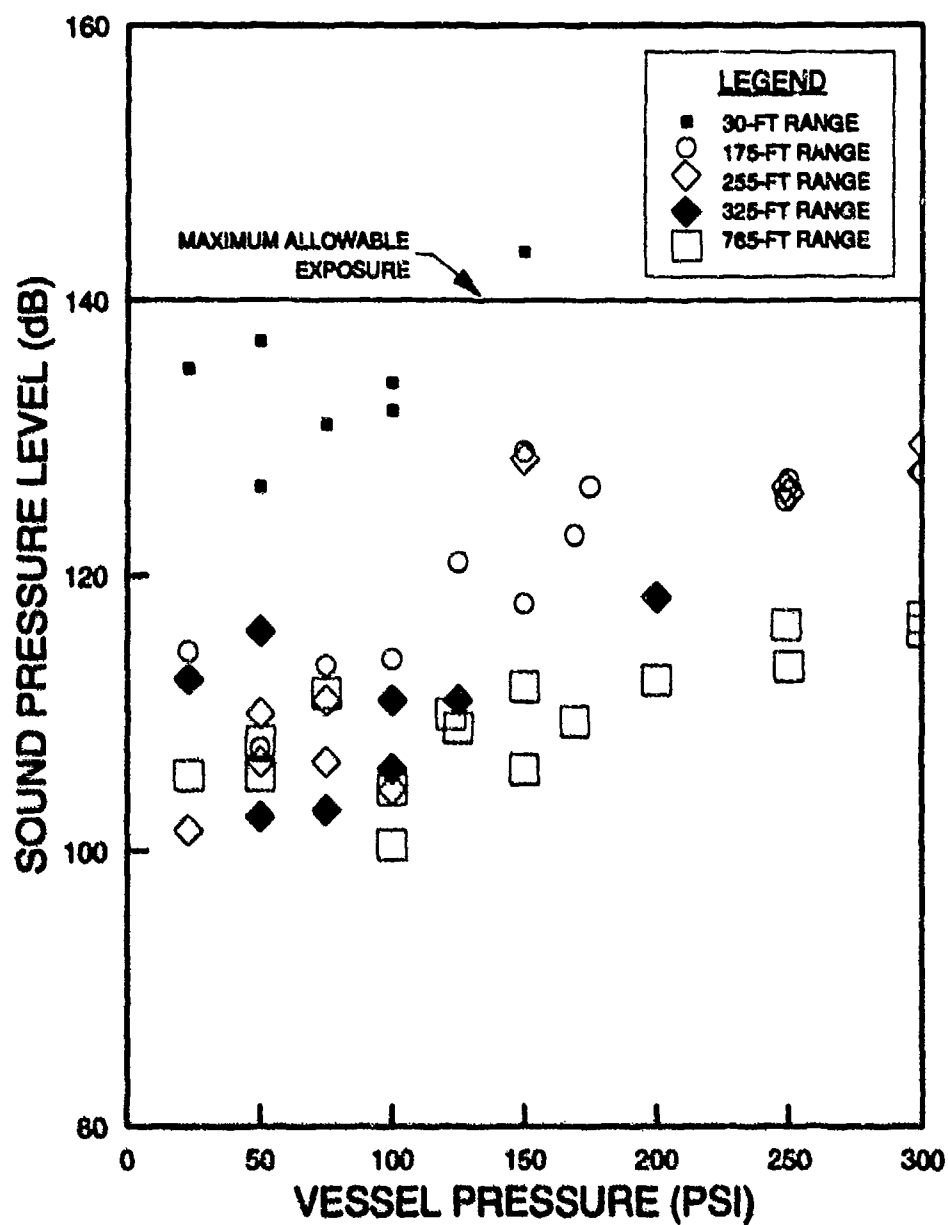


Figure 4-7. Measured sound pressure levels generated by the 4-ft gas gun as a function of vessel pressure, for various ranges of interest.

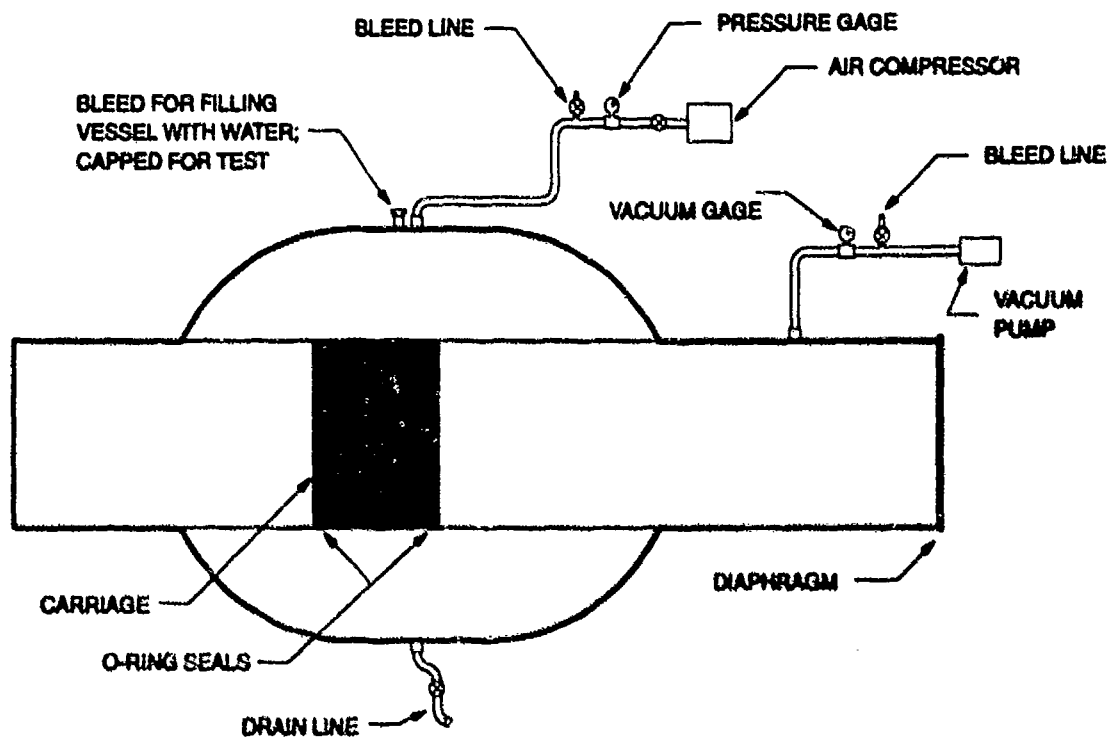


Figure 5-1. Test setup for initial hydrostatic and vacuum testing of the 4-ft gas gun.

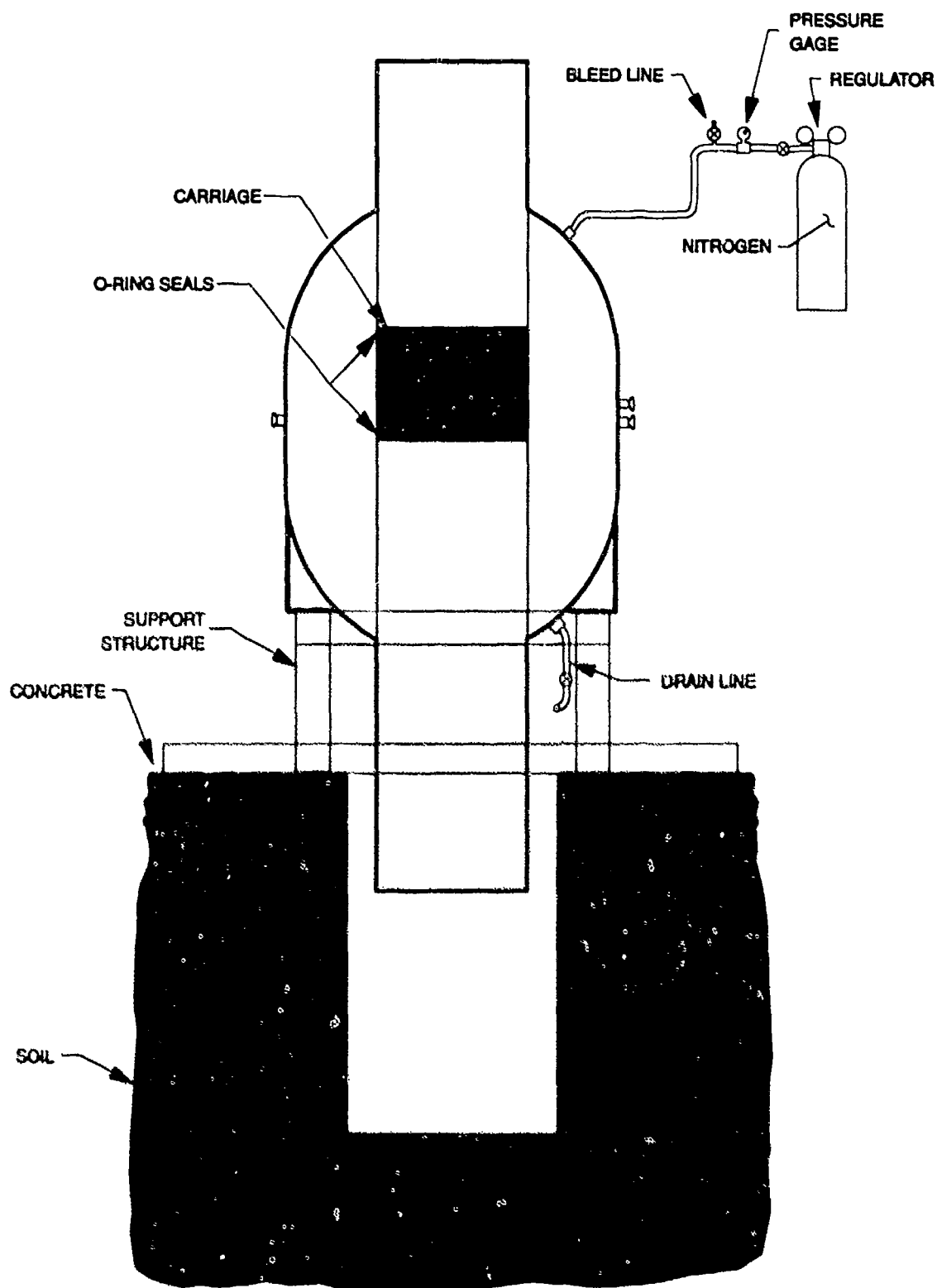


Figure 5-2. Test setup for high-pressure hydrostatic testing of the 4-ft gas gun.



Figure 5-3. Control panel used for operating the gas gun.

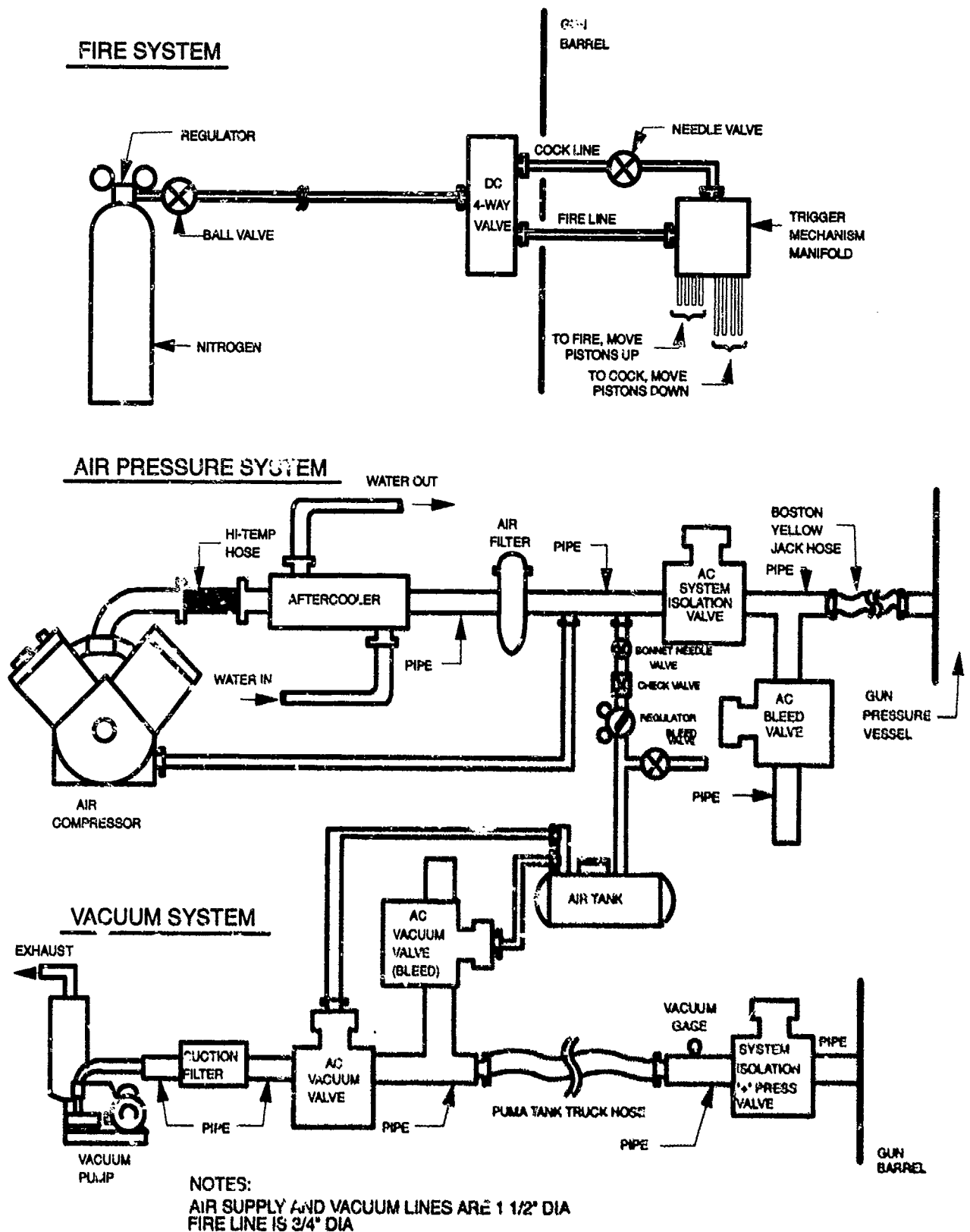


Figure 5-4. Schematic of the fill system used for conducting tests with the gas gun.

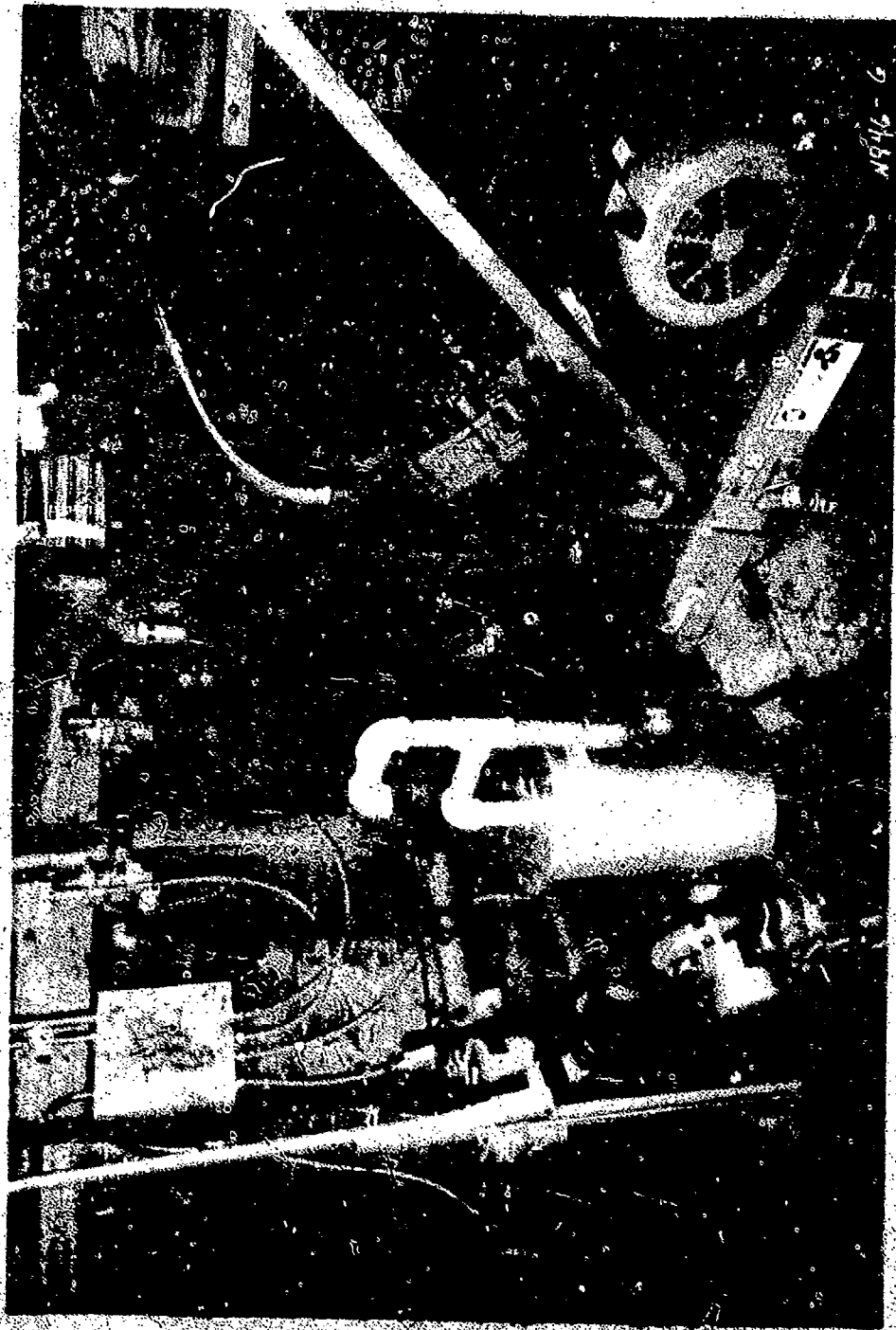


Figure 5-5. Components of the pressure and vacuum systems located in a shed adjacent to the 4-ft gas gun.



Figure 5-6. Photograph of target construction. Several 6 to 8 in. lifts of sand were placed in the target container.



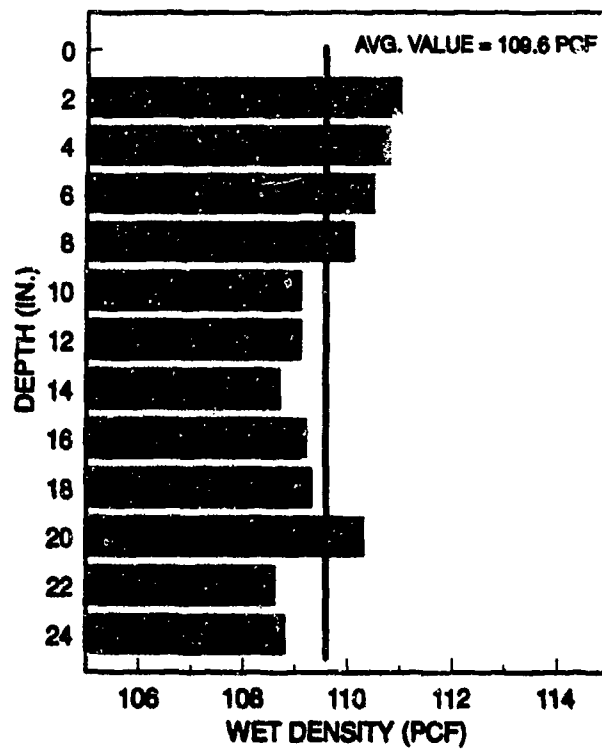
Figure 5-7. Photograph of personnel vibrating a lift of sand.



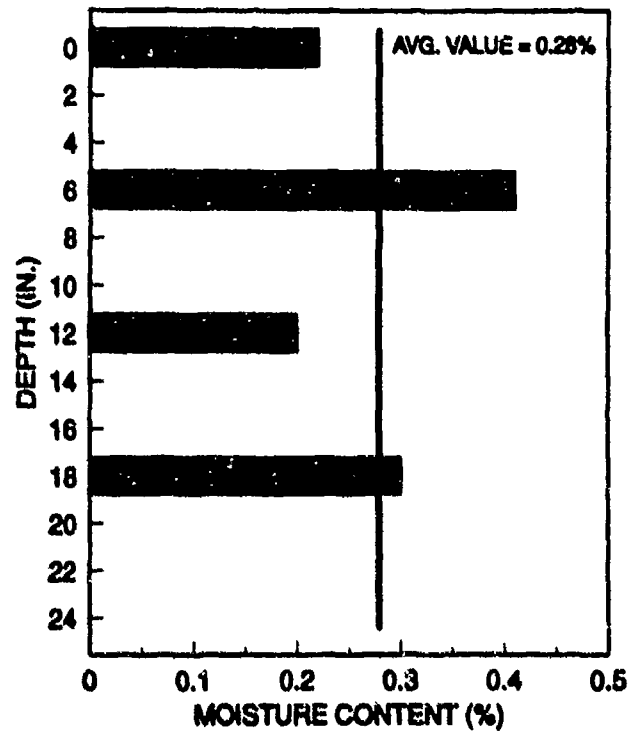
Figure 5-8. Photograph of the nuclear densitometer used to measure density through each lift of the target.



Figure 5-9. Photograph of personnel using a microwave oven to determine the moisture content of each lift of sand.



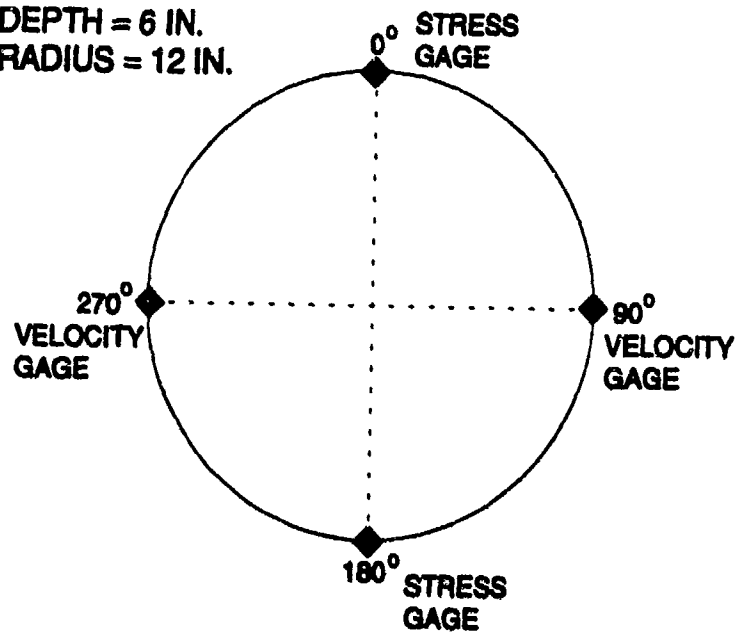
a. Profile of wet density



b. Profile of moisture content

Figure 5-10. Example density and moisture content profiles for a target tested with the gas gun.

DEPTH = 6 IN.
RADIUS = 12 IN.



DEPTH = 12 IN.
RADIUS = 6 IN.

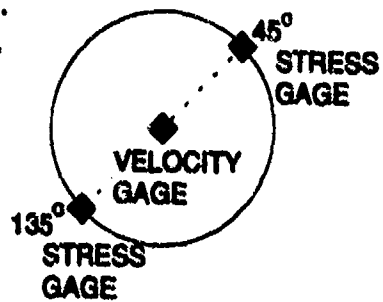


Figure 5-11. Typical layout for target instrumentation.



Figure 5-12. Photograph of personnel placing gages in the target.

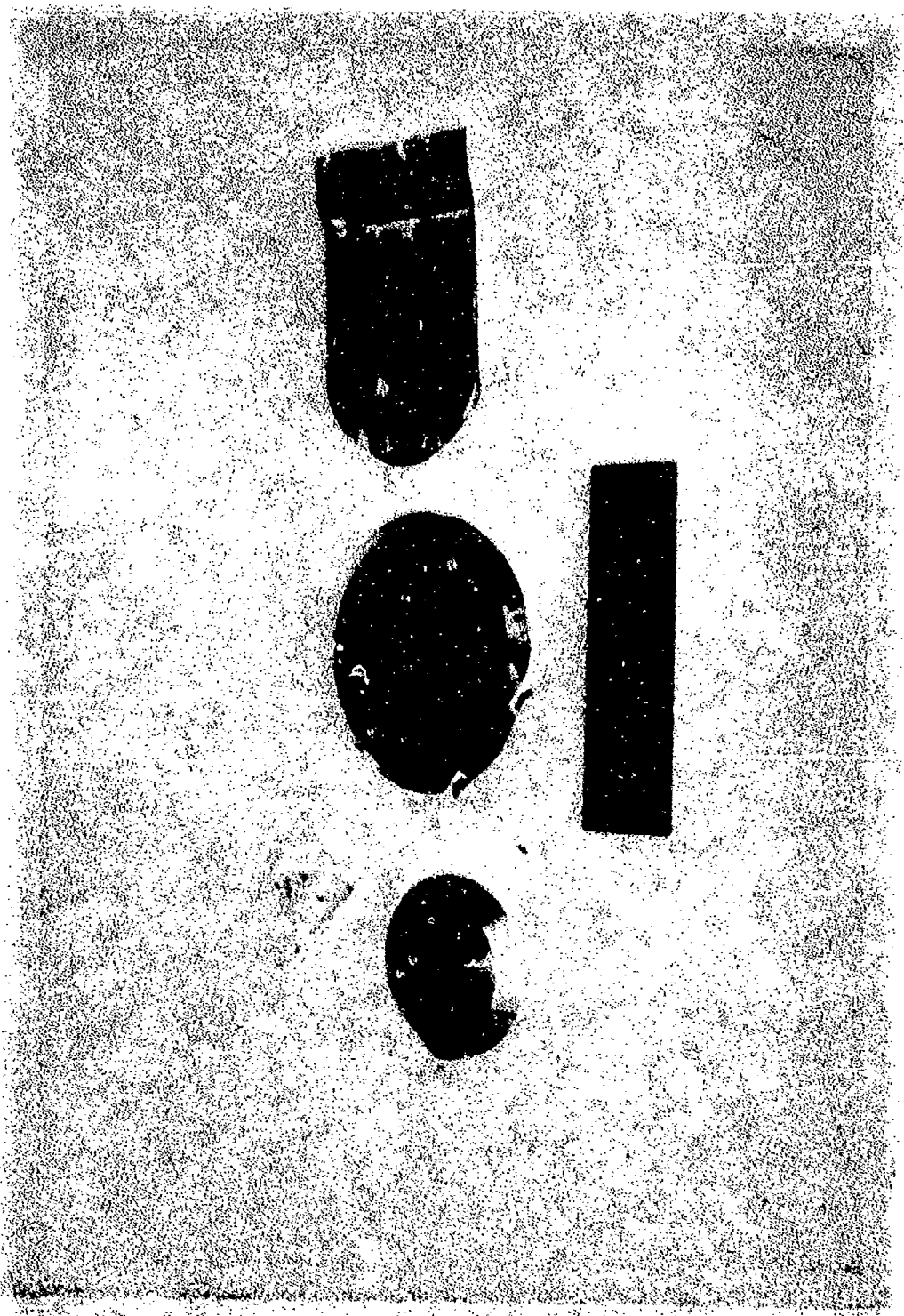


Figure 5-13. Stress, velocity, and TOA gages located at the 12-in. depth in a target.

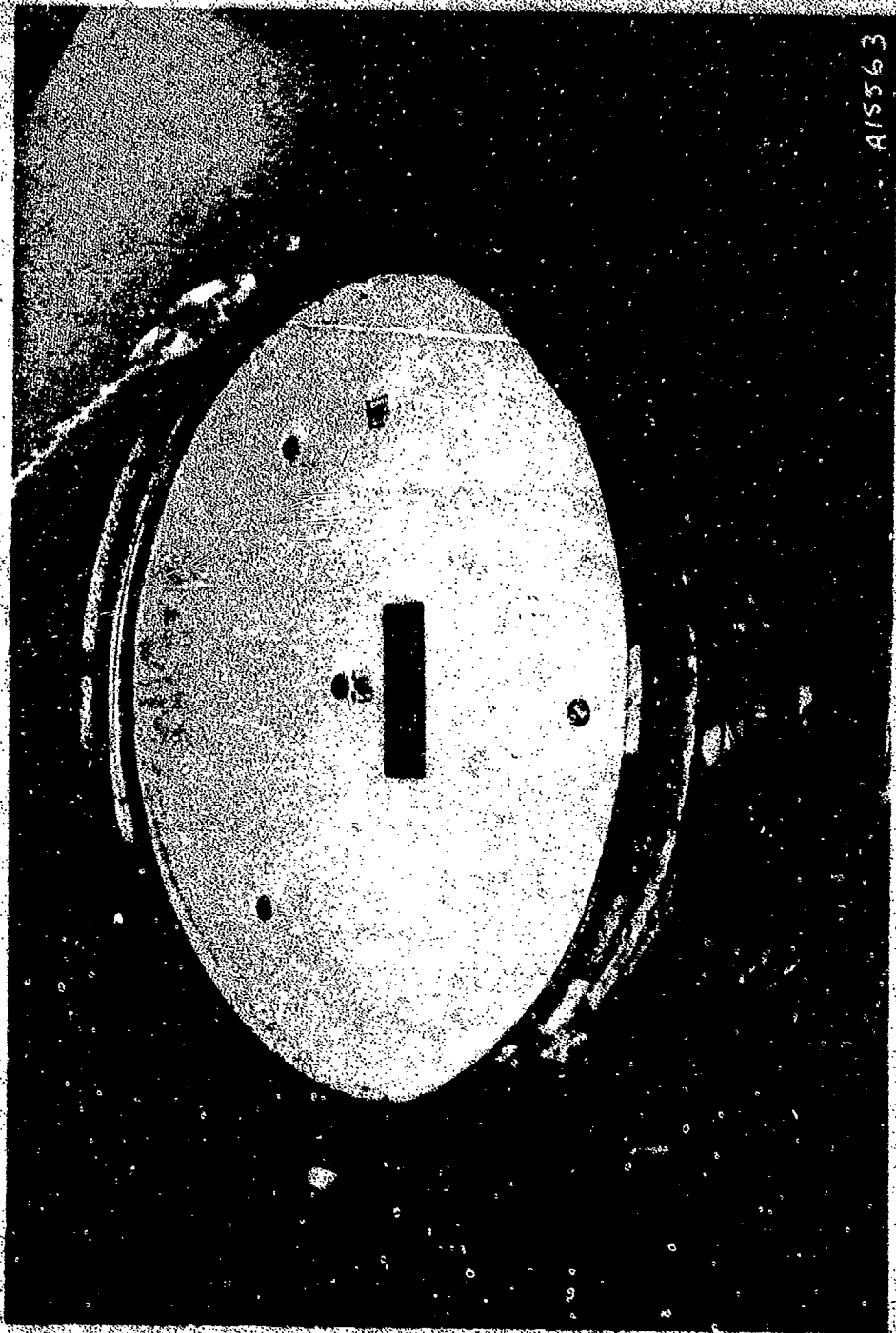


Figure 5-14. A completed target, ready to be relocated to the testing area.
Note: the circular gages at the surface receive piezoelectric pins used to measure impact velocity and planarity.

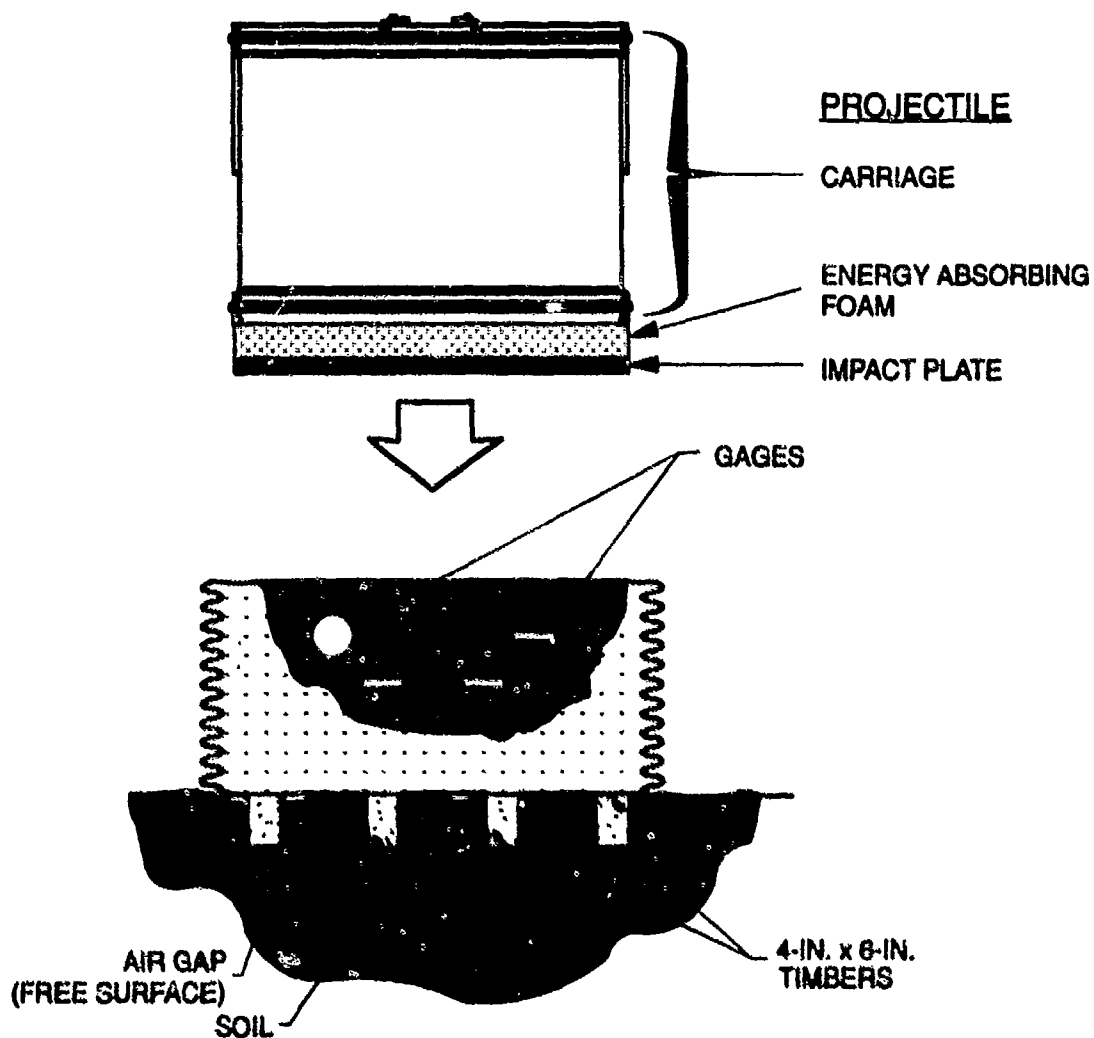


Figure 5-15. Cross section of the gas gun projectile and container of target material.

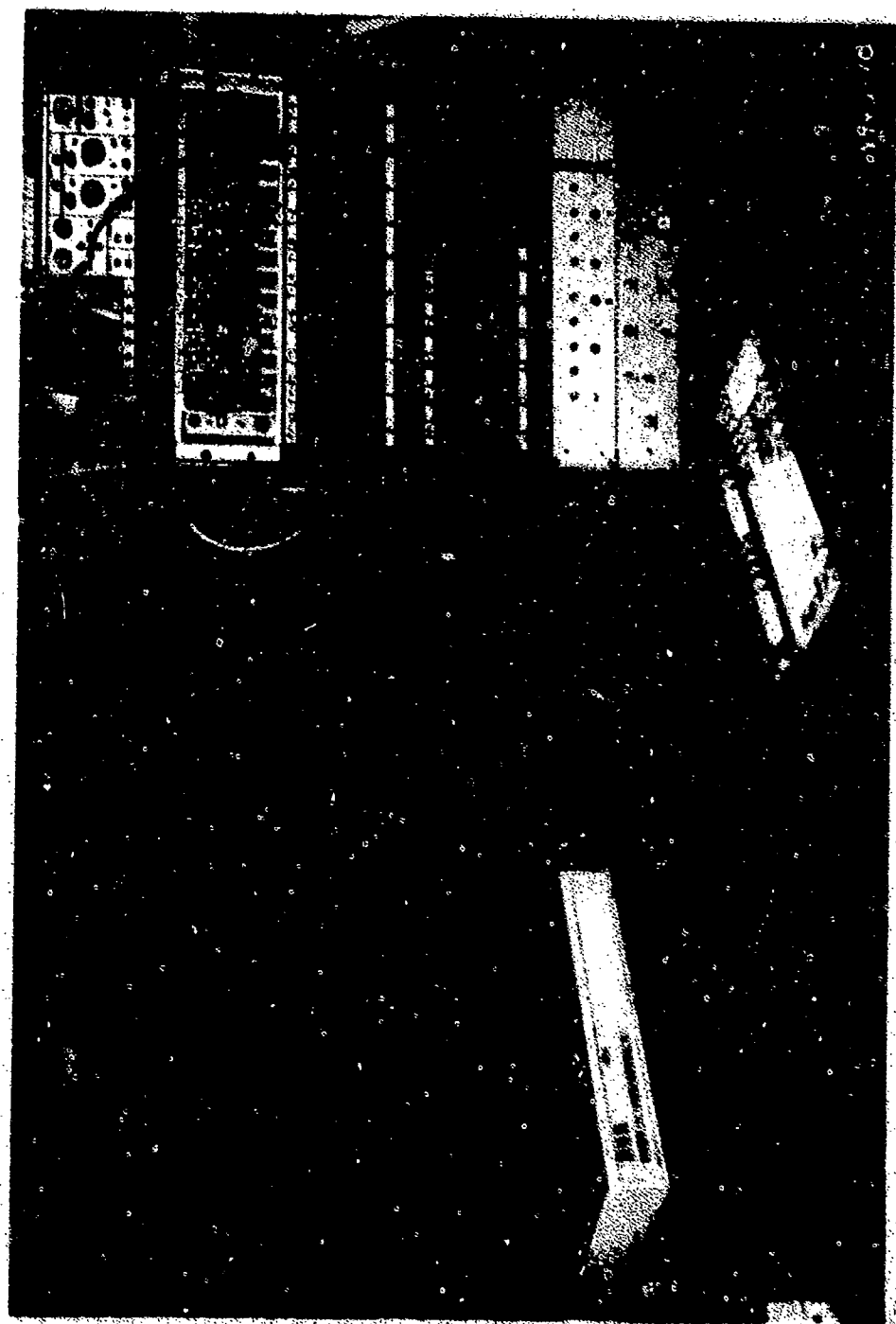


Figure 5-16. Recording equipment used for tests with the 4-ft gas gun.

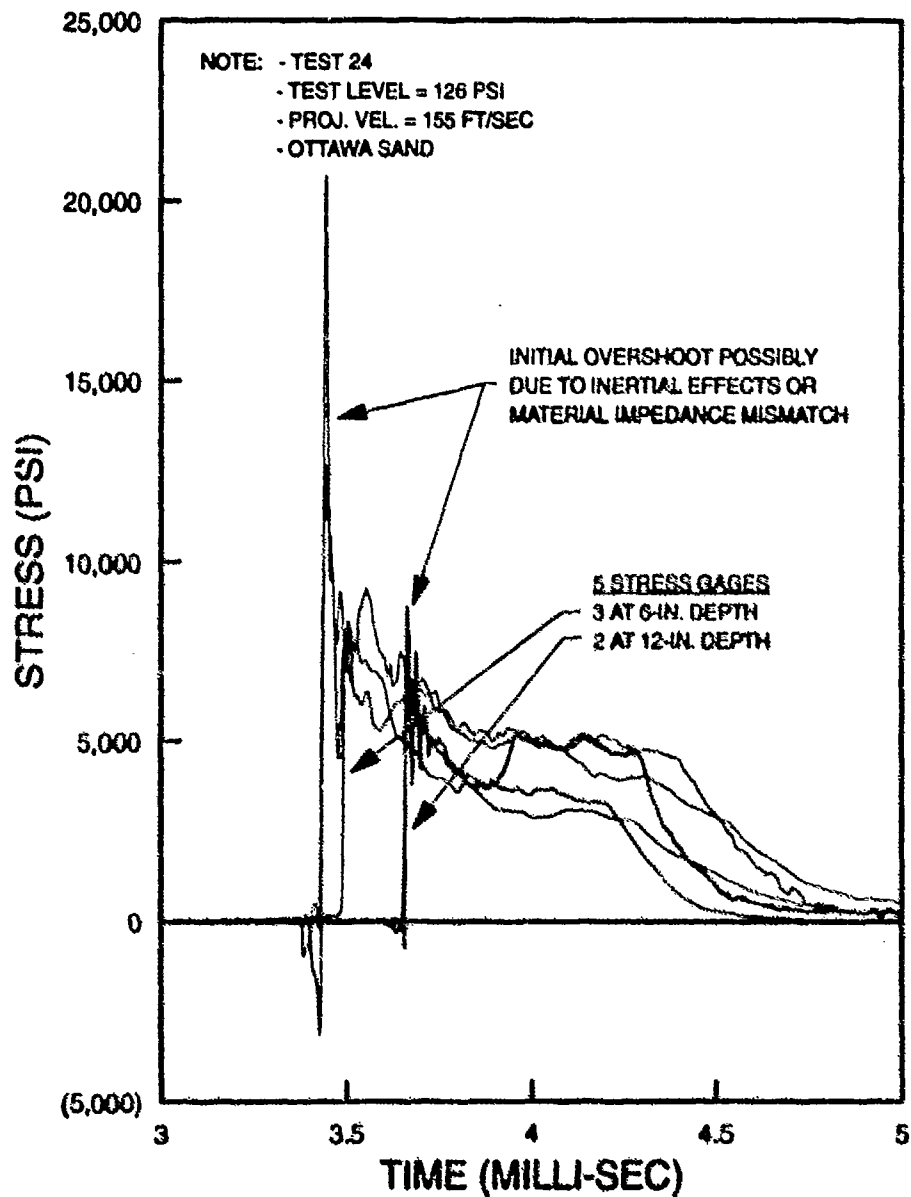


Figure 6-1. Stress measurements from Test 24 with the 4-ft gas gun. Data recorders were triggered at time $t=0$ sec.

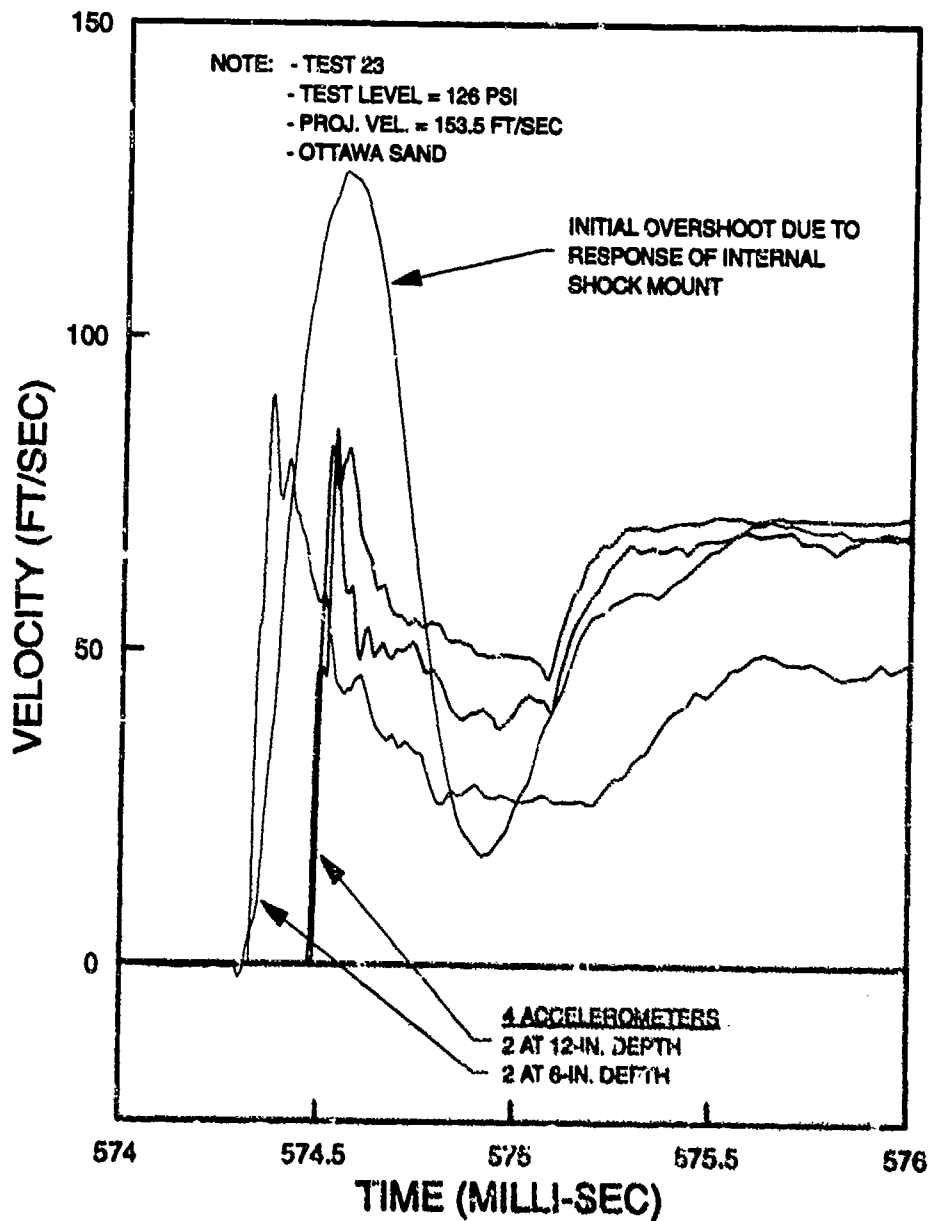


Figure 6-2. Velocity measurements from Test 23 with the 4-ft gas gun. Data recorders were triggered at time $t=0$ sec.

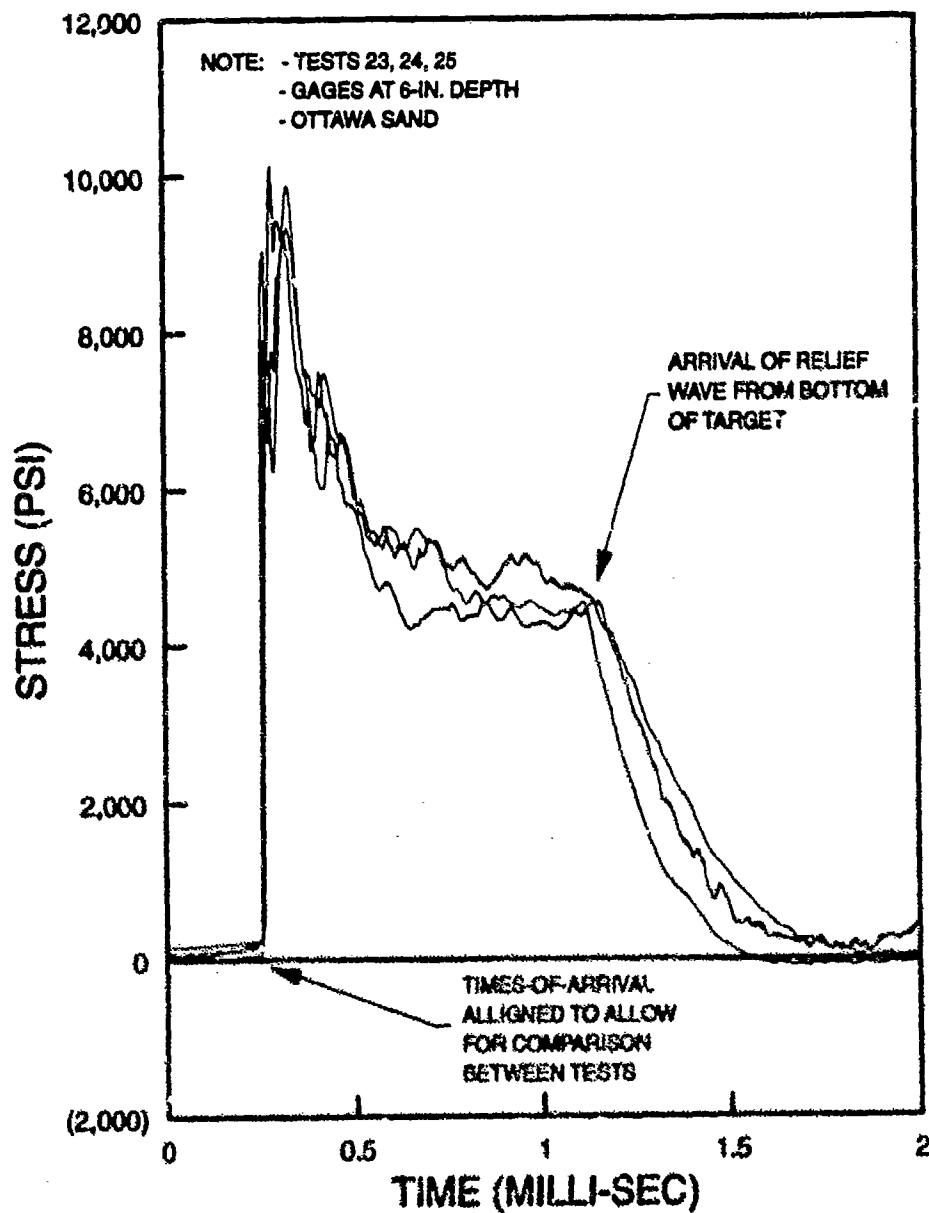


Figure 6-3. Stress measurements from three identical tests with the 4-ft gas gun, as monitored by a single type of stress gage.

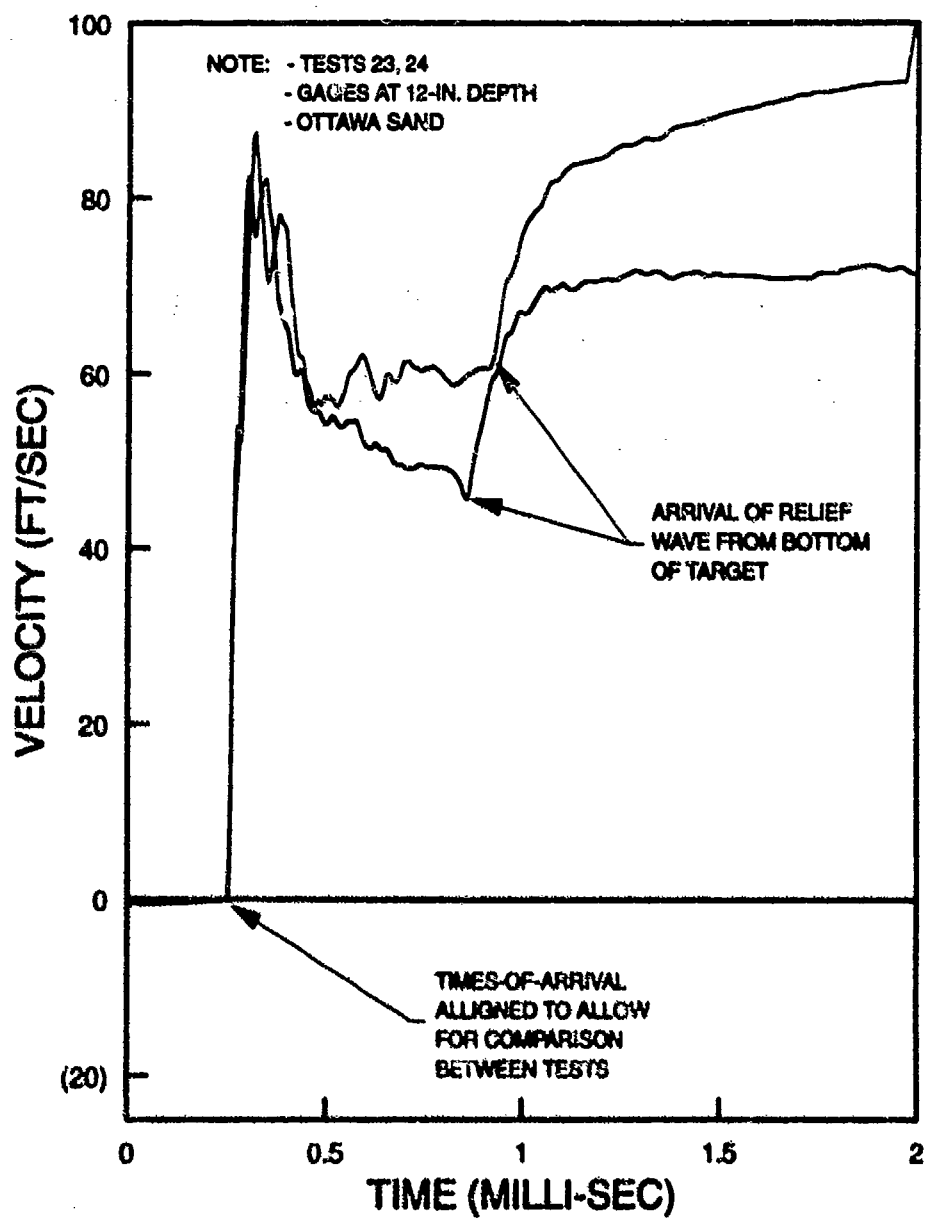


Figure 6-4. Velocity measurements from two identical tests with the 4-ft gas gun.

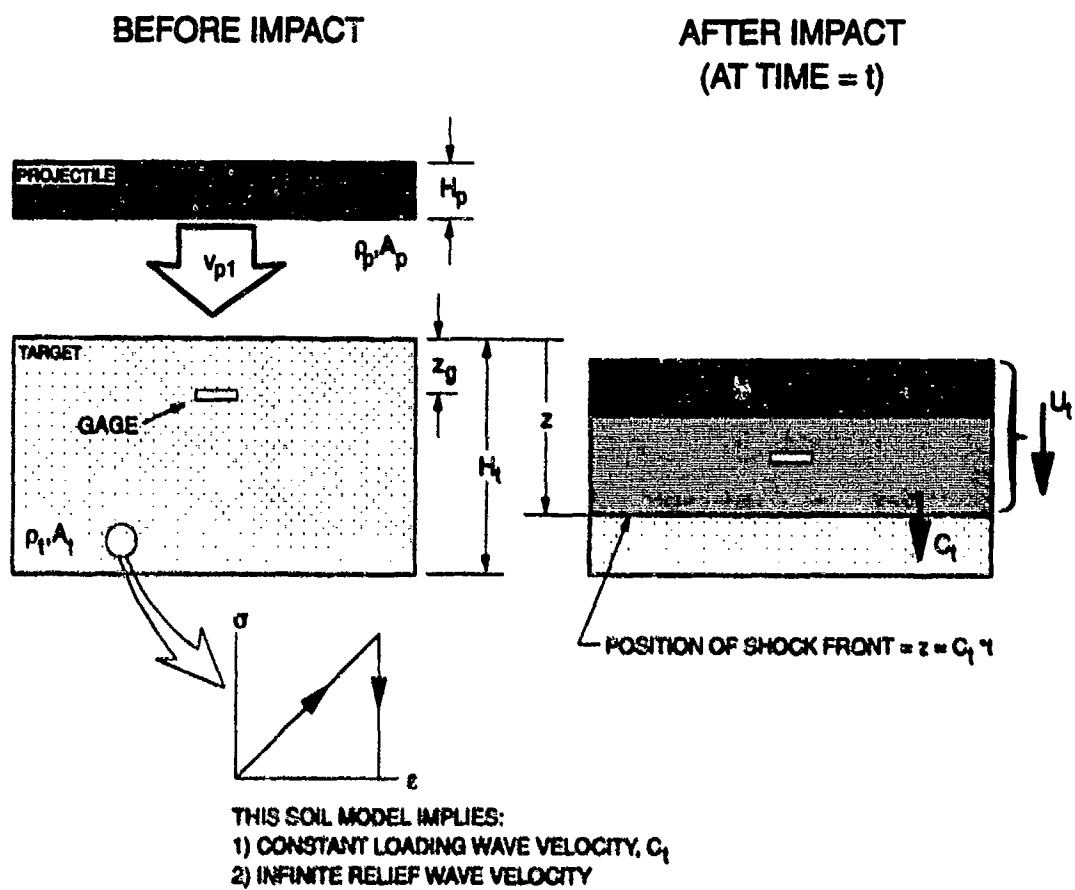


Figure 6-5. Projectile-soil interaction (PSI) model.

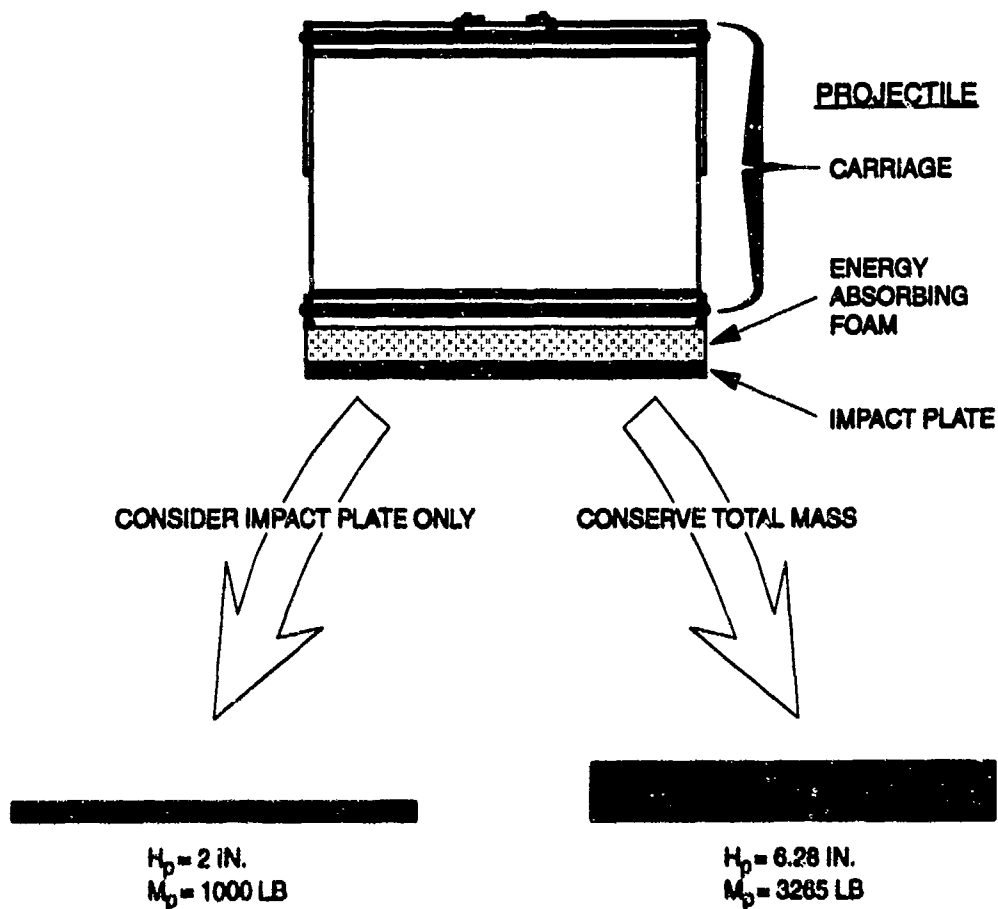


Figure 6-6. Schematic of lower and upper bounds on ways to represent the gas gun projectile in PSI model calculations.

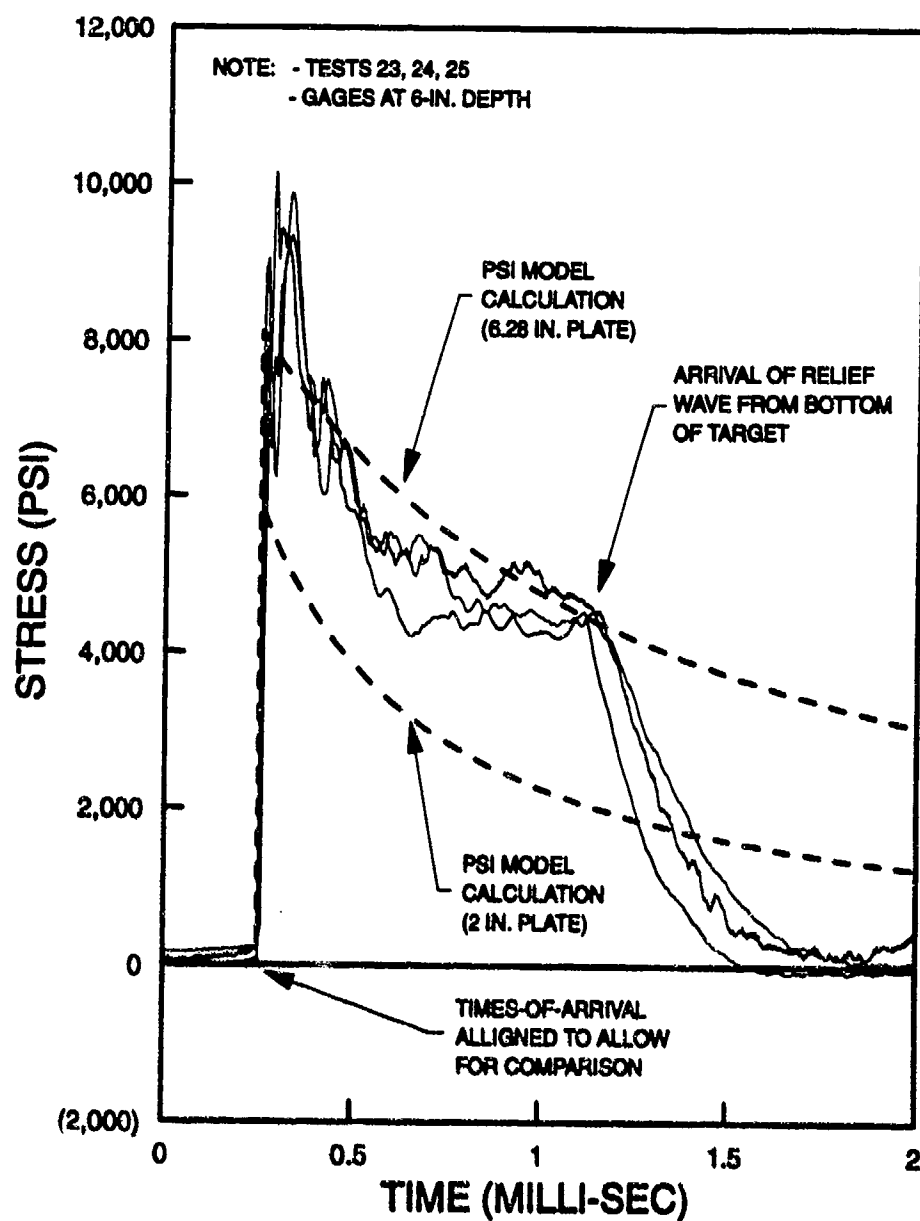


Figure 6-7. Comparison between the PSI model and stress data at the 6-in. depth in Ottawa sand targets.

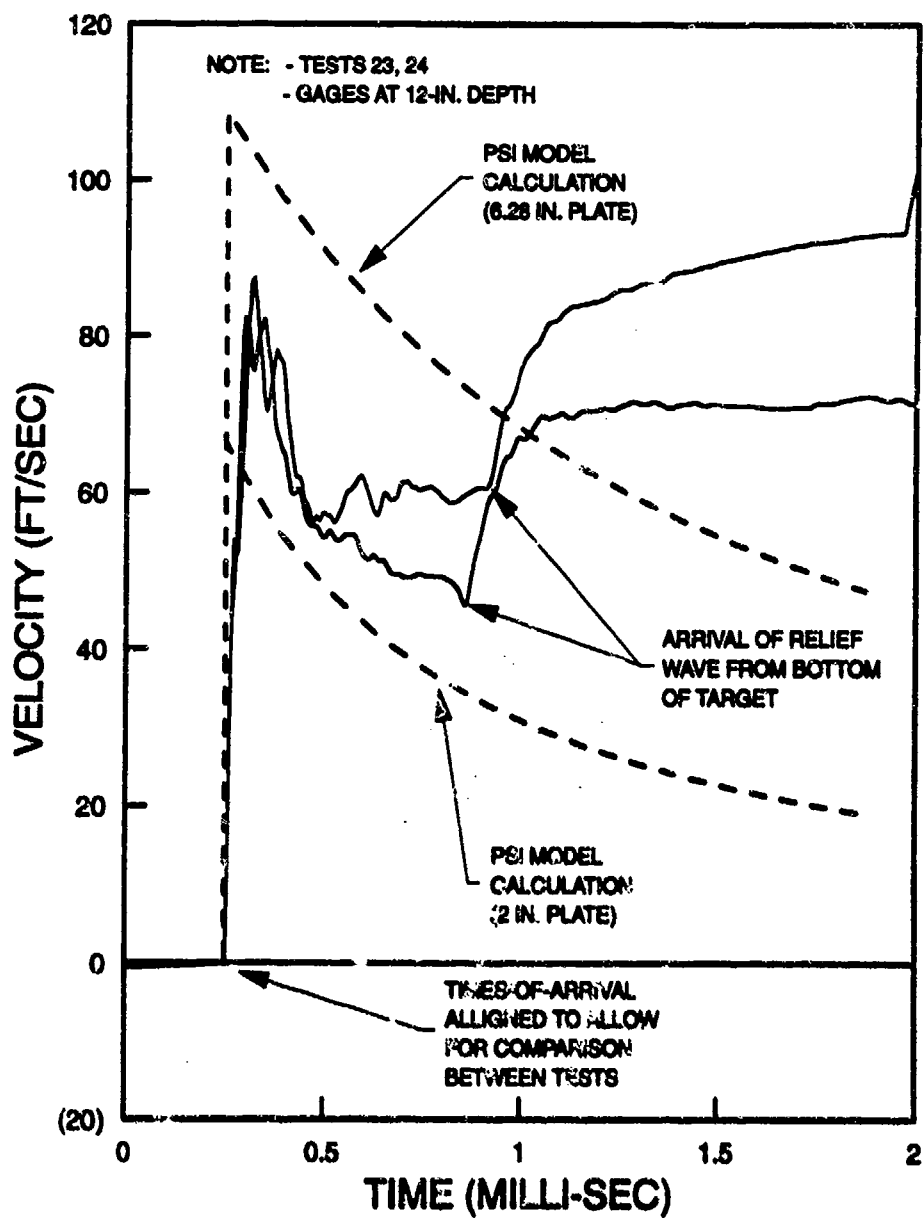


Figure 6-8. Comparison between the PSI model and velocity data at the 12-in. depth in Ottawa sand targets.

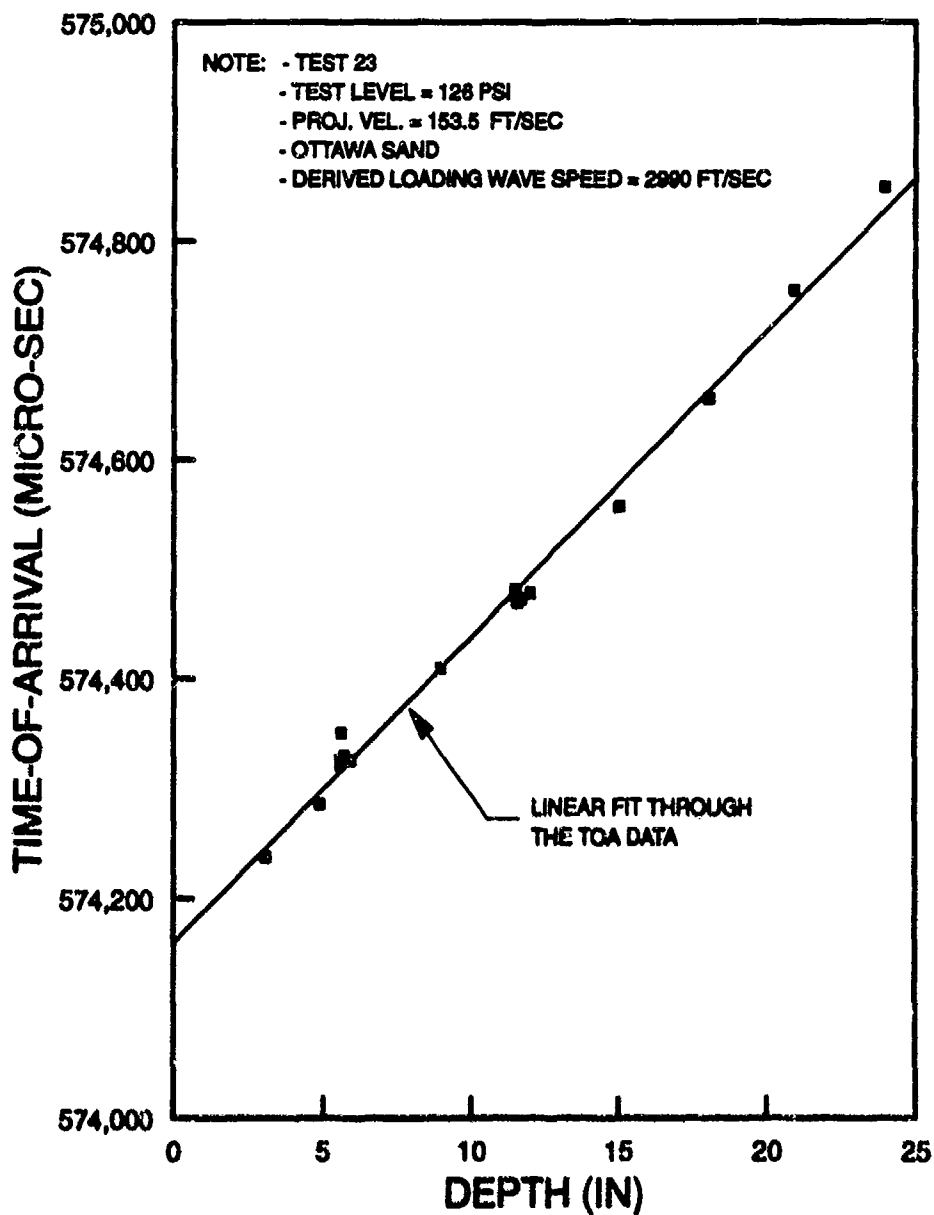


Figure 6-9. Time-of-arrival vs. depth, for Test 23, used to determine the propagation velocity of the loading shock wave.

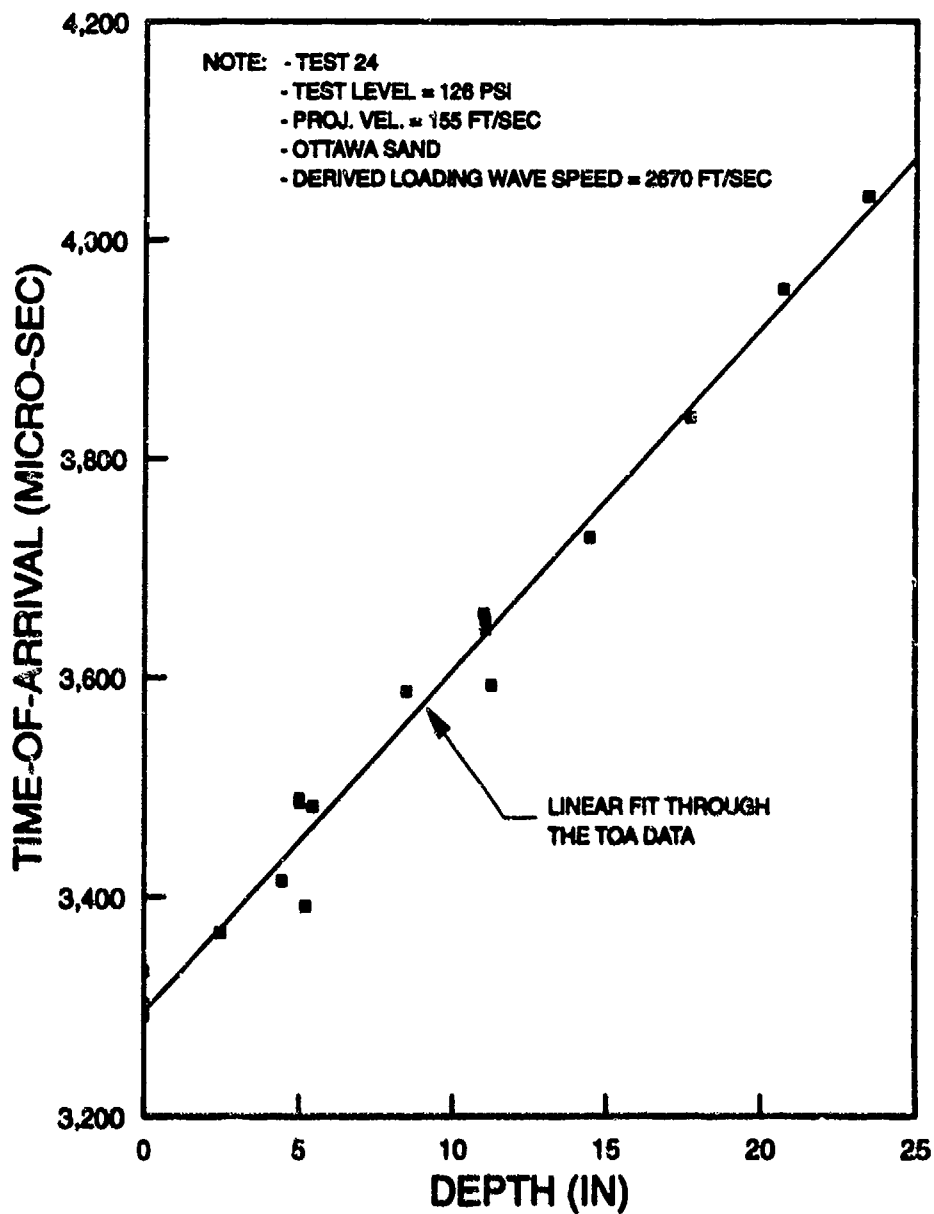


Figure 6-10. Time-of-arrival vs. depth, for Test 24, used to determine the propagation velocity of the loading shock wave.

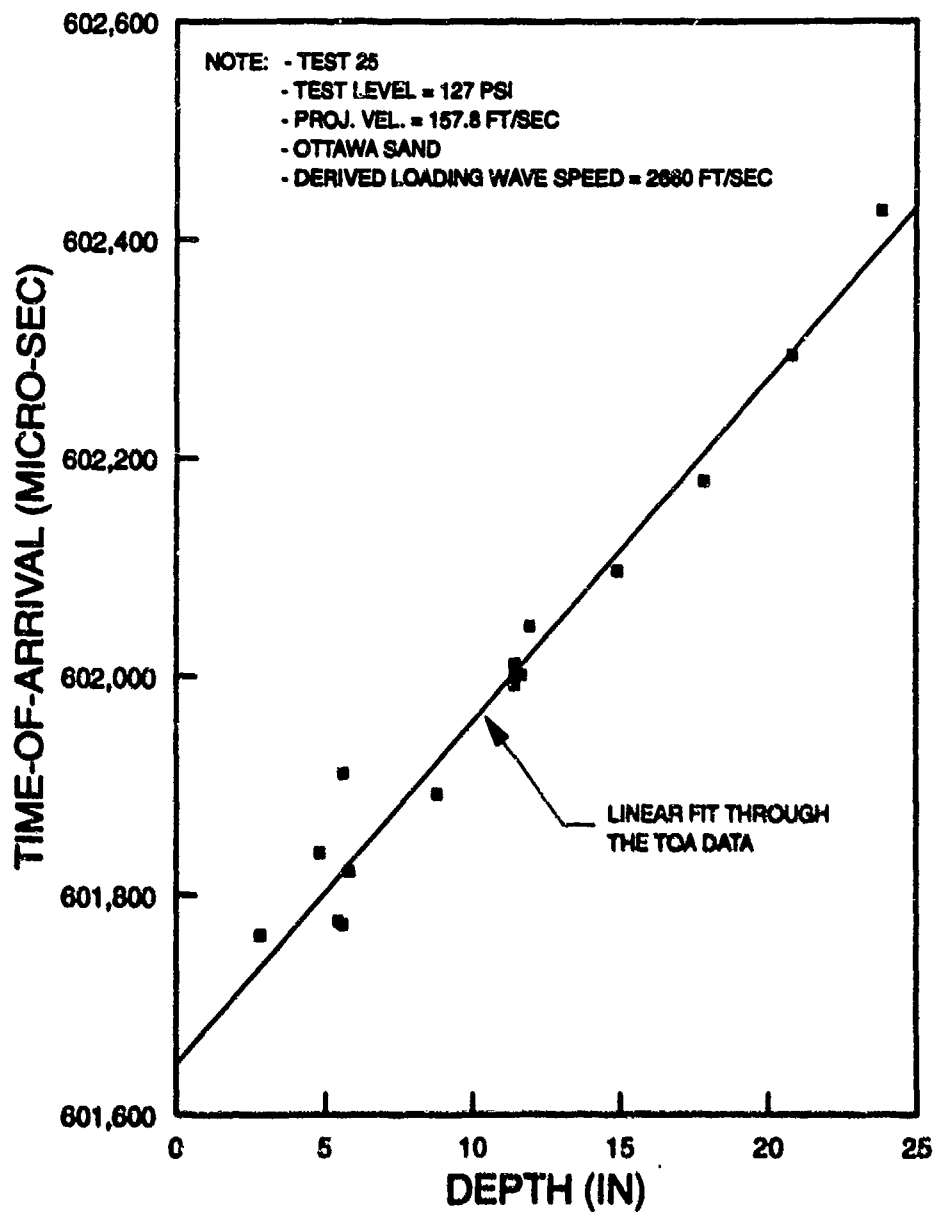


Figure 6-11. Time-of-arrival vs. depth, for Test 25, used to determine the propagation velocity of the loading shock wave.

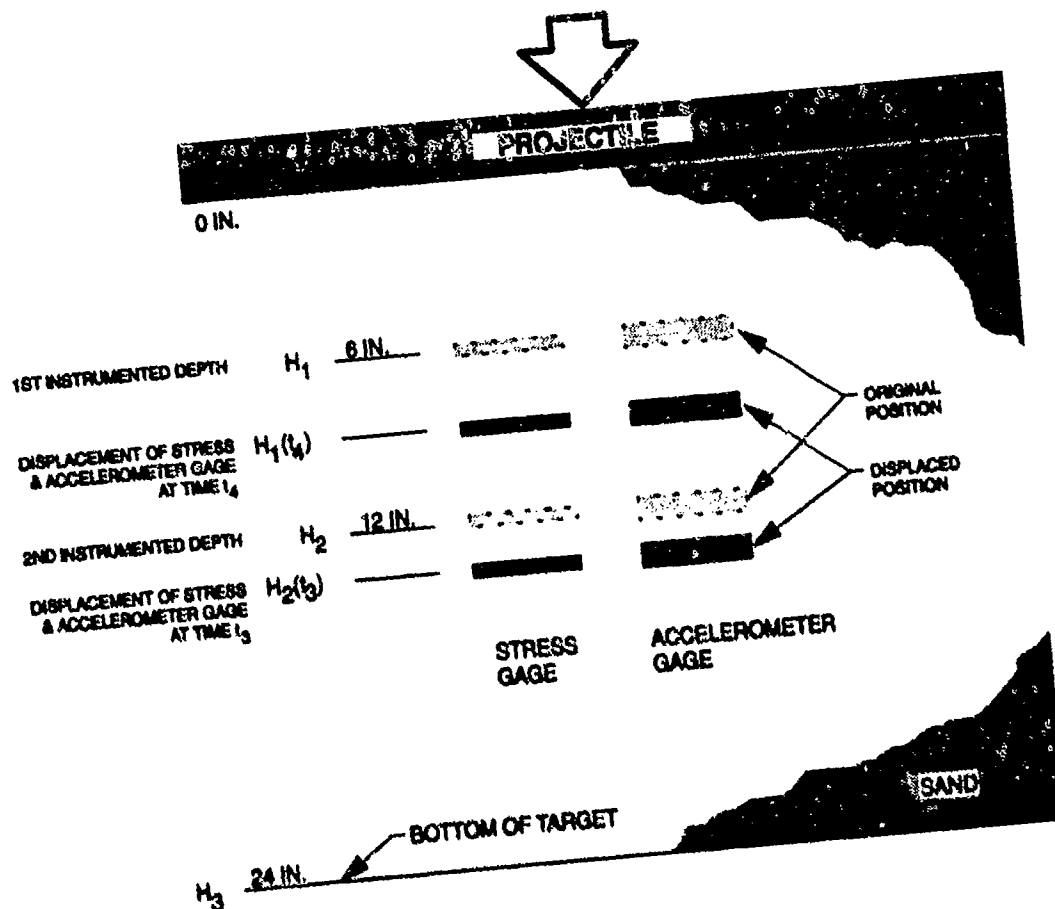


Figure 6-12. Schematic of canister positions at TOA of the loading and relief waves.

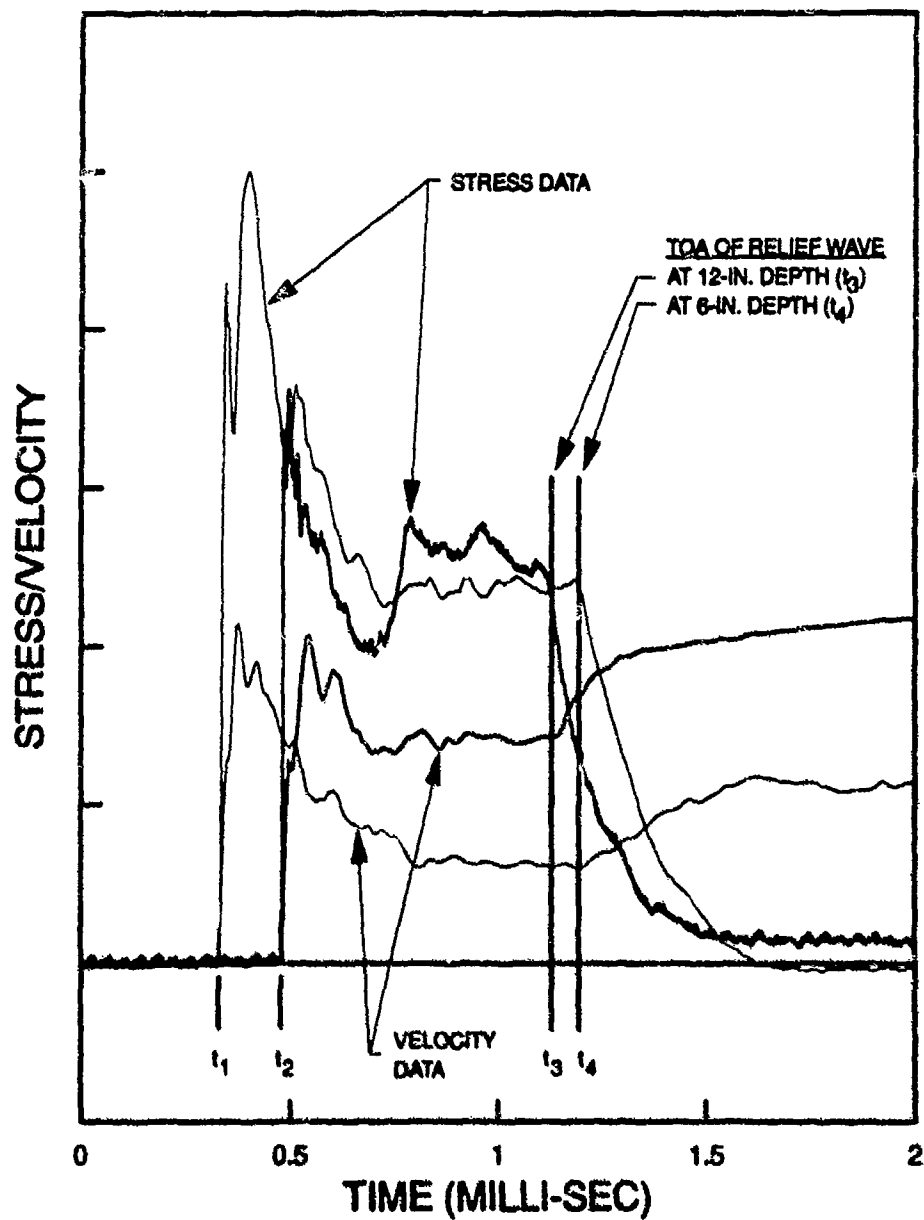


Figure 6-13. Stress and velocity measurements at the two instrumented depths, indicating the TOA of the loading (t_1 and t_2) and relief (t_3 and t_4) waves.

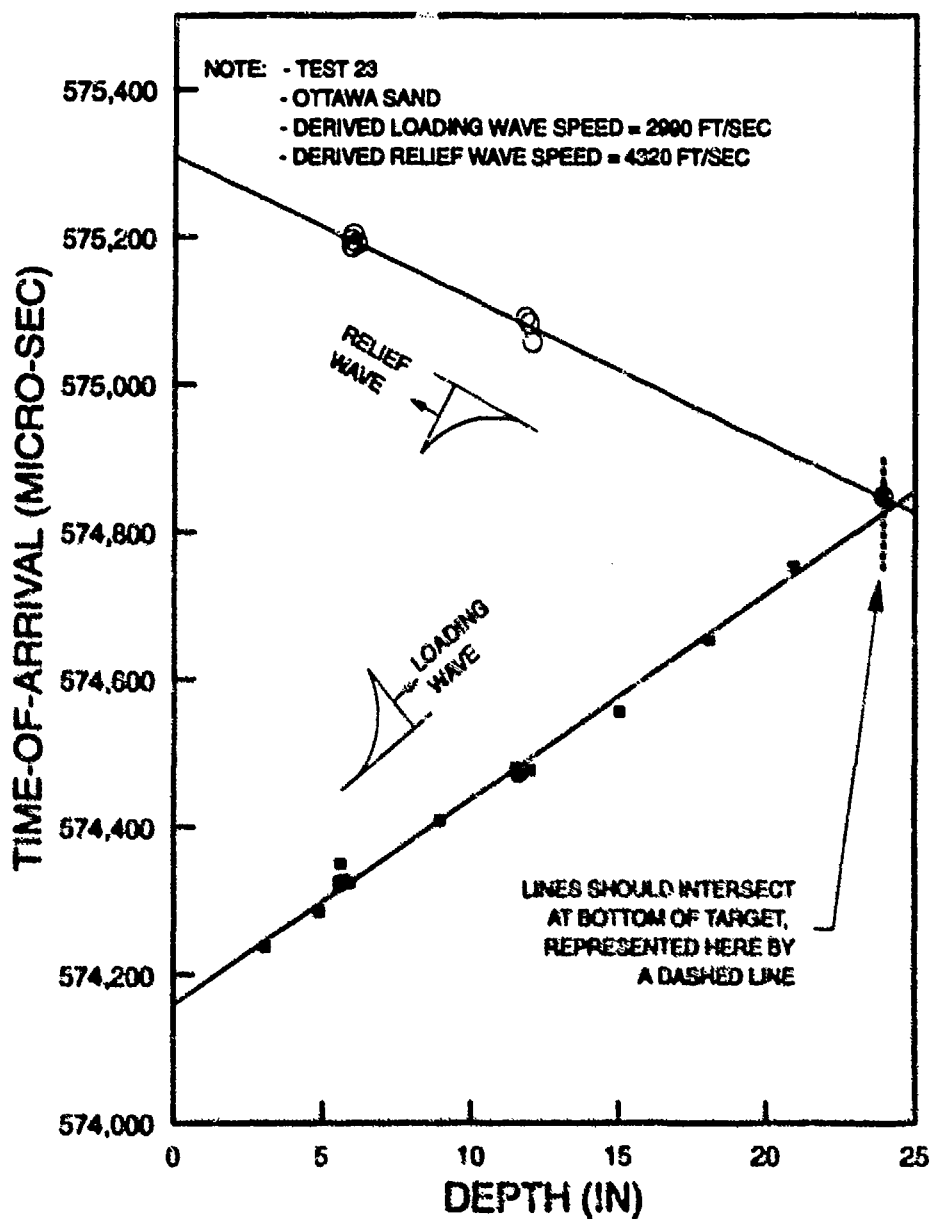


Figure 6-14. Graphical determination of the relief wave speed for Test 23.

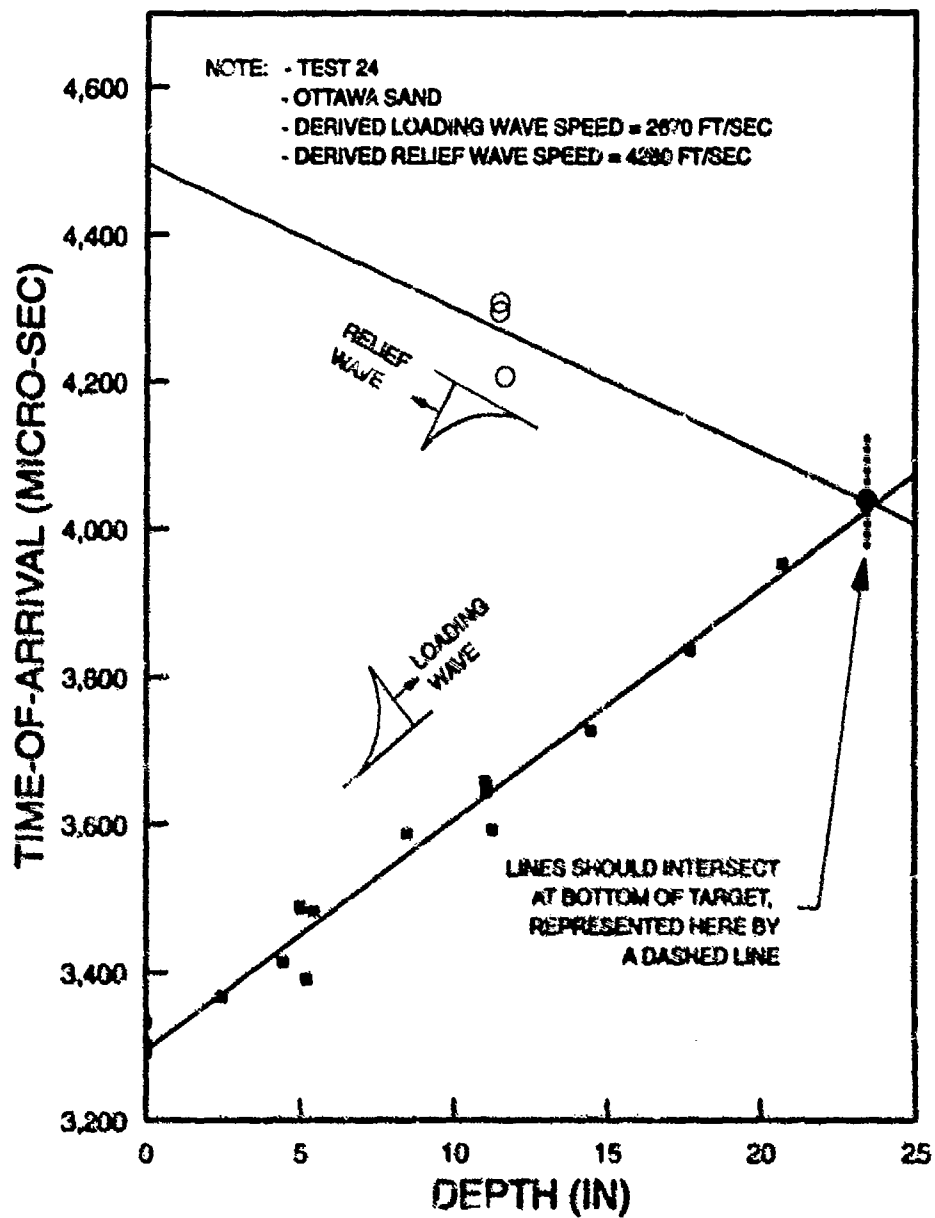


Figure 6-15. Graphical determination of the relief wave speed for Test 24.

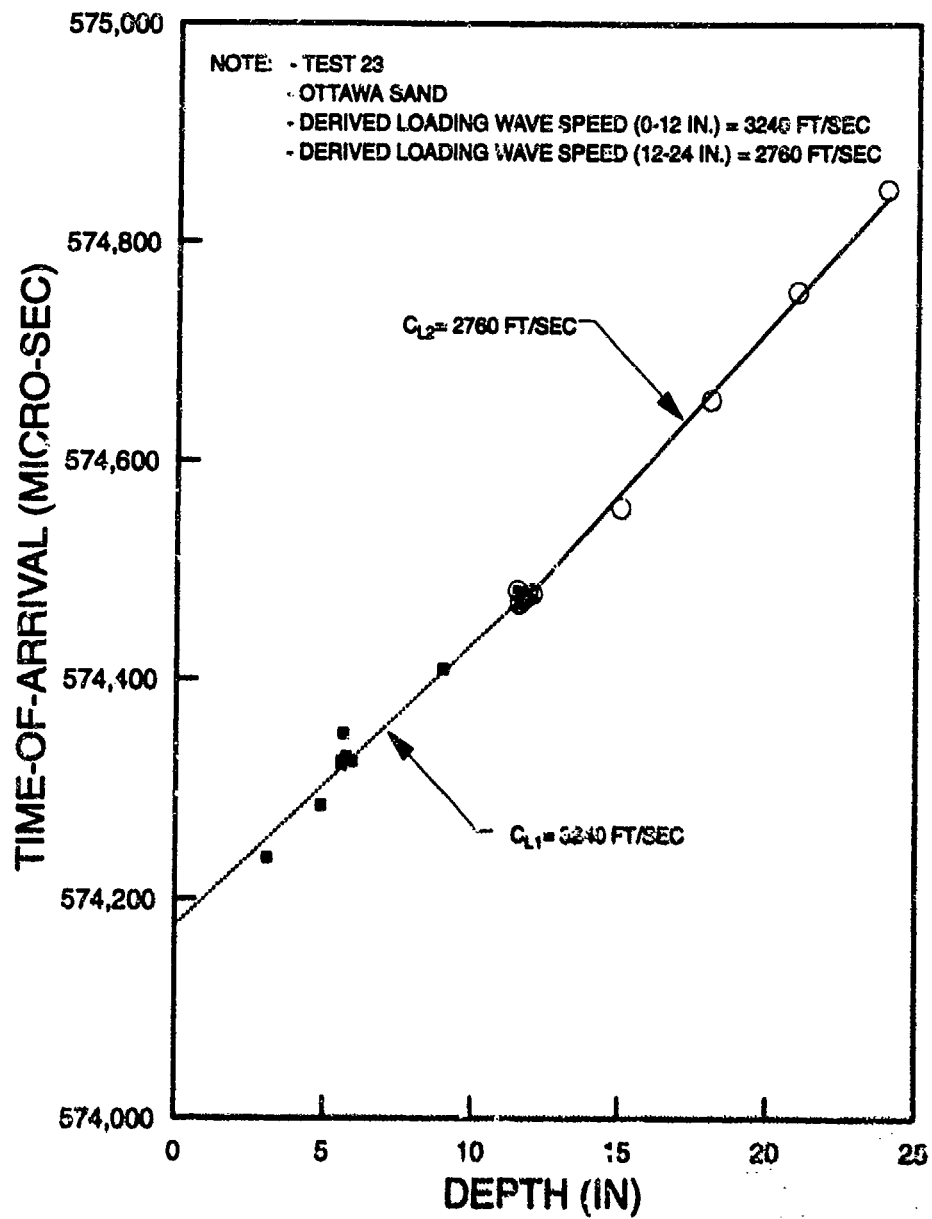


Figure 6-16. Determination of a varying loading wave speed through the depth of the target for Test 23.

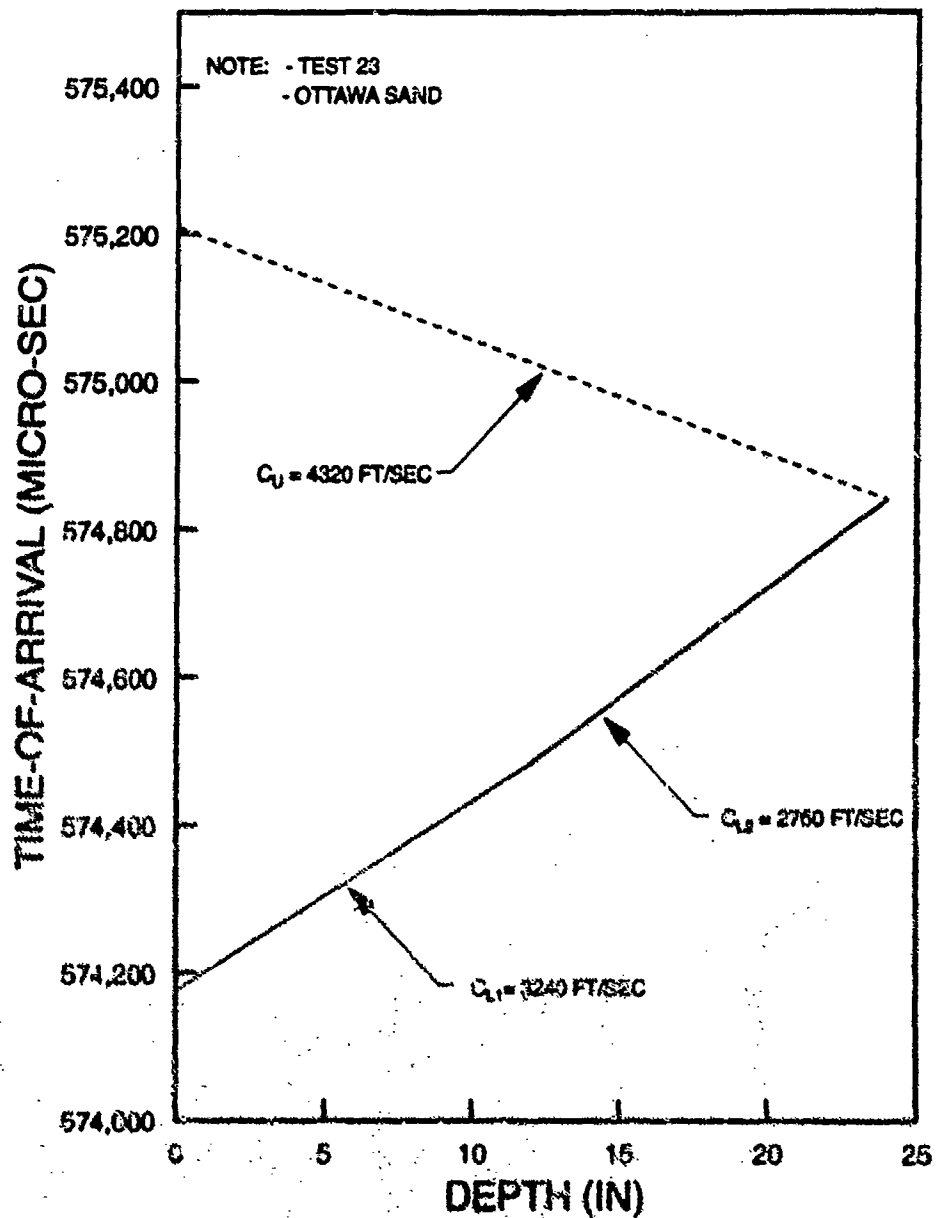


Figure 6-17. Loading and relief wave speeds used to determine a material model for Test 23.

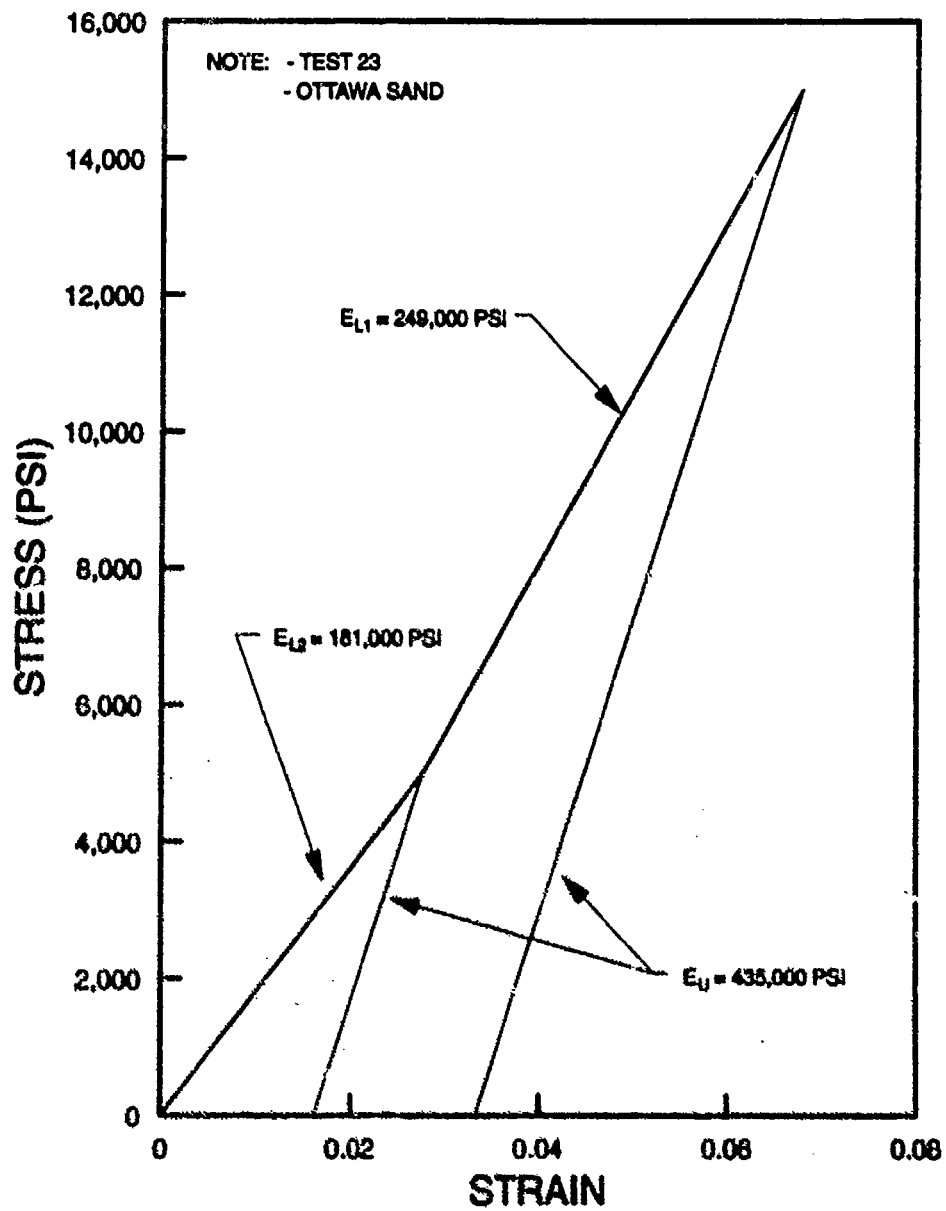


Figure 6-18. Material model for Ottawa sand, determined from TOA measurements in the target for Test 23.

REFERENCES

- Anderson, C. E., O'Donoghue, P. E., Renick, J. D., O'Kelley, D. K., and Felice, C. (1987). "Flyer Plate Impact of Dry Soils: An Instrumentation Calibration Technique." Proceedings of the Defense Nuclear Agency Instrumentation for Nuclear Weapons Effects Testing (INWET) Conference, 6-8 October 1987. Defense Nuclear Agency, Alexandria, VA 22310-3398.
- Blaster's Handbook, 16 ed. (1980). E. I. du Pont de Nemours & Co., Wilmington, Delaware.
- EM 385-1-1 (1987). Safety and Health Requirements Manual. US Army Corps of Engineers, Washington, DC 20314-1000.
- Federal Register, May 29, 1971.
- Germain, L. (1993). "Borehole Correction Factors." Proceedings of the Defense Nuclear Agency Verification Technology - HYDRO-PLUS Ground Shock Measurement Technology and Yield Determination (VERITECH) Symposium, 2-4 February, 1992, Volume 1 - Unclassified Papers, DASIAC TR-92-002-V1, Defense Nuclear Agency, Alexandria, VA 22310-3398.
- Gibson, L. J., and Ashby M. F. (1988). Cellular Solids. Structure & Properties. Pergamon Press, New York.
- Gilbert, P. A. (1988). "Computer Controlled Microwave Oven System for Rapid Water Content Determination." WES Technical Report GL-88-21, USAE Waterways Experiment Station, Vicksburg, MS 39180-6199.
- Gilbert, P. A. (1990). "Computer-Controlled Microwave Drying of Potentially Difficult Organic and Inorganic Soils." WES Technical Report GL-90-26, USAE Waterways Experiment Station, Vicksburg, MS 39180-6199.
- Gould, K. (1990). "Guide to Nuclear Weapons Effects Simulation Facilities and Techniques (1990 Edition)." Technical Report DASIAC SR-90-252, Defense Nuclear Agency, Alexandria, VA 22310-3398.
- Henry, F. (1991). "General Plastics Last-A-Foam FR-3700 for Crash & Fire Protection of Nuclear Material Shipping Containers." General Plastics Manufacturing Company, Tacoma, WA 98409.
- Ingram, J. K. (1968). "Development of a Free-Field Soil Stress Gage for Static and Dynamic Measurements." WES Technical Report 1-814, USAE Waterways Experiment Station, Vicksburg, MS 39180-6199.

Joachim, C. E. (1985). Unpublished design calculations and sketches on the 12-in. diameter vertical gas gun. USAE Waterways Experiment Station, Vicksburg, MS 39180-6199.

Joachim, C. E., Welch, C. R. (1985). "Design and Experience with the WES 10-Kbar Airblast and Stress Gages." Shock and Vibration Bulletin 55, Part 2, The Shock and Vibration Information Center, Naval Research Laboratory, Washington, DC.

King, P. K. (1992). "Study of Gage/Borehole Inclusion Effects." Briefing to FC/DNA (Dr. Eric Rinehart), USAE Waterways Experiment Station, Vicksburg, MS 39180-6199.

Kinsler, L. E., Frey, A. R., Coppens, A. B., and Sanders, J. V. (1982). Fundamentals of Acoustics, 3rd ed. Wiley, New York.

Landry, M. (1994). "High Bandwidth Fiber Optic Accelerometer." Proceedings of the Defense Nuclear Agency Instrumentation for Nuclear Weapons Effects Testing (INWET) Conference, 2-5 November 1993. Defense Nuclear Agency, Alexandria, VA 22310-3398.

Langefors, U., Westerberg, H., Kihlström, B. (1958). "Ground Vibrations in Blasting," Water Power.

Miller, R. E. (1990). Personal communication with Prof. R. E. Miller, Department of Theoretical and Applied Mechanics, University of Illinois, during H. G. White's thesis proposal presentation.

McPherson, J. A. (1989). "Blasting Vibration Damage and Noise Prediction and Control." Engineer Technical Letter 1110-1-142, U.S. Army Corps of Engineers.

Nicholls, H. R., Johnson, C. F., and Duvall, W. I. (1971). "Blasting Vibrations and Their Effects on Structures." Bulletin 656, U.S. Department of the Interior, Bureau of Mines.

Ohrt, A. P. (1988). Unpublished design calculations and sketches for 4-ft-diameter vertical gas gun. USAE Waterways Experiment Station, Vicksburg, MS 39180-6199.

Ohrt, A. P. and Welch, C. R. (1989). "Development of a 4-ft Diameter Vertical Gas Gun - Summary Progress Report - FY88," USAE Waterways Experiment Station, Vicksburg, MS 39180-6199.

Ohrt, A. P. (1994). Personal communication with Mr. Ohrt, USAE Waterways Experiment Station, Explosion Effects Division, regarding a series of tests he conducted in 1985, using the WES Large Blast Load Generator for static instrumentation studies in various soils.

Parker O-Ring Handbook (1990). Parker Hannifin Corporation, Cleveland, Ohio.

Peekna, A. (1972). "Ground Motion Canister Design and Evaluation." Unpublished report, USAE Waterways Experiment Station, Vicksburg, MS 39180-6199.

Phillips, B. R. (1991). "Backfilling of Test Container for Gas Gun Tests - Report of Telephone Conversation." USAE Waterways Experiment Station, Vicksburg, MS 39180-6199.

Renick, J. D., Goodfellow, G. M., and Flores, L. E. (1987). "Large High Explosive Driven Flyer Plate Technique for the Calibration of Soil Stress and Motion Instrumentation." Informal Report, Air Force Weapons Laboratory, Kirtland AFB, NM.

Rickman, D. D., and White, H. G. (1986). "Procedure for Assembling WES Column-Based Soil Stress Gages." WES Instruction Report SL-86-1, USAE Waterways Experiment Station, Vicksburg, MS 39180-6199.

Rinehart, E. J. (1987). "Gage Validation Using a 2.4 M Diameter Flyer Plate." Technical Report CRTA-TR-3750-2. California Research and Technology, Inc., Albuquerque, NM.

Rinehart E. J. (1993). "The Effect of Geometry on Stress Measurements." Proceedings of the 64th Shock and Vibration Symposium, Volume 2, 26-28 October 1993. Naval Surface Warfare Center, Silver Spring, MD.

Ristvet, B. L. (1987). "Environmental Assessment and Finding of No Significant Impact for the Deep Underground Simulator Test Program, Continental Mine, Silver City, NM." prepared for the Director, Defense Nuclear Agency, Washington, DC.

Rocco, J. R., Rinehart, E. J., Welch, C. R., White, H. G., and Thomsen J. M. (1994). "Response of WES Column-Based Stress Gages to Kilobar Level Shocks in Dry Sand and Saturated Limestone." Proceedings of the Defense Nuclear Agency Instrumentation for Nuclear Weapons Effects Testing (INWET) Conference, 2-5 November 1993. Defense Nuclear Agency, Alexandria, VA 22310-3398.

Schneider, J. F. (1989). "Time-of-Arrival Data System Test Results." AFWL-TR-88-123, Air Force Weapons Laboratory, Kirtland Air Force Base, NM.

Siskind, D. E., Crum, S. V., and Plis, M. M. (1990). "Vibration Environment and Damage Characterization for Houses in McCutchanville and Daylight, Indiana." Contract Research Report, U.S. Department of the Interior, Bureau of Mines.

Stewart, W. N., and Tatu, W. J. (1972). "Artillery Gun Shock Simulator." U.S. Patent No. 3,693,432, U.S. Department of Commerce, Patent and Trademark Office, Washington, D.C. 20231.

Veyera, G. E. and Rinehart, E. J. (1986). "Inertial Effects on Field Gage Records." Technical Report CRTA-TR-3810-2. California Research and Technology, Inc., Albuquerque, NM.

Wallace, J. G., and Fowler, J. (1973). "Fundamental Experiments in Ground Shock Phenomenology." Miscellaneous Paper N-73-2. USAE Waterways Experiment Station, Vicksburg, MS 39180-6199.

Welch, C. R. (1982). "Perturbation of Free-Field Stress Measurements In Rock By Backfill Materials." Conference on Instrumentation for Nuclear Weapons Effects, 30 March - 1 April, 1982, Volume 1 - Proceedings, DNA-TR-82-17-V1, Defense Nuclear Agency, Alexandria, VA 22310-3398.

Welch, C. R. (Editor) (1986). "Silo Test Program (STP) 3.5A Event, Volume 1 - The Test Environment." WES Technical Report SL-84-11, USAE Waterways Experiment Station, Vicksburg, MS 39180-6199.

Welch, C. R. (1993). "A Full-Engulfment Engineering Model, and Its Experimental and Numerical Verification, for the Response of a Rigid Body to Ground-Shock." Dissertation, Virginia Polytechnic Institute and State University, Blacksburg, Virginia.

Welch, C. R., and White H. G. (1987). "Shock-Isolated Accelerometer Systems For Measuring Velocities In High-G Environments." Shock and Vibration Bulletin 57, The Shock and Vibration Information Center, Naval Research Laboratory, Washington, DC.

Welch, C. R., White, H. G., and King, P. K. (1992). "HydroPlus TID Program Work Accomplished To Date - 18 September 1992." USAE Waterways Experiment Station, Vicksburg, MS 39180-6199.

Welch, C. R., White, H. G., Fuller, B. D., and Rickman D. D. (1994). "WES Third-Generation, High-Fidelity, Particle Velocity Gage." Proceedings of the Defense Nuclear Agency Instrumentation for Nuclear Weapons Effects Testing (INWET) Conference, 2-5 November 1993. Defense Nuclear Agency, Alexandria, VA 22310-3398.

White, H. G. (1989a). "Development Of A High-Range Particle-Velocity Gage." WES Technical Report SL-89-3, USAE Waterways Experiment Station, Vicksburg, MS 39180-6199.

- White, H. G. (1989b). "Overview of Polymer Materials and Their Use for Packaging in High-G Environments." Final report for independent study course TAM 493 at the University of Illinois, under the direction of Prof. H. T. Corten.
- White, H. G. (1990). "Hydrostatic and Vacuum Testing of the WES 4-ft Diameter Vertical Gas Gun." USAE Waterways Experiment Station, Vicksburg, MS 39180-6199.
- White, H. G. (1991a). "Safety Plan for Testing with the WES 4-ft-Diameter Vertical Gas Gun." USAE Waterways Experiment Station, Vicksburg, MS 39180-6199.
- White, H. G. (1991b). "Test Plan for the WES 4-ft Diameter Vertical Gas Gun." USAE Waterways Experiment Station, Vicksburg, MS 39180-6199.
- White, H. G. (1991c). "Standard Operating Procedure for the WES 4-ft Diameter Vertical Gas Gun." USAE Waterways Experiment Station, Vicksburg, MS 39180-6199.
- White, H. G. (1991d). "Nuisance and Damage Calculations for Testing with the WES 4-ft-Diameter Vertical Gas Gun." USAE Waterways Experiment Station, Vicksburg, MS 39180-6199.
- White, H. G., Ohrt, A. P., Welch, C. R., and Joachim C. E. (1991). "Design and Testing Experiences with the WES 12-in. and 4-ft Diameter Vertical Gas Guns." Proceedings of the Defense Nuclear Agency Instrumentation for Nuclear Weapons Effects Testing (INWET) Conference, 16-19 April 1991. Volume 1-General Session and Sessions I and II, DASIAC-TR-91-001-V1, Defense Nuclear Agency, Alexandria, VA 22310-3398.
- White, H. G. (1991-1993). "Test Plan for Tests 1-28 with the WES 4-ft Diameter Vertical Gas Gun." 28 vols. USAE Waterways Experiment Station, Vicksburg, MS 39180-6199.
- White, H. G. (1992). "Test Plan for the WES 4-ft Diameter Vertical Gas Gun." USAE Waterways Experiment Station, Vicksburg, MS 39180-6199.
- White, H. G. (1993). "Performance Tests with the WES 4-ft-Diameter Vertical Gas Gun." DNA-TR-93-16, Defense Nuclear Agency, Alexandria, VA 22310-3398.
- White, H. G. and Byrne, J. T. (1994). "DNA/WES Ground Motion Test Facility - Results and Analysis of Impact Tests Against Masonry and Socorro Plaster Sand Testbeds." DNA-TR-93-114, Defense Nuclear Agency, Alexandria, VA 22310-3398.

White, H. G., and Welch, C. R. (1994). "Initial Ground Shock Tests in Sand Using the WES 4-ft Diameter Vertical Gas Gun." Proceedings of the Defense Nuclear Agency Instrumentation for Nuclear Weapons Effects Testing (INWET) Conference, 2-5 November 1993. Defense Nuclear Agency, Alexandria, VA 22310-3398.

Young, C., Ascher, J., and Callant D. (1992). "Electromagnetic Gage Techniques for HEST Measurements (Phase II)." DNA-TR-92-46, Defense Nuclear Agency, Alexandria, VA 22310-3398.

APPENDIX A

LISTING OF THE COMPUTER CODE GG4PV

C PROGRAM NAME: GG4PV.FOR
C UPDATED: DECEMBER 20, 1993
C DATE: JULY 10, 1991

C WRITTEN BY: HOWARD G. WHITE
C USAE WATERWAYS EXPERIMENT STATION
C 3909 HALLS FERRY ROAD
C VICKSBURG, MS 39180-6199
C PH: (601) 634-3391

C THIS PROGRAM CALCULATES THE PROJECTILE VELOCITY FOR THE 4-FT
C GAS GUN, FOR A GIVEN VESSEL PRESSURE, OR RANGE OF PRESSURES,
C AND A GIVEN PROJECTILE WEIGHT.

C VARIABLE DEFINITION
C C = CONVENIENT CONSTANT
C COEFF1 = CONVENIENT CONSTANT
C COEFF2 = CONVENIENT CONSTANT
C COEFF3 = CONVENIENT CONSTANT
C DENRM = DENSITY OF REACTION MASS (SLUGS/FT^3)
C I = DUMMY VARIABLE
C IALC = 1 IF CALC VEL AS FRONT EXITS BARREL, 2 IF REAR
C IPPLATE = 2 IF PRESSURE PLATE IS USED ON PROJECTILE, 1 IF NOT
C OUTFILE = OUTPUT FILENAME FOR CALCULATED DATA
C PINC = PRESSURE INCREMENT FOR CALCULATIONS (PSI, CHANGED TO LB/FT^2)
C PINIT = INITIAL VESSEL PRESSURE (PSI)
C PMASSLB = PROJECTILE MASS (LBm, CHANGED TO SLUGS)
C PMASS = PROJECTILE MASS (SLUGS)
C PMAX = MAX PRESSURE FOR CALCULATIONS (PSI)
C RATIO = RATIO OF PROJECTILE MASS TO REACTION MASS
C RBAR = RADIUS OF BARREL (FT)
C RMASS = REACTION MASS (SLUGS)
C VCHAM = VOL OF CHAMBER BETWEEN PROJECTILE AND REACTION MASS (FT^3)
C VEL = VELOCITY OF PROJECTILE (FT/SEC)
C VINIT = INITIAL PRESSURIZED VOL, BEFORE MASSES BEGIN MOVING (FT^3)
C VTANK = VOLUME OF TANK (FT^3)
C XFOAM = LENGTH OF FOAM ADDED TO FRONT OF PROJECTILE (IN CHANGED TO FT)
C XL = LENGTH OF PROJECTILE TRAVEL PRIOR TO IMPACTING RATE PINS (FT)
C XPLATE = LENGTH OF IMPACT PLATE (IN CHANGED TO FT)
C YL = LENGTH OF REACTION MASS HEIGHT (AND TRAVEL) (FT)

C
C CHARACTER OUTFILE*15

C **** INPUT PROJECTILE MASS ****

```

10  WRITE(*,90)
90  FORMAT(///,5X,'PROGRAM GG4PV (LAST UPDATED: 20 DECEMBER 1993)')

      WRITE(*,100)
100  FORMAT(///,5X,'INPUT PROJECTILE MASS (LBm) : ')
      READ(*,*)PMASSLB

      WRITE(*,110)
110  FORMAT(///,5X,'INPUT LENGTH OF FOAM ON PROJECTILE (IN) : ')
      READ(*,*)XFOAM

      WRITE(*,120)
120  FORMAT(///,5X,'INPUT LENGTH OF IMPACT PLATE (IN) : ')
      READ(*,*)XPLATE

125  WRITE(*,130)
130  FORMAT(///,5X,'WAS A PRESSURE PLATE USED ON THE PROJECTILE?',
1      /,5X,'1 = NO      2 = YES',
2      //,5X,'ENTER OPTION : ')
      READ(*,*)IPPLATE
      IF(IPPLATE.LT.1 .OR. IPPLATE.GT.2) THEN
          WRITE(6,*)'YOU ENTERED : ',IPPLATE
          WRITE(6,*)'PLEASE ENTER A 1 OR 2'
          GOTO 125
      END IF

135  WRITE(*,140)
140  FORMAT(///,5X,'CALCULATE THE VELOCITY AS:',
1      /,5X,'1 = THE FRONT OF THE PROJECTILE EXITS THE BARREL',
2      /,5X,'2 = THE REAR OF THE PROJECTILE EXITS THE BARREL',
3      //,5X,'ENTER OPTION : ')
      READ(*,*)ICALC
      IF(ICALC.LT.1 .OR. ICALC.GT.2) THEN
          WRITE(6,*)'YOU ENTERED : ',ICALC
          WRITE(6,*)'PLEASE ENTER A 1 OR 2'
          GOTO 135
      END IF

```

C **** INITIAL CONSTANTS AND CALCULATIONS ****

```

PI = 3.141592654
RBAR = 2.0
DENRM = 1.939
IF (ICALC .EQ. 1) THEN
    XL = (128.375-XFOAM-XPLATE)/12.
ELSE
    XL = 166/12.
END IF
PMASS = PMASSLB/32.174
VTANK = 355.0
IF (IPPLATE .EQ. 1) THEN
    VCHAM = 63.7

```

```

ELSE
  VCHAM = 33.0
END IF
VINIT = VTANK+VCHAM

```

C **** CALCULATE REACTION MASS TRAVEL DISTANCE AND MASS ****

```

ZZ = XL*PMASS
Z = PI*RBAR*RBAR*DENRM
YL = SQRT(ZZ/Z)
RMASS = YL*Z

```

C **** CALCULATE CONVENIENT CONSTANTS ****

```

RATIO = PMASS/RMASS
C = PI*RBAR*RBAR*(1.+RATIO)
COEFF1 = (1.-(VINIT/(VINIT+XL*C)))**0.4
COEFF3 = ((VTANK/VINIT)**1.4)/0.4*2.
COEFF2 = (COEFF3*VINIT)/(PMASS*(1.+RATIO))

```

C **** CALCULATE ONE OR MANY POINTS? ****

```

150 WRITE(*,160)
160 FORMAT(///,5X,'          OPTIONS',
1      //,5X,'1 = GENERATE DATA FILE FOR RANGE OF PRESSURES',
2      //,5X,'2 = INVESTIGATE SINGLE PRESSURE',
3      //,5X,'ENTER OPTION : ')
READ(*,*)IOPT
IF(IOPT.LT.1 .OR. IOPT.GT.2) THEN
  WRITE(6,*)'YOU ENTERED : ',IOPT
  WRITE(6,*)'PLEASE ENTER A 1 OR 2'
  GOTO 150
END IF

```

```

IF(IOPT.EQ.2) GOTO 300

```

C **** SECTION TO CALCULATE FOR A RANGE OF PRESSURES ****

```

200 WRITE(*,210)
210 FORMAT(///,5X,'INPUT MAXIMUM PRESSURE OF INTEREST (PSI) : ')
READ(*,*)PMAX

WRITE(*,220)
220 FORMAT(//,5X,'INPUT INCREMENT FOR PRESSURE STEPS (PSI) : ')
READ(*,*)PINC

WRITE(*,230)
230 FORMAT(//,5X,'ENTER THE NAME OF THE OUTPUT FILE : ')
READ(*,240)OUTFILE
240 FORMAT(A15)

NPTS = INT(PMAX/PINC)+1
PINC = PINC*144.

```

```

OPEN(UNIT=10,FILE=OUTFILE)
WRITE(10,250)NPTS
250 FORMAT(15)

```

C **** BEGIN LOOP CALCULATIONS ****

```

DO 260 I=1,NPTS
  PRES = (I-1)*PINC
  VEL = (PRES*COEFF1*COEFF2)**0.5
  PRES = PRES/144.
  WRITE(10,*)PRES,VEL
260 CONTINUE
CLOSE(UNIT=10)
GOTO 400

```

C **** SECTION TO CALCULATE VELOCITY FOR A SINGLE POINT ****

```

300 WRITE(*,310)
310 FORMAT(///,5X,'INPUT INITIAL VESSEL PRESSURE (PSI) : ')
  READ(*,*)PINIT
  VEL = (PINIT*144.*COEFF1*COEFF2)**0.5
  YL = YL*12.
  RMASS = RMASS*32.174
  WRITE(*,320)PINIT,VEL,YL,RMASS,PMASSLB
320 FORMAT(//,5X,'INITIAL PRESSURE = ',F4.0,' PSI',
1      /,5X,'PROJECTILE VELOCITY = ',F4.0,' FT/SEC',
2      /,5X,'REACTION-MASS HEIGHT = ',F5.1,' INCHES',
3      /,5X,'REACTION-MASS MASS = ',F5.0,' LBm',
4      /,5X,'PROJECTILE MASS = ',F5.0,' LBm')

```

C **** END CALCULATIONS ****

C **** RUN THE PROGRAM AGAIN? ****

```

400 WRITE(*,410)
410 FORMAT(///,5X,' OPTIONS',
1      /,5X,'1 = RUN PROGRAM AGAIN',
2      /,5X,'2 = END PROGRAM',
3      /,5X,'ENTER OPTION : ')
  READ(*,*)IOPT
  IF(IOPT.LT.1 OR IOPT.GT.2) THEN
    WRITE(6,*)'YOU ENTERED : ',IOPT
    WRITE(6,*)'PLEASE ENTER A 1 OR 2'
    GOTO 400
  END IF
  IF (IOPT.EQ.1) GOTO 10

```

1000 END

APPENDIX B

LISTING OF THE COMPUTER CODE PARTVEL

C PROGRAM NAME: PARTVELFOR
C DATE: APRIL 27, 1991

C WRITTEN BY: HOWARD G. WHITE
C USAE WATERWAYS EXPERIMENT STATION
C 3909 HALLS FERRY ROAD
C VICKSBURG, MS 39180-8199
C PH: (601) 634-3391

C THIS PROGRAM CALCULATES THE PEAK VERTICAL PARTICLE VELOCITY
C FOR IMPACTS AS A FUNCTION OF RANGE AND PROJECTILE SEISMIC ENERGY
C LEVEL ASSUMING A TNT EQUIVALENCE OF 1.41E6 FT-LB/LB-TNT. THE
C PROJECTILE'S KINETIC ENERGY IS FOUND FROM ITS MASS AND VELOCITY.

C REFERENCE: FUNDAMENTAL EXPERIMENTS IN GROUND SHOCK PHENOMENOLOGY
C WES MISCELLANEOUS PAPER N-73-2
C J.G. WALLACE AND J. FOWLER
C MARCH 1973
C PARAGRAPH 28, P36.

C VARIABLE DEFINITION

C GC = GRAVITATIONAL CONSTANT (LBm-FT/LB-SEC²)
C E = ENERGY OF IMPACT (LB-TNT)
C MP = MASS OF PROJECTILE (LBm)
C PARTVEL = PARTICLE VELOCITY AT RANGE R (IN/SEC)
C PROJVEL = PROJECTILE VELOCITY (FT/SEC)
C R = RANGE (FT)
C TNT = TNT EQUIVALENCE
C VMIN = MINIMUM VELOCITY USED IN CALCULATION (FT/SEC)
C VMAX = MAXIMUM VELOCITY USED IN CALCULATION (FT/SEC)

C
C INTEGER VMIN,VMAX
C REAL MP
C CHARACTER OUTFILE*15

10 CONTINUE

C **** DEFINE CONSTANTS ****

GC=32.174
TNT=1410000.0
MP=3260.
VMIN=1
VMAX=300

```

WRITE(*,50)GC,TNT,MP,VMIN,VMAX
50  FORMAT(//,5X,'CURRENT PARAMETER SETTINGS ARE : ',
1//,5X,'GRAVITATIONAL CONSTANT = ',F6.3,' (LBm-FT)/(LBf-SEC^2)',
2//,5X,'TNT EQUIVALENCE = ',F8.0,' (FY-LBf)/(LBf-TNT)',
3//,5X,'PROJECTILE MASS = ',F5.0,' LBm',
4//,5X,'RANGE OF PROJECTILE VELOCITY CALCULATED : ',I2,' TO ',
5  I3,' FT/SEC',/)

WRITE(*,60)
60  FORMAT(5X,'UNITS OF THE RESULTING PARTICLE VELOCITY ARE IN/SEC')

WRITE(*,70)
70  FORMAT(//,5X,'INPUT THE RANGE OF THE OBSERVATION POINT (FT) : ')
READ(*,*)R

WRITE(*,80)
80  FORMAT(//,5X,'OUTPUT FILE NAME : ')
READ(*,90)OUTFILE
90  FORMAT(A15)
OPEN(UNIT=17,FILE=OUTFILE)
WRITE(17,*)VMAX

C **** CALC. ATION SECTION ****

DO 100 I=VMIN,VMAX
  PROJVEL=I*1.0

  E=MP*PROJVEL*PROJVEL/(2.0*GC*1410000.)

C **** PARTVEL HAS UNITS OF IN/SEC ****
  PARTVEL=600.0*(E/R**3)**0.5

  WRITE(17,*)PROJVEL,PARTVEL

100 CONTINUE

CLOSE (UNIT=17)

350 WRITE(*,*) ' DO YOU WISH TO RUN THIS PROGRAM AGAIN?'
WRITE(*,*) ' YES = 1 NO = 2'
WRITE(*,*) ' PREFERENCE: '
READ(*,*)IPREF
IF(IPREF.EQ.1) GOTO 10

1000 END

```

APPENDIX C

LISTING OF THE COMPUTER CODE 1DWAVE

C PROGRAM NAME: 1DWAVE.FOR

C DATE: JULY 14, 1992

C LAST REVISED: JULY 24, 1992

C WRITTEN BY: HOWARD G. WHITE

C USAE WATERWAYS EXPERIMENT STATION

C STRUCTURES LABORATORY/EXPLOSION EFFECTS DIVISION

C ATTN: CEWES-SE-R

C 3909 HALLS FERRY ROAD

C VICKSBURG, MS 39180-6199

C (601) 634-3391

C REFERENCES: FUNDAMENTALS OF PHYSICS, 2ND EDITION

C HALLIDAY AND RESNICK, PP 153-7

C GAGE VALIDATION USING A 2.4 M DIAMETER FLYER PLATE

C ERIC RINEHART, JULY 1987.

C "LARGE HIGH EXPLOSIVE DRIVEN FLYER PLATE TECHNIQUE

C FOR THE CALIBRATION OF SOIL STRESS AND MOTION

C INSTRUMENTATION"

C RENICK, GOODFELLOW, AND FLORES

C GAS GUN CALCULATIONS NOTEBOOK

C SECTION ON 1-D ANALYSIS OF WAVE PROPAGATION

C "MECHANICAL PROPERTY RECOMMENDATIONS FOR POSTTEST

C EVALUATION OF THE MIDNIGHT HOUR 2 TEST"

C BRUCE PHILLIPS, CEWES-SD, JULY 1991

C FOR AN INELASTIC COLLISION, 2 PARTICLES WITH INITIAL MASSES AND
C VELOCITIES WILL "STICK" TOGETHER AFTER IMPACT, AND HAVE A SINGLE
C VELOCITY THEREAFTER. FOR OUR CASE OF THE GAS GUN PROJECTILE
C IMPACTING A TARGET, THE TOTAL MASS INCREASES AS THE WAVE TRAVERSES
C THE TARGET (AT A PROPAGATION VELOCITY C_2) THEREBY REDUCING THE
C VELOCITY OF THE "SYSTEM". WE WILL MODEL THE CARRIAGE, SHOCK-
C ISOLATING FOAM, AND IMPACT PLATE OF THE PROJECTILE BY CONSIDERING
C A SINGLE IMPACTING PLATE (EFFECTIVELY THROWING OUT THE CARRIAGE AND
C FOAM). WE WILL NOT ACCOUNT FOR THE RELIEF WAVE IMMEDIATELY COMING
C IN FROM THE SIDES OF THE TARGET, IN ORDER TO REMAIN 1-D.
C WE HAVE TWO GOVERNING EQUATIONS.

C FOR A PULSE WITH MAGNITUDE "STRESS", TRAVELLING INTO A BAR WITH AREA
C "A", PROPAGATION VELOCITY "C", DENSITY "RHO", FOR A TIME "DELTA T",
C AND EQUATING THE IMPULSE APPLIED TO THE END OF A BAR TO THE CHANGE
C IN MOMENTUM OF THE EFFECTED REGION, WE FIND:

C $STRESS = RHO (DENSITY) * C (WAVE SPEED) * V (PARTICLE VELOCITY)$

C FROM CONSERVATION OF MOMENTUM FOR AN INELASTIC COLLISION; FOR AN
 C IMPACTOR WITH DENSITY "RHO1", PROPAGATION VELOCITY "C1", AREA "A",
 C THICKNESS "H1", AND VELOCITY "V1", AND A TARGET WITH DENSITY "RHO2",
 C PROPAGATION VELOCITY "C2", AREA "A", & A GIVEN DEPTH "H", THE VELOCITY
 C OF THE "SYSTEM", "V2", AS A FUNCTION OF TIME "T", IS GIVEN BY:

$$C \quad V2(T) = (RHO1 * H1 * V1) / [(RHO1 * H1) + (RHO2 * C2 * T)]$$

C THE VELOCITY VARIES WITH TIME BECAUSE THE EFFECTED MASS IS A
 C FUNCTION OF TIME, IE, $H(T)=C2*T$. $V2(T)$ MAY BE SUBSTITUTED INTO
 C THE PREVIOUS EQUATION TO FIND THE STRESS IN THE TARGET.

C THIS DEVELOPMENT ASSUMES A LINEAR WAVESPEED DURING LOADING, IE, A
 C LINEAR STRESS-STRAIN CURVE FOR THE TARGET MATERIAL, AND IT ASSUMES
 C AN INFINITE UNLOADING WAVESPEED, IE, THE ENTIRE MASS BEHIND THE WAVE
 C FRONT IS TRAVELLING AT THE SAME SPEED (AS A RIGID BODY). THESE
 C ASSUMPTIONS ARE PERHAPS NOT EXTREMELY INCORRECT FOR LOW STRESS LEVELS
 C IN SAND. ALSO, AS A RESULT OF THE INFINITE UNLOADING WAVE SPEED IN
 C TARGET, THE VELOCITY/STRESS STATE OF THE "SYSTEM" BEHIND THE INITIAL
 C WAVE FRONT, IS CONSTANT (WITH DEPTH), FOR A GIVEN INSTANT IN TIME.

C VARIABLES USED IN THIS PROGRAM INCLUDE

C C2=PROPAGATION VELOCITY IN THE TARGET (FPS)
 C D=DEPTH WITHIN A TARGET (FT, THEN IN OR M)
 C DOP=DEPTH OF OBSERVATION POINT (IN, THEN FT)
 C GC=GRAVITATIONAL CONSTANT ((LBM-FT)/(LBF-S^2))
 C H1=THICKNESS OF THE IMPACTOR (IN, THEN FT)
 C I=DUMMY VARIABLE
 C IPREF1=SEC OR MSEC TIMEBASE FOR OUTPUT FILE?
 C IPREF2=ENGLISH OR METRIC UNITS FOR OUTPUT FILE?
 C IPREF3=OUTPUT VELOCITY DATA?
 C IPREF4=OUTPUT STRESS DATA?
 C IPREF5=RUN PROGRAM AGAIN OR NOT?
 C IPREF6=TIME OR DEPTH FOR X-AXIS DATA FOR OUTPUT FILE?
 C NN=PARAMETER TO SET SIZE OF ARRAYS
 C NPTS=NUMBER OF POINTS IN CALCULATION
 C OUTFILE1=FILENAME FOR VELOCITY DATA
 C OUTFILE2=FILENAME FOR STRESS DATA
 C REDUCE=TIME NEEDED TO REDUCE TMAX BY TO ALLOW PROGRAM TO RUN (MSEC)
 C RHO1=DENSITY OF THE IMPACTOR (PCF)
 C RHO2=DENSITY OF THE TARGET (PCF)
 C STRESS(T)=STRESS IN THE TARGET (PSI OR MPA) AT & BEHIND LOCATION H
 C T=TIME (SEC, THEN SEC OR MSEC)
 C TINC=TIME INCREMENT BETWEEN CALCULATIONS (SEC)
 C TMAX=DURATION OF CALCULATION (SEC)
 C TOP=TIME TO REACH THE OBSERVATION POINT (SEC)
 C V1=VELOCITY OF THE IMPACTOR (FPS)
 C V2(T)=VELOCITY IN THE TARGET (FPS OR MPS) AT & BEHIND LOCATION H
 C X(I)=DUMMY ARRAY FOR TIME OR DEPTH AS X-AXIS DATA FOR OUTPUT FILE
 C

5 CONTINUE

CHARACTER OUTFILE1*15, OUTFILE2*15
PARAMETER(NN=1001)
DIMENSION D(NN), STRESS(NN), T(NN), V2(NN), X(NN)
GC=32.174

WRITE(*,10)
10 FORMAT(/,5X,'PROGRAM NAME: 1DWAVE')

WRITE(*,20)
20 FORMAT(/,5X,'PROBLEM DEFINITION: ')

WRITE(*,30)
30 FORMAT(/,15X,'DENSITY OF THE IMPACTOR (PCF): ')
READ(*,*)RHO1

WRITE(*,40)
40 FORMAT(/,15X,'THICKNESS OF THE IMPACTOR (IN): ')
READ(*,*)H1

WRITE(*,50)
50 FORMAT(/,15X,'VELOCITY OF THE IMPACTOR (FPS): ')
READ(*,*)V1

WRITE(*,60)
60 FORMAT(/,15X,'DENSITY OF THE TARGET (PCF): ')
READ(*,*)RHO2

WRITE(*,85)
85 FORMAT(/,15X,'PROPAGATION VELOCITY IN THE TARGET (FPS): ')
READ(*,*)C2

WRITE(*,75)
75 FORMAT(/,15X,'DEPTH OF OBSERVATION POINT (IN): ')
READ(*,*)DOP

85 WRITE(*,90)
90 FORMAT(/,15X,'DURATION OF THE CALCULATION (SEC): ')
READ(*,*)TMAX

WRITE(*,100)
100 FORMAT(/,15X,'INCREMENT BETWEEN CALCULATIONS (SEC): ')
READ(*,*)TINC

NPTS = INT(TMAX/TINC)+1

IF(NPTS.GT.NN) THEN
REDUCE = (NPTS-NN)*TINC
WRITE(*,110)NN,REDUCE
110 FORMAT(/,5X,'CANNOT PERFORM OVER ',I4,' CALCULATIONS!!!',
1 //,5X,'PLEASE REDUCE TMAX BY ',F8.6,' SECONDS.')

```

      GOTO 85
    ELSE
      WRITE(*,120)
120  FORMAT(/,15X,'**** DATA ENTRY COMPLETE ****')
    END IF

```

C **** INITIAL CALCULATIONS ****

```

      H1 = H1/12.
      DOP = DOP/12.
      TOP = DOP/C2
      FACTOR1 = RHO1 * H1
      FACTOR2 = FACTOR1 * V1
      FACTOR3 = RHO2 * C2

```

C **** BEGIN CALCULATIONS ****

```

      D(1) = 0.
      T(1) = 0.
      V2(1) = 0.
      STRESS(1) = 0.

```

```

      DO 200 I=2,NPTS
        T(I) = (I-1)*TINC
        D(I) = T(I)*C2

```

C DO NOT START CALCULATIONS TIL THE OBSERVATION POINT HAS BEEN REACHED

```

      IF(T(I).LT.TOP) THEN

```

```

        V2(I) = 0.
        STRESS(I) = 0.

```

```

      ELSE

```

```

        V2(I) = FACTOR2/(FACTOR1 + FACTOR3*T(I))
        STRESS(I) = V2(I)*FACTOR3

```

C CHANGE UNITS TO PSI

```

        STRESS(I) = STRESS(I)/144./GC

```

```

      END IF

```

```

200  CONTINUE

```

C **** END CALCULATIONS ****

C **** OUTPUT DATA TO FILE ****

C **** CHOOSE ENGLISH OR METRIC UNITS ****

```

290  WRITE(*,295)

```

```

295  FORMAT(/,15X,'UNITS OPTIONS: 1 = ENGLISH (PSI, FPS, FT)',

```

```

      1    /,15X,'          2 = METRIC (MPA, MPS, M)',

```

```

      2    //,15X,'PREFERENCE: ')

```

```

      READ(*,*)IPREF2

```

```

      IF(IPREF2.LT.1 .OR. IPREF2.GT.2) THEN

```

```

        WRITE(6,*)'YOU ENTERED: ',IPREF2

```

```

        WRITE(6,*)'PLEASE ENTER A 1 OR 2'

```

```

        GOTO 290

```

```

END IF

C **** CHOOSE THE OUTPUT X-AXIS AS TIME T(I) OR DEPTH D(I) ****

300 WRITE(*,310)
310 FORMAT(/,15X,'OUTPUT TO FILE TIME OR DEPTH FOR X-AXIS?',
1    //,15X,'1 = TIME',
2    //,15X,'2 = TARGET DEPTH',
3    //,15X,'PREFERENCE: ')
READ(*,*)IPREF6
IF(IPREF6.LT.1 .OR. IPREF6.GT.2) THEN
WRITE(6,*)'YOU ENTERED: ',IPREF6
WRITE(6,*)'PLEASE ENTER A 1 OR 2'
GOTO 300
END IF

IF(IPREF6.EQ.2) THEN
DO 315 I=1,NPTS
IF(IPREF2.EQ.2) THEN
X(I)=D(I)/3.28
ELSE
X(I)=D(I)
END IF
315 CONTINUE
ELSE
C **** CHOOSE SEC OR MSEC FOR TIMEBASE ****
320 WRITE(*,330)
330 FORMAT(/,15X,'TIME BASE OPTIONS (1 = SEC 2 = MSEC)',
1    //,15X,'PREFERENCE: ')
READ(*,*)IPREF1
IF(IPREF1.LT.1 .OR. IPREF1.GT.2) THEN
WRITE(6,*)'YOU ENTERED: ',IPREF1
WRITE(6,*)'PLEASE ENTER A 1 OR 2'
GOTO 320
END IF

C **** CHANGE FROM SEC TO MSEC IF NECESSARY ****
IF(IPREF1.EQ.2) THEN
DO 335 I=1,NPTS
X(I)=T(I)*1000.
335 CONTINUE
ELSE
C **** OUTPUT TIME ARRAY IS SECONDS HERE ****
DO 340 I=1,NPTS
X(I)=T(I)
340 CONTINUE
END IF
END IF

C **** SELECT WHICH DATA TO OUTPUT TO A FILE ****

400 WRITE(*,410)

```

```

410  FORMAT(//,15X,'DO YOU WISH TO OUTPUT THE VELOCITY DATA?',
1      /,15X,'1 = YES, 2 = NO',
2      //,15X,'PREFERENCE: ')
      READ(*,*)IPREF3
      IF(IPREF3.LT.1 .OR. IPREF3.GT.2) THEN
          WRITE(6,*)'YOU ENTERED: ',IPREF3
          WRITE(6,*)'PLEASE ENTER A 1 OR 2'
          GOTO 400
      END IF

      IF(IPREF3.EQ.1) THEN
          WRITE(*,420)
420  FORMAT(///,15X,'ENTER OUTPUT FILENAME FOR THE VELOCITY DATA: ')
          READ(*,430)OUTFILE1
430  FORMAT(A15)
          OPEN(UNIT=10,FILE=OUTFILE1)
          WRITE(10,440)NPTS
440  FORMAT(I5)
          DO 450 I=1,NPTS
              IF(IPREF2.EQ.2) THEN
C  CHANGING FROM ENGLISH UNITS (FPS) TO METRIC UNITS (MPS) IF NECESSARY
                  V2(I)=V2(I)/3.28
                  END IF
                  WRITE(10,*)X(I),V2(I)
450  CONTINUE
                  CLOSE(UNIT=10)
                  END IF

500  WRITE(*,510)
510  FORMAT(//,15X,'DO YOU WISH TO OUTPUT THE STRESS DATA?',
1      /,15X,'1 = YES, 2 = NO',
2      //,15X,'PREFERENCE: ')
          READ(*,*)IPREF4
          IF(IPREF4.LT.1 .OR. IPREF4.GT.2) THEN
              WRITE(6,*)'YOU ENTERED: ',IPREF4
              WRITE(6,*)'PLEASE ENTER A 1 OR 2'
              GOTO 500
          END IF

          IF(IPREF4.EQ.1) THEN
              WRITE(*,520)
520  FORMAT(///,15X,'ENTER OUTPUT FILENAME FOR THE STRESS DATA: ')
              READ(*,530)OUTFILE2
530  FORMAT(A15)
              OPEN(UNIT=10,FILE=OUTFILE2)
              WRITE(10,540)NPTS
540  FORMAT(I5)
              DO 550 I=1,NPTS
                  IF(IPREF2.EQ.2) THEN
C  CHANGING FROM ENGLISH UNITS (PSI) TO METRIC UNITS (MPA) IF NECESSARY
                      STRESS(I)=STRESS(I)/145.
                      END IF

```

```

        WRITE(10,*)X(I),STRESS(I)
550   CONTINUE
        CLOSE(UNIT=10)
        END IF

600   WRITE(*,610)
610   FORMAT(/,15X,'DO YOU WISH TO RUN THIS PROGRAM AGAIN?',
1      /,15X,'1 = YES, 2 = NO',
2      //,15X,'PREFERENCE: ')
        READ(*,*)IPREF5
        IF(IPREF5.LT.1 .OR. IPREF5.GT.2) THEN
            WRITE(6,*)'YOU ENTERED: ',IPREF5
            WRITE(6,*)'PLEASE ENTER A 1 OR 2'
            GOTO 600
        END IF

        IF(IPREF5.EQ.1) THEN
            GOTO 5
        END IF

1000  END

```

REPORT DOCUMENTATION PAGE

Form Approved
OMB No. 0704-0188

Public reporting burden for this collection of information is estimated to average 1 hour per response, including the time for reviewing instructions, searching existing data sources, gathering and maintaining the data needed, and completing and reviewing the collection of information. Send comments regarding this burden estimate or any other aspect of this collection of information, including suggestions for reducing this burden, to Washington Headquarters Services, Directorate for Information Operations and Reports, 1215 Jefferson Davis Highway, Suite 1204, Arlington, VA 22202-4302, and to the Office of Management and Budget, Paperwork Reduction Project (0704-0188), Washington, DC 20503.

1. AGENCY USE ONLY (Leave blank)		2. REPORT DATE July 1994	3. REPORT TYPE AND DATES COVERED Final report	
4. TITLE AND SUBTITLE Development of a Large-Diameter Gas Gun for Studies of Gage Validation and Dynamic Material Properties			5. FUNDING NUMBERS	
6. AUTHOR(S) Howard G. White				
7. PERFORMING ORGANIZATION NAME(S) AND ADDRESS(ES) U.S. Army Engineer Waterways Experiment Station 3909 Halls Ferry Road Vicksburg, MS 39180-6199			8. PERFORMING ORGANIZATION REPORT NUMBER Technical Report SL-94-16	
9. SPONSORING/MONITORING AGENCY NAME(S) AND ADDRESS(ES) Defense Nuclear Agency 6801 Telegraph Road Alexandria, VA 22310-3398			10. SPONSORING/MONITORING AGENCY REPORT NUMBER	
11. SUPPLEMENTARY NOTES Report also submitted to the University of Illinois in partial fulfillment of the requirements for the degree of Doctor of Philosophy in Theoretical and Applied Mechanics.				
12a. DISTRIBUTION/AVAILABILITY STATEMENT Approved for public release; distribution is unlimited.			12b. DISTRIBUTION CODE	
13. ABSTRACT (Maximum 200 words) A large-diameter gas gun has been developed which fires a 4-ft diameter, 3,200-lb projectile downward at velocities up to 230 ft/sec. The impact of the projectile onto geologic or other material specimens beneath the gun provides precise shock environments for shock physics studies, especially the evaluation and validation of ground-motion instruments, and the development of dynamic material properties data for large specimens. This report describes the operating principle of the gun. A mathematical model of the gun is developed and compared with experiment results. Predictions of nuisance effects associated with testing, e.g., far-field ground motion and airblast, are compared with experiment results. Descriptions of target construction and testing procedures are given. Examples of stress and ground-motion data collected in sand targets are presented, as well as typical data-analysis procedures.				
14. SUBJECT TERMS Gas gun Ground motion Ground shock Projectile impact			15. NUMBER OF PAGES 170	
			16. PRICE CODE	
17. SECURITY CLASSIFICATION OF REPORT UNCLASSIFIED	18. SECURITY CLASSIFICATION OF THIS PAGE UNCLASSIFIED	19. SECURITY CLASSIFICATION OF ABSTRACT	20. LIMITATION OF ABSTRACT	